GEOCHEMISTRY OF POST-SHIELD LAVAS FROM KEA- AND LOA-TREND HAWAIIAN VOLCANOES: CONSTRAINTS ON THE ORIGIN AND DISTRIBUTION OF HETEROGENEITIES IN THE HAWAIIAN MANTLE PLUME

by

DIANE HANANO

B.Sc.H., The University of British Columbia, 2004

A THESIS SUBMITTED IN PARTIAL FULFILLMENT OF

THE REQUIREMENTS FOR THE DEGREE OF

MASTER OF SCIENCE

in

THE FACULTY OF GRADUATE STUDIES

(GEOLOGICAL SCIENCES)

THE UNIVERSITY OF BRITISH COLUMBIA

July 2008

ABSTRACT

The alteration mineralogy, major and trace element chemistry, and Sr-Nd-Pb-Hf isotopic compositions of post-shield lavas from Mauna Kea, Kohala, and Hualalai on the island of Hawaii in the Pacific Ocean are used to constrain the origin and distribution of heterogeneities in the Hawaiian mantle plume. Ocean island basalts contain a variety of secondary minerals that must be removed by acid-leaching to achieve high-precision Pb isotopic compositions, a powerful geochemical tracer of variation in plume source composition. Post-shield lavas range from transitional/alkalic basalt to trachyte and are enriched in incompatible trace elements (e.g. La_N/Yb_N = 6.0-16.2) relative to shield stage tholeiites. Post-shield lavas are characterized by a limited range of Sr-Nd-Hf isotopic compositions ($^{87}Sr/^{86}Sr$ = 0.70343-0.70365; $^{143}Nd/^{144}Nd$ = 0.51292-0.51301; $^{176}Hf/^{177}Hf$ = 0.28311-0.28314) and have Pb isotopic compositions ($^{206}Pb/^{204}Pb$ = 17.89-18.44; $^{207}Pb/^{204}Pb$ = 15.44-15.49; $^{208}Pb/^{204}Pb$ = 37.68-38.01) that belong to their respective Kea or Loa side of the Pb-Pb boundary. Mauna Kea lavas show a systematic shift to less radiogenic Pb isotopic compositions from the shield to post-shield stage and trend to low $^{87}Sr/^{86}Sr$ towards compositions characteristic of rejuvenated stage lavas. Hualalai post-shield lavas lie distinctly above the Hf-Nd Hawaiian array (ε_{Hf} = +12 to +13; ε_{Nd} = +5.5 to +6.5) and have some of the least radiogenic Pb isotopic compositions (e.g. $^{206}Pb/^{204}Pb$ = 17.89-18.01) of recent Hawaiian volcanoes. In contrast, comparison of Kohala with the adjacent Mahukona shows that lavas from these volcanoes become more radiogenic in Pb during the late stages of volcanism. The Sr-Nd-Pb-Hf isotope systematics of the post-shield lavas cannot be explained by mixing between the Kea and Koolau end-members or by assimilation of Pacific lithosphere and are consistent with the presence of ancient

recycled lower oceanic crust and sediments in their source. More than one depleted component is sampled by the post-shield lavas and these components are long-lived features of the Hawaiian plume that are present in both the Kea and Loa source regions. The geochemistry of the post-shield lavas provide evidence for a bilaterally zoned plume, where the compositional boundary between the Kea and Loa sources is complex and vertical components of heterogeneity are also significant.

TABLE OF CONTENTS

LIST OF TABLES

LIST OF FIGURES

ACKNOWLEDGEMENTS

There have been many people who have helped me over the years that have led up to the completion of this thesis. Firstly, I would like to thank my supervisors Dominique Weis and James Scoates, whose enthusiasm for science and dedication to their students have been a great source of inspiration. Since the day I began working with them as an undergraduate student just over 5 years ago, they have continued to support and encourage me. Thanks also to Kelly Russell for being part of my supervisory committee. I thank the staff of the Pacific Centre for Isotopic and Geochemical Research (PCIGR) including Jane Barling, Bruno Kieffer, Bert Mueller, and Wilma Pretorius for their help with MC-ICP-MS, TIMS, and HR-ICP-MS analyses, as well as Claude Maerschalk and Rich Friedman for support in the lab. Mati Raudsepp and Sasha Wilson are also thanked for assistance with SEM and XRD analyses.

I would like to thank Don DePaolo for giving me the opportunity to work on the Hawaiian post-shield lavas. This project interested me from the start and I am grateful to have been a part of it. I would also like to thank Sarah Aciego for her assistance with the post-shield samples. Mike Garcia and Mark Kurz are thanked for allowing me to work on the Mahukona basalts, and Dave Clague is also thanked for providing the submarine basalts from Hualalai, Kohala, and Penguin Bank. These additional samples brought a unique perspective to this project that would not have otherwise been possible.

I am thankful for the support that my family and friends have given me throughout this process. My parents have always encouraged my studies and I thank them for their love and guidance. My fellow students of the PCIGR have shared in the emotional ups and downs of being a graduate student and have become my good friends. I would especially

like to thank Ryan Fisher for being there for me from the very beginning. For understanding when I had to study, for driving me to UBC every morning even though I made him late for work, and for his unconditional love and support even during the most difficult times, I will always be grateful.

CO-AUTHORSHIP STATEMENT

All research, analytical work (except as indicated below), and manuscript preparation was carried out by the author with contributions from my co-authors of each manuscript. As co-authors, my supervisors Dominique Weis and James Scoates provided research advice and ideas, careful editing of both manuscripts, as well as financial support.

CHAPTER 2
Alteration mineralogy and the effect of acid-leaching on the Pb isotope systematics of ocean island basalts
Authors: Diane Hanano, James S. Scoates, Dominique Weis

CHAPTER 3
Trace element and isotope geochemistry of post-shield lavas from Mauna Kea, Kohala, and Hualalai: Evidence for ancient depleted components in the Hawaiian plume
Authors: Diane Hanano, Dominique Weis, Sarah Aciego, James S. Scoates, Donald J. DePaolo

Donald DePaolo and Sarah Aciego (University of California, Berkeley) carried out field work and sample collection.
Sarah Aciego provided the major and trace element XRF analyses as well as the Sr and Nd isotopic compositions for the post-shield samples.
Donald DePaolo was responsible for the development of the research project.

CHAPTER 1

GEOCHEMICAL EVOLUTION OF THE HAWAIIAN ISLANDS AND THE IMPORTANCE OF POST-SHIELD VOLCANISM

1.1 INTRODUCTION

This study focuses on the geochemistry of post-shield lavas from Mauna Kea, Kohala, and Hualalai volcanoes on the island of Hawaii, part of the Hawaiian-Emperor Seamount Chain in the Pacific Ocean (Figure 1.1). The ~6000 km long chain of at least 129 islands, atolls, and seamounts extends from ~19°N to the Aleutian subduction zone at ~55°N. The chain displays a systematic age progression from >76 Ma in the north at Meiji and Detroit seamounts to active volcanism in the south at Kilauea volcano and Loihi seamount [*Duncan and Keller*, 2004]. The prominent bend in the chain at ~50 Ma records a change in the direction of Pacific plate motion from N10°W to N65°W and is thought to be due to a major reorganization of Pacific spreading centres [*Sharp and Clague*, 2006]. Hawaii is the archetype of intraplate ocean island volcanism, whereby an age-progressive hotspot track is created as the lithosphere migrates over a relatively stationary source (i.e., a plume) [*Wilson*, 1963; *Morgan*, 1971]. The Hawaiian mantle plume in particular is one of the most robust plumes on Earth and is inferred to have an origin in the deep mantle [e.g., *Sleep*, 1990; *Courtillot et al.*, 2003; *Lei and Zhao*, 2006; *Montelli et al.*, 2006; *Nolet et al.*, 2007].

The Hawaiian Islands, at the southern end of the Hawaiian-Emperor Seamount Chain, preserve the last ~5 million years of volcanism related to the Hawaiian mantle plume (Figure 1.1). A striking feature of the Hawaiian Islands is the two geographically distinct chains of volcanoes [*Dana*, 1849; *Jackson et al.*, 1972]. These two chains, termed Loa and Kea after their largest volcanoes (Mauna Loa and Mauna Kea), are sub-parallel to each other and separated by a distance of approximately 40 km. Lavas erupted from volcanoes belonging to each chain are characterized by persistent differences in major elements, trace

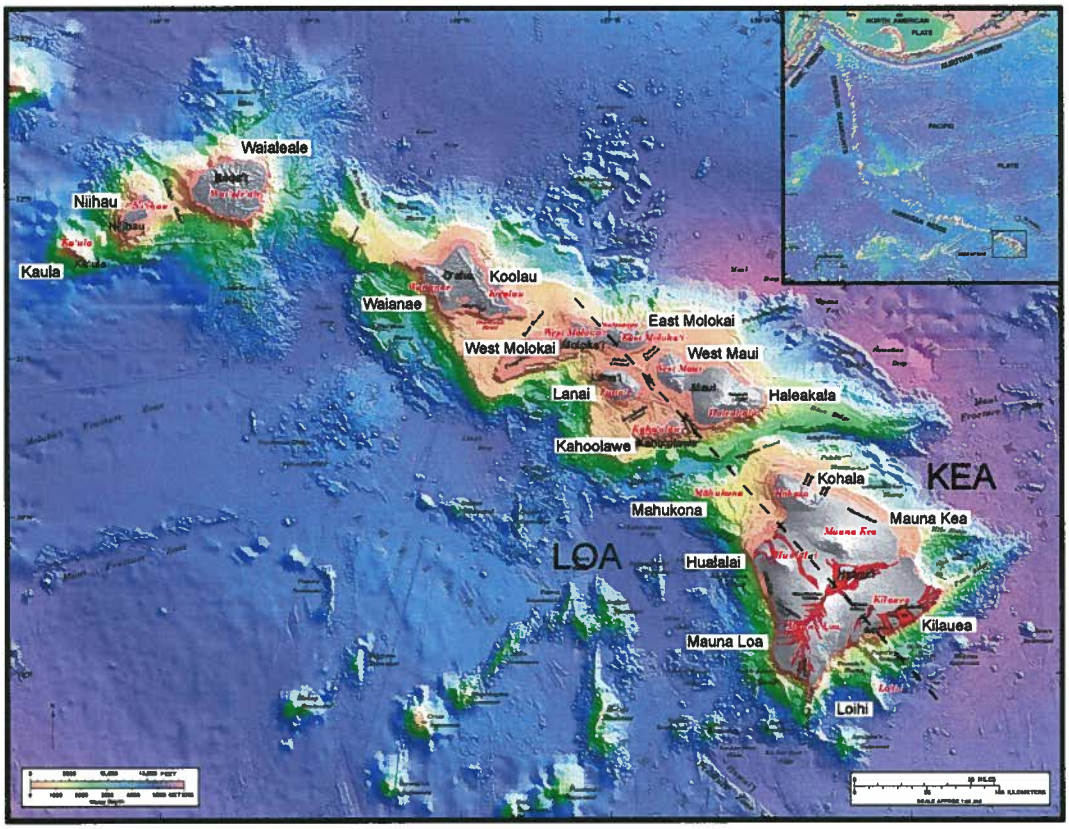

Figure 1.1: Bathymetric map of the seafloor around the Hawaiian Islands [*Eakins et al.*, 2003]. Subaerial topography is represented by shades of grey and historical lava flows are shown in red. Broad terraces that surround the islands represent paleo-coastlines and prominent ridges extending from the islands represent submarine rift zones. Fields of blocky debris were created by landslides and slumps. The numerous seamounts distributed across the seafloor are Late Cretaceous in age (~80 Ma) and are unrelated to the Hawaiian plume. The inset map shows the bathymetry of the northwest Pacific Ocean and the ~6000 km long Hawaiian-Emperor Seamount Chain.

elements, and isotope ratios [e.g., *Tatsumoto*, 1978; *Frey and Rhodes*, 1993; *Hauri*, 1996; *Lassiter et al.*, 1996; *Abouchami et al.*, 2005]. Variations in chemistry are also observed in lavas from a single volcano, which has led to the recognition that Hawaiian volcanoes evolve through four distinct stages during their ~600,000 year lifetime [e.g., *Macdonald*, 1968; *Moore et al.*, 1982; *Macdonald et al.*, 1983; *Clague and Dalrymple*, 1987]. The initial submarine pre-shield stage is characterized by a heterogeneous mixture of mostly alkalic lavas and accounts for only ~3% of the total volume of the volcano. The majority of the volcano (95-98%) is produced by the eruption of tholeiitic basalts that build the volcano above sea level during the subsequent shield stage. As the volcano migrates away from the plume axis, magma supply and eruption rates decrease and the volcano enters the post-shield stage, where lavas typically form a thin veneer of alkalic basalts, hawaiites and mugearites that contribute ~1% of the volcano's volume. After a period of subsidence, extensive erosion, and volcanic quiescence that may last between 0.5 and 2.5 million years, some volcanoes experience rejuvenated (or "post-erosional" or "secondary") volcanism, which is volumetrically minor (<<1%) and characterized by strongly alkalic lavas.

The geochemical variability observed in Hawaiian lavas requires involvement of at least three compositionally distinct source components [e.g., *Staudigel et al.*, 1984; *Stille et al.*, 1986; *West et al.*, 1987; *Eiler et al.*, 1996; *Hauri*, 1996]. Recent studies have shown that a depleted component may also be required to explain the depleted isotopic signatures observed in some Hawaiian lavas [e.g., *Mukhopadhyay et al.*, 2003; *Frey et al.*, 2005]. However, much debate currently exists over the origin of this component as being related to either the Pacific lithosphere [e.g., *Chen and Frey*, 1985; *Gaffney et al.*, 2004] or material intrinsic to the plume [e.g., *Frey et al.*, 2005; *Fekiacova et al.*, 2007]. Furthermore, the

geochemical structure of the plume, commonly inferred to be concentrically or bilaterally zoned, is another controversial aspect of Hawaiian volcanism [e.g., *DePaolo et al.*, 2001 *Abouchami et al.*, 2005; *Bryce et al.*, 2005; *Xu et al.*, 2007]. Post-shield lavas, which are derived from low degrees of partial melting and small volumes within the melting region, are especially useful for helping to resolve such questions and are the focus of this study.

The island of Hawaii, the youngest in the Hawaiian chain, is made up of five coalesced volcanoes; two additional volcanoes (Mahukona and Loihi) that are presently below sea level also contribute to the island's submarine base (Figure 1.2). Mauna Loa and Kilauea, which make up the southern part of the island, are in the shield-building stage of growth, whereas the older Hualalai, Mauna Kea, and Kohala volcanoes to the north have experienced post-shield volcanism. A fair amount of previous work has been carried out on post-shield lavas from Mauna Kea and Kohala [e.g., *Spengler and Garcia*, 1988; *West et al.*, 1988; *Frey et al.*, 1990; *Kennedy et al.*, 1991]. Relatively less work has been carried out on post-shield lavas from Hualalai; the isotopic compositions of several lavas from Hualalai were determined as part of a regional survey of ocean island basalts [*Park*, 1990] and in a recent study of post-shield trachytes [*Cousens et al.*, 2003]. However, in the older studies, the ages and vent locations of the studied samples were not well-constrained, and very few, if any, Hf isotopic data were reported. Furthermore, recent advances in analytical techniques, particularly the development of MC-ICP-MS, permit the isotope ratios of numerous elements (including Hf and Pb) to be determined with significantly improved precision [e.g., *Albarède et al.*, 2004]. Specifically, the ability of the plasma source to more efficiently ionize Hf has resulted in external precision better than 40 ppm [*Blichert-Toft et al.*, 1997; *Weis et al.*, 2007]. For Pb, the use of Tl to correct for instrumental mass

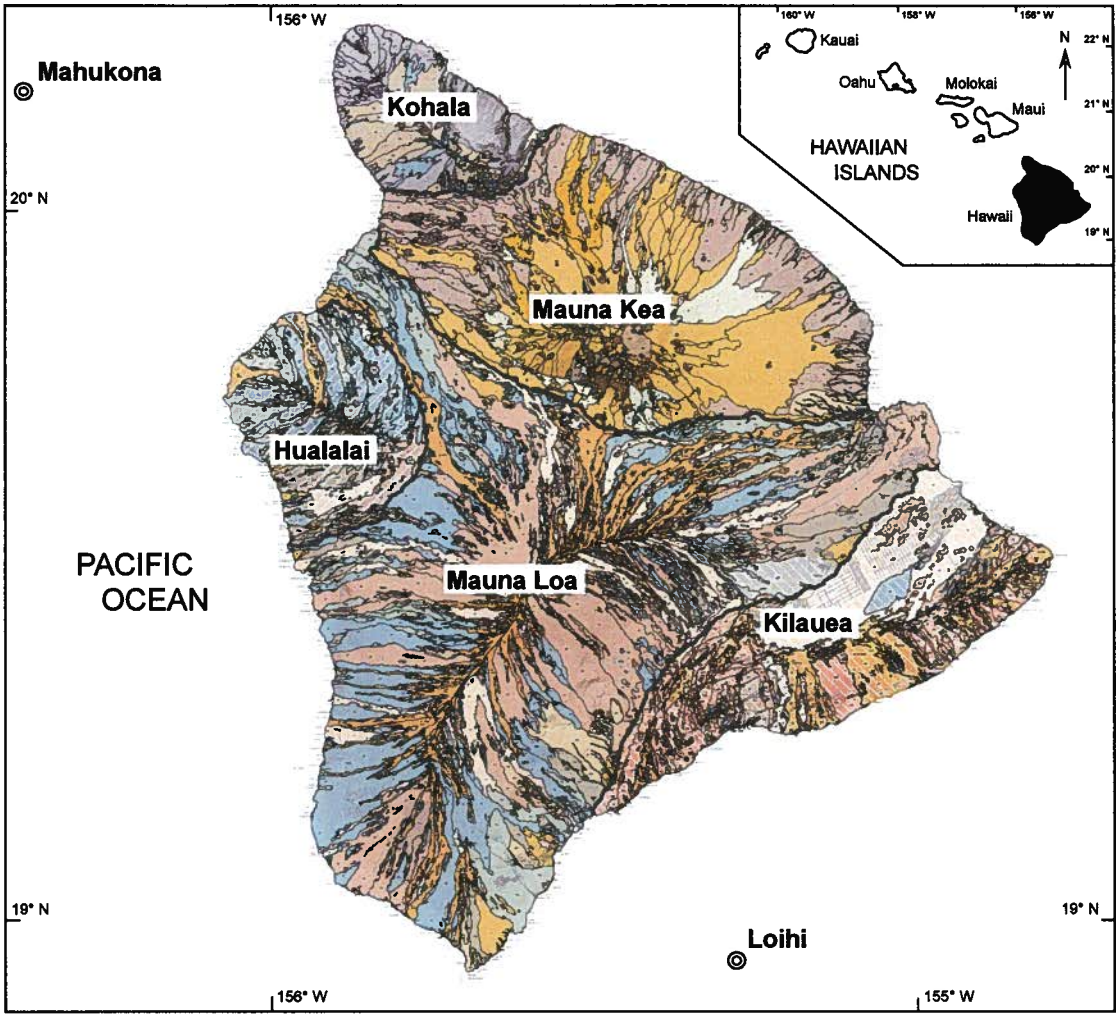

Figure 1.2: Geological map of the island of Hawaii [*Wolfe and Morris*, 1996]. Different colours and patterns represent distinct lithologic units (mainly lavas flows of varying age). The thick grey lines mark the approximate boundaries between lavas from Kilauea, Mauna Loa, Hualalai, Mauna Kea, and Kohala volcanoes. The approximate locations of the submarine summits of Mahukona and Loihi volcanoes are also shown. The inset map shows the location of the island of Hawaii with respect to the other Hawaiian Islands in the Pacific Ocean.

fractionation, combined with enhanced acid-leaching techniques, have allowed for external precision in the 100 ppm range [e.g., *White et al.*, 2000; *Woodhead*, 2002; *Weis et al.*, 2006].

1.2 OVERVIEW OF THE THESIS

This thesis comprises two distinct studies, which are presented in Chapters 2 and 3. The main objectives of this thesis were to (1) characterize the geochemistry of lavas from the post-shield stage of Hawaiian volcanism, (2) determine the extent and origin of depleted components in Hawaiian lavas, and ultimately (3) provide constraints on the geochemical structure of the Hawaiian plume. Due to the potential susceptibility of Pb isotopes to modification by post-magmatic alteration, and their importance in helping to answer the objectives of this research, we first undertook a mineralogical study of the alteration phases present in ocean island basalts, the results of which are presented in Chapter 2. Chapter 3 represents the central work of this thesis and involves the trace element and isotope geochemistry of post-shield lavas from Mauna Kea, Kohala, and Hualalai volcanoes on the island of Hawaii. The results of this work have been presented by the author at a number of international conferences including the 2005 and 2006 AGU Fall Meetings (*Hanano et al.*, 2005; *Hanano et al.*, 2006a), the 2006 GAC-MAC Joint Annual Meeting (*Hanano et al.*, 2006b), and the 17th Annual Goldschmidt Conference (*Hanano et al.*, 2007). Both chapters were prepared in manuscript format appropriate for submission to international scientific journals. Chapter 2 is the revised version of the manuscript submitted to American Mineralogist after undergoing peer-review. Chapter 4 presents a summary of the major findings of the thesis.

Chapter 2 explores the alteration mineralogy of four weakly altered basalts from two major ocean island volcanic systems, Hawaii and Kerguelen, using scanning electron microscopy and X-ray diffraction. This work was initiated as part of a research project for EOSC 521 (Microbeam Diffraction Methods for the Characterization of Minerals and Materials) taught by Mati Raudsepp at UBC, and the initial results were included in a final report required for partial completion of the course. Many studies have documented the changes in Pb isotopic compositions resulting from acid-leaching, but very few have tried to link these changes with the alteration mineralogy of the samples. A wide variety of secondary minerals are identified, and the effectiveness of their removal by acid-leaching is evaluated. These results are then integrated with Pb isotope data on the same samples (from *Nobre Silva et al.*, in revision, 2008) to identify possible sources of contamination and to determine the effect of incomplete removal of alteration phases on the reproducibility of Pb isotopic compositions. The results of this study have important implications for high-precision Pb isotope studies of ocean island basalts.

Chapter 3 documents the geochemistry of 32 post-shield lavas from Mauna Kea, Kohala, and Hualalai (Figure 1.2). The samples were collected by Don DePaolo and Sarah Aciego of the University of California, Berkeley as part of a larger project to better define the geochemical structure of the Hawaiian mantle plume. Of the data reported in this chapter, the trace element concentrations and Pb and Hf isotopic compositions were acquired by the author, whereas the major element and Sr and Nd isotope analyses were carried out by Sarah Aciego at the University of California, Berkeley. The major and trace element results provide the framework for investigating the origin and source of the post-shield lavas. The Sr, Nd, Pb, and Hf isotopic compositions allow for identification of

discrete mantle components sampled by each volcano and have implications for the origin and distribution of small-scale heterogeneities and large-scale zoning within the Hawaiian plume. Literature data from other Hawaiian volcanoes were compiled in an effort to determine if the post-shield lavas were derived from the same sources as shield lavas and to provide the appropriate context for interpretation of the post-shield results. The post-shield lavas are compared to potential depleted sources to identify the origin of the depleted signature observed in the post-shield lavas. The post-shield lavas are also compared to late-shield, post-shield, and rejuvenated stage lavas from other Hawaiian volcanoes to constrain the extent of the depleted component related to Hawaiian volcanism. Lastly, the isotope systematics of two consecutive pairs of Hawaiian volcanoes (Mahukona-Kohala and Hualalai-Mauna Kea) are used to evaluate models of horizontal zoning and to determine the importance of vertical heterogeneity within the plume.

Appendix A reports the analytical quality assurance, quality control (QA-QC) results for the chemical analyses reported in this study including: a comparison between trace element abundances determined by XRF and ICP-MS (A1), the trace element abundances of USGS reference materials (A2), and the reproducibility of the Pb and Hf isotopic analyses (A3). Appendix B is a brief summary and preliminary interpretation of the isotopic results for offshore submarine Hawaiian basalts. The Sr, Nd, Pb, and Hf isotopic compositions were determined for 13 samples from Mahukona (B1) and 10 samples from Penguin Bank, Hualalai, and Kohala (B2). These supplementary samples, provided by Dave Clague, Mike Garcia, and Mark Kurz, were analyzed in an effort to better understand the onshore post-shield volcanism and to increase the geographical sampling area. The isotopic compositions of the submarine basalts are used in Chapter 3 to provide additional constraints on the large-

scale geochemical structure of the Hawaiian plume. The isotopic results for Mahukona will form part of a larger manuscript on the geology of this volcano (*Garcia et al.*, in preparation, 2008). The geochemistry of this submerged Hawaiian shield volcano is not well characterized and is particularly important to our understanding of Hawaiian volcanism because it fills the gap between Hualalai and Kahoolawe in the paired sequence of Hawaiian volcanoes.

1.3 REFERENCES

Abouchami, W., A. W. Hofmann, S. J. G. Galer, F. A. Frey, J. Eisele, and M. Feigenson (2005), Lead isotopes reveal bilateral asymmetry and vertical continuity in the Hawaiian mantle plume, *Nature*, *434*, 851-856.

Albarède, F., P. Telouk, J. Blichert-Toft, M. Boyet, A. Agranier, and B. Nelson (2004), Precise and accurate isotopic measurements using multiple-collector ICPMS, *Geochimica et Cosmochimica Acta*, *68*(12), 2725-2744.

Blichert-Toft, J., C. Chauvel, and F. Albarède (1997), Separation of Hf and Lu for high-precision isotope analysis of rock samples by magnetic sector-multiple collector ICP-MS, *Contributions to Mineralogy and Petrology*, *127*, 248-260.

Bryce, J. G., D. J. DePaolo, and J. C. Lassiter (2005), Geochemical structure of the Hawaiian plume: Sr, Nd, and Os isotopes in the 2.8 km HSDP-2 section of Mauna Kea volcano, *Geochemistry Geophysics Geosystems*, *6*(9), doi:10.1029/2004GC000809.

Chen, C. Y., and F. A. Frey (1985), Trace element and isotopic geochemistry of lavas from Haleakala volcano, East Maui, Hawaii: Implications for the origin of Hawaiian basalts, *Journal of Geophysical Research*, *90*, 8743-8768.

Clague, D. A., and G. B. Dalrymple (1987), The Hawaiian-Emperor volcanic chain, Part 1: Geologic evolution, in *Volcanism in Hawaii*, edited by R.W. Decker, T.L. Wright, and P.H. Stauffer, pp. 1667, US Geological Survey Professional Paper 1350, Denver.

Courtillot, V., A. Davaille, J. Besse, and J. Stock (2003), Three distinct types of hotspots in the Earth's mantle, *Earth and Planetary Science Letters*, *205*, 295-308.

Cousens, B. L., D. A. Clague, and W. D. Sharp (2003), Chronology, chemistry, and origin of trachytes from Hualalai Volcano, Hawaii, *Geochemistry Geophysics Geosystems*, *4*(9), 1078, doi:10.1029/2003GC000560.

Dana, J. D. (1849), Geology, in *United States Exploring Expedition, 1838-1842*, vol. 10, pp. 756, C. Sherman, Philadelphia.

DePaolo, D. J., J. G. Bryce, A. Dodson, D. L. Shuster, and B. M. Kennedy (2001), Isotopic evolution of Mauna Loa and the chemical structure of the Hawaiian plume, *Geochemistry Geophysics Geosystems*, *2*, doi: 10.1029/2000GC000139.

Duncan, R. A., and R. A. Keller (2004), Radiometric ages for basement rocks from the Emperor Seamounts, ODP Leg 197, *Geochemistry Geophysics Geosystems*, *5*, doi:10.1029/2004GC000704.

Eakins, B. W., J. E. Robinson, T. Kanamatsu, J. Naka, J. R. Smith, E. Takahashi, and D. A. Clague (2003), Hawaii's volcanoes revealed, *Map I-2809*, United States Geological Survey, Denver, CO.

Eiler, J. M., K. A. Farley, J. W. Valley, A. W. Hofmann, and E. M. Stolper (1996), Oxygen isotope constraints on the sources of Hawaiian volcanism, *Earth and Planetary Science Letters*, *144*, 453-468.

Fekiacova, Z., W. Abouchami, S. J. G. Galer, M. O. Garcia, and A. W. Hofmann (2007), Origin and temporal evolution of Koolau volcano, Hawaii: Inferences from isotope data on the Koolau Scientific Drilling Project (KSDP), the Honolulu Volcanics and ODP Site 843, *Earth and Planetary Science Letters*, *261*, 65-83.

Frey, F., and J. Rhodes (1993), Intershield geochemical differences among Hawaiian volcanoes: Implications for source compositions, melting process and magma ascent paths, *Philosophical Transactions Royal Society of London Part A*, *342*, 121-136.

Frey, F. A., S. Huang, J. Blichert-Toft, M. Regelous, and M. Boyet (2005), Origin of depleted components in basalt related to the Hawaiian hot spot: Evidence from isotopic and incompatible element ratios, *Geochemistry Geophysics Geosystems*, *6*(1), doi: 10.1029/2004GC000757.

Frey, F. A., W. S. Wise, M. O. Garcia, H. B. West, S.-T. Kwon, and A. K. Kennedy (1990), Evolution of Mauna Kea volcano, Hawaii: Petrologic and geochemical constraints on postshield volcanism, *Journal of Geophysical Research*, *95*(B2), 1271-1300.

Gaffney, A. M., B. K. Nelson, and J. Blichert-Toft (2004), Geochemical constraints on the role of oceanic lithosphere in intra-volcano heterogeneity at West Maui, Hawaii, *Journal of Petrology*, *45*(8), 1663-1687.

Hanano, D., D. Weis, S. Aciego, J. S. Scoates, and D. J. DePaolo (2005), Geochemical systematics of Hawaiian post-shield lavas: Implications for the chemical structure of the Hawaiian mantle plume, *Eos Transactions, AGU*, *86*(52), Fall Meeting Supplement, Abstract V41D-1497.

Hanano, D., D. Weis, S. Aciego, J. S. Scoates, and D. J. DePaolo (2006a), Geochemistry of post-shield lavas and submarine tholeiites from the Kea and Loa trends of Hawaiian volcanoes, *Eos Transactions, AGU*, *87*(52), Fall Meeting Supplement, Abstract V13B-0673.

Hanano, D., D. Weis, S. Aciego, J. S. Scoates, and D. J. DePaolo (2006b), Pb isotopic systematics of Mauna Kea, Kohala, and Hualalai post-shield lavas: Heterogeneity at the periphery of the Hawaiian plume, *GAC-MAC Program with Abstracts*, *31*, 63.

Hanano, D., D. Weis, S. Aciego, J. S. Scoates, and D. J. DePaolo (2007), Geochemistry of post-shield lavas from paired Loa- and Kea-trend Hawaiian volcanoes, *Geochimica et Cosmochimica Acta*, *71-15*, Supplement 1: A375.

Hauri, E. H. (1996), Major-element variability in the Hawaiian mantle plume, *Nature*, *382*, 415-419.

Jackson, E. D., E. A. Silver, and G. B. Dalrymple (1972), Hawaiian-Emperor chain and its relation to Cenozoic circum-Pacific tectonics, *Geological Society of America Bulletin*, *83*, 601-618.

Kennedy, A. K., S.-T. Kwon, F. A. Frey, and H. B. West (1991), The isotopic composition of postshield lavas from Mauna Kea volcano, Hawaii, *Earth and Planetary Science Letters*, *103*, 339-353.

Lassiter, J. C., D. J. DePaolo, and M. Tatsumoto (1996), Isotopic evolution of Mauna Kea Volcano: results from the initial phase of the Hawaii Scientific Drilling Project, *Journal of Geophysical Research*, *101*(B5), 11,769-11,780.

Lei, J., and D. Zhao (2006), A new insight into the Hawaiian plume, *Earth and Planetary Science Letters*, *241*, 438-453.

Macdonald, G. A. (1968), Composition and origin of Hawaiian lavas, *Geological Society of America Memoir*, *116*, 477-522.

Macdonald, G. A., A. T. Abbott, and F. L. Peterson (1983), The Geology of Hawaii, in *Volcanoes in the Sea*, pp. 517, University of Hawaii Press, Honolulu.

Montelli, R., G. Nolet, F. A. Dahlen, and G. Masters (2006), A catalogue of deep mantle plumes: New results from finite-frequency tomography, *Geochemistry Geophysics Geosystems*, *7*(11), doi:10.1029/2006GC001248.

Moore, J. G., D. A. Clague, and W. R. Normark (1982), Diverse basalt types from Loihi Seamount, Hawaii, *Geology*, *10*, 88-92.

Morgan, W. J. (1971), Convection plumes in the lower mantle, *Nature*, *230*, 42-43.

Mukhopadhyay, S., J. C. Lassiter, K. A. Farley, and S. W. Bogue (2003), Geochemistry of Kauai shield-stage lavas: Implications for the chemical evolution of the Hawaiian plume, *Geochemistry Geophysics Geosystems*, *4*(1), 1009, doi:10.1029/2002GC000342.

Nobre Silva, I. G., D. Weis, J. Barling, and J. S. Scoates (2008), Leaching systematics for the determination of high-precision Pb isotope compositions of ocean island basalts, *Geochemistry Geophysics Geosystems*, paper # 2007GC001891 (in revision).

Nolet, G., R. Allen, and D. Zhao (2007), Mantle plume tomography, *Chemical Geology*, *241*, 248-263.

Park, K.-H., Strontium, neodymium, and lead isotopic studies of ocean island basalts: Constraints on their evolution and origin, Ph.D. thesis, Columbia University, Palisades, N.Y., 1990.

Sharp, W. D., and D. A. Clague (2006), 50-Ma initiation of Hawaiian-Emperor bend records major change in Pacific plate motion, *Science*, *313*, 1281-1284.

Sleep, N. H. (1990), Hotspots and mantle plumes: Some phenomenology, *Journal of Geophysical Research*, *95*, 6715-6736.

Spengler, S. R., and M. O. Garcia (1988), Geochemistry of the Hawi lavas, Kohala volcano, Hawaii, *Contributions to Mineralogy and Petrology*, *99*, 90-104.

Staudigel, H. A., A. Zindler, S. R. Hart, T. Leslie, C.-Y. Chen, and D. Clague (1984), The isotope systematics of a juvenile intraplate volcano: Pb, Nd and Sr isotope ratios of basalts from Loihi Seamount, Hawaii, *Earth and Planetary Science Letters*, *69*, 13-29.

Stille, P., D. M. Unruh, and M. Tatsumoto (1986), Pb, Sr, Nd, and Hf isotopic constraints on the origin of Hawaiian basalts and evidence for a unique mantle source, *Geochimica et Cosmochimica Acta*, *50*(10), 2303-2319.

Tatsumoto, M. (1978), Isotopic composition of lead in oceanic basalt and implication to mantle evolution, *Earth and Planetary Science Letters*, *38*, 63-87.

Weis, D., B. Kieffer, D. Hanano, I. N. Silva, J. Barling, W. Pretorius, C. Maerschalk, and N. Mattielli (2007), Hf isotope compositions of U.S. Geological Survey reference materials, *Geochemistry Geophysics Geosystems*, *8*(6), doi:10.1029/2006GC001473.

Weis, D., B. Kieffer, C. Maerschalk, J. Barling, J. deJong, G. A. Williams, D. Hanano, W. Pretorius, N. Mattielli, J. S. Scoates, A. Goolaerts, R. M. Friedman, and J. B. Mahoney (2006), High-precision isotopic characterization of USGS reference materials by TIMS and MC-ICP-MS, *Geochemistry Geophysics Geosystems*, *7*(8), doi:10.1029/2006GC001283.

West, H. B., M. O. Garcia, F. A. Frey, and A. Kennedy (1988), Nature and cause of compositional variation among the alkalic cap lavas of Mauna Kea volcano, Hawaii, *Contributions to Mineralogy and Petrology*, *100*, 383-397.

West, H. B., D. C. Gerlach, W. P. Leeman, and M. O. Garcia (1987), Isotopic constraints on the origin of Hawaiian lavas from the Maui volcanic complex, Hawaii, *Nature*, *330*, 216-220.

White, W. M., F. Albarède, and P. Telouk (2000), High-precision analysis of Pb isotope ratios by multi-collector ICP-MS, *Chemical Geology*, *167*, 257-270.

Wilson, J. T. (1963), A possible origin of the Hawaiian Islands, *Canadian Journal of Physics*, *41*(6), 863-870.

Wolfe, E. W., and J. Morris (1996), Geologic map of the island of Hawaii, *Map 2524-A*, United States Geological Survey, Denver, CO.

Woodhead, J. D. (2002), A simple method for obtaining highly accurate Pb-isotope data by MC-ICPMS, *Journal of Analytical Atomic Spectrometry*, *17*, 1381-1385.

Xu, G., F. A. Frey, D. A. Clague, W. Abouchami, J. Blichert-Toft, B. Cousens, and M. Weisler (2007), Geochemical characteristics of West Molokai shield- and postshield-stage lavas: Constraints on Hawaiian plume models, *Geochemistry Geophysics Geosystems*, *8*, doi:10.1029/2006GC001554.

CHAPTER 2

ALTERATION MINERALOGY AND THE EFFECT OF ACID-LEACHING ON THE Pb ISOTOPE SYSTEMATICS OF OCEAN ISLAND BASALTS

2.1 INTRODUCTION[1]

The Pb isotopic compositions of ocean island basalts are a powerful tool for the characterization of their mantle source components, especially with recent improvements in precision and reproducibility offered by the triple spike method [e.g., *Abouchami et al.*, 2000] and by multiple collector inductively coupled plasma mass spectrometry (MC-ICP-MS) [e.g., *White et al.*, 2000; *Weis et al.*, 2005]. However, Pb isotopic compositions of ocean island basalts are highly susceptible to modification by non-magmatic Pb from seawater, hydrothermal alteration, aeolian dust, subaerial weathering, as well as by contamination during sample recovery and processing [e.g., *McDonough and Chauvel*, 1991; *Thirlwall*, 2000; *Weis et al.*, 2005]. Acid-leaching of basaltic rock powders or chips may not remove the foreign Pb component completely or in a reproducible way [e.g., *Abouchami et al.*, 2000; *Eisele et al.*, 2003], resulting in erroneous values, data scatter, and poor reproducibility, which reduces the effectiveness of the Pb isotopic system as a geochemical tracer. It is therefore critical to understand the types, quantities, and distribution of alteration phases in ocean island basalts that are analyzed for Pb isotope ratios. Most research concerning the alteration of basalt has focused on strongly altered samples [e.g., *Böhlke et al.*, 1980; *Alt and Honnorez*, 1984; *Banerjee et al.*, 2004], which are typically not selected for geochemical analysis in igneous studies. In this study, we present a mineralogical investigation of alteration phases in a select group of weakly altered basalts from two major ocean island volcanic systems (Hawaii and Kerguelen) based on scanning

[1] A version of this chapter has been submitted for publication. Hanano, D., J. S. Scoates, and D. Weis (2008), Alteration mineralogy and the effect of acid-leaching on the Pb isotope systematics of ocean island basalts, *American Mineralogist*, paper # 2845R.

electron microscopy (SEM), X-ray diffraction (XRD), and acid-leaching experiments that were specifically designed to test the effectiveness of leaching at removing alteration phases and the resulting effect on Pb isotope systematics.

2.2 SAMPLE DESCRIPTION

Basalts from four volcanic centers from Hawaii and Kerguelen were examined to cover a range of ages, eruptive environments, lava compositions, and alteration styles (Table 2.1; Figure 2.1). The basalts selected for this study display only minor to moderate alteration, and are typical samples analyzed for geochemical studies. Loss-on-ignition (LOI), a commonly used parameter for helping to assess the degree of alteration in a sample and thus its suitability for geochemical work, varies from 0-2 wt% in the four samples (Table 2.1), within the range of values that are considered acceptable.

The two Hawaiian basalts are from the two largest Hawaiian volcanoes, Mauna Loa (J2-019-04) and Mauna Kea (SR0954-8.00), which belong to the "Loa" and "Kea" trends, respectively [*Dana*, 1849; *Jackson et al.*, 1972]. Basaltic lavas from the two chains are distinguished both geographically and geochemically, exhibiting systematic differences in radiogenic isotopic compositions [e.g., *Tatsumoto*, 1978; *Lassiter et al.*, 1996; *Abouchami et al.*, 2005]. Alteration of Hawaiian basalts mainly involves the partial to complete replacement of glass and olivine by secondary minerals, including clays (mostly smectite), zeolites (most commonly chabazite and phillipsite), as well as Ca-silicate minerals, gypsum, and rare pyrite [e.g., *Walton and Shiffman*, 2003; *Garcia et al.*, 2007].

The two Kerguelen basalts are from Mont des Ruches on the Kerguelen Archipelago (BY96-27) and Site 1140 on the Northern Kerguelen Plateau (1140A 31R-1 57-61), which

Table 2.1: Sample characteristics and alteration indicators of studied Hawaiian and Kerguelen basalts

	Hawaii		Kerguelen	
Sample	J2-019-04	SR0954-8.00	BY96-27	1140A 31R-1 57-61
Location	Mile High Section, Southwest Rift Zone, Mauna Loa ("Loa-trend")	HSDP-2, Mauna Kea ("Kea-trend")	Mont des Ruches, Loranchet Peninsula, Kerguelen Archipelago	ODP Leg 183 Site 1140, Northern Kerguelen Plateau
Sampling Method	ROV Jason2	drilling	hammer	drilling
Depth/Elevation[a]	1986 mbsl	3009.3 mbsl	455 masl	270.07 mbsf
Age[b]	~450 ka	~550 ka	~28 Ma	~34 Ma
Eruption Environment	submarine	submarine	subaerial	submarine
Composition	tholeiitic basalt	tholeiitic basalt (picritic)	transitional basalt	tholeiitic basalt
MgO (wt%)[c]	14.2	18.2	10.7	5.7
Olivine Phenocryst Abundance (vol%)	~25	~19	~12	~20 (plagioclase, clinopyroxene, olivine)
General Alteration Description	trace groundmass alteration	minor alteration of olivine; moderate groundmass alteration	moderate alteration of olivine; moderate groundmass alteration	complete iddingsite replacement of olivine; secondary minerals in vesicles
LOI (wt%)[c]	0	0.85	2.01	1.65
Leaching Steps[d]	7	6	15	15
Leaching Weight Loss (%)[d]	34.8	32.2	51.0	50.4
Reproducibility (ppm)[e]	170	254	288	359

[a]mbsl = meters below sea level; masl = meters above sea level; mbsf = meters below the sea floor.

[b]J2-019-04: B. Singer (personal communication); SR0954-8.00: *DePaolo and Stolper* [1996]; BY96-27: *Doucet et al.* [2002]; 1140A 31R-1 57-61: *Duncan et al.* [2002].

[c]J2-019-04: D. Weis (unpublished data); SR0954-8.00: *Rhodes and Vollinger* [2004]; BY96-27: *Doucet et al.* [2002]; 1140A 31R-1 57-61: *Weis and Frey* [2002].

[d]Hawaii: *Nobre Silva et al.* (in revision, 2008); leaching weight loss is the mean of 2-3 separate powder aliquots. Kerguelen: this study; leaching weight loss is the mean of 6 separate powder aliquots.

[e]Reproducibility of the MC-ICP-MS Pb isotopic analyses is represented by the external reproducibility (2SD/mean x 10^6) of $^{206}Pb/^{204}Pb$ on acid-leached whole rock powders.

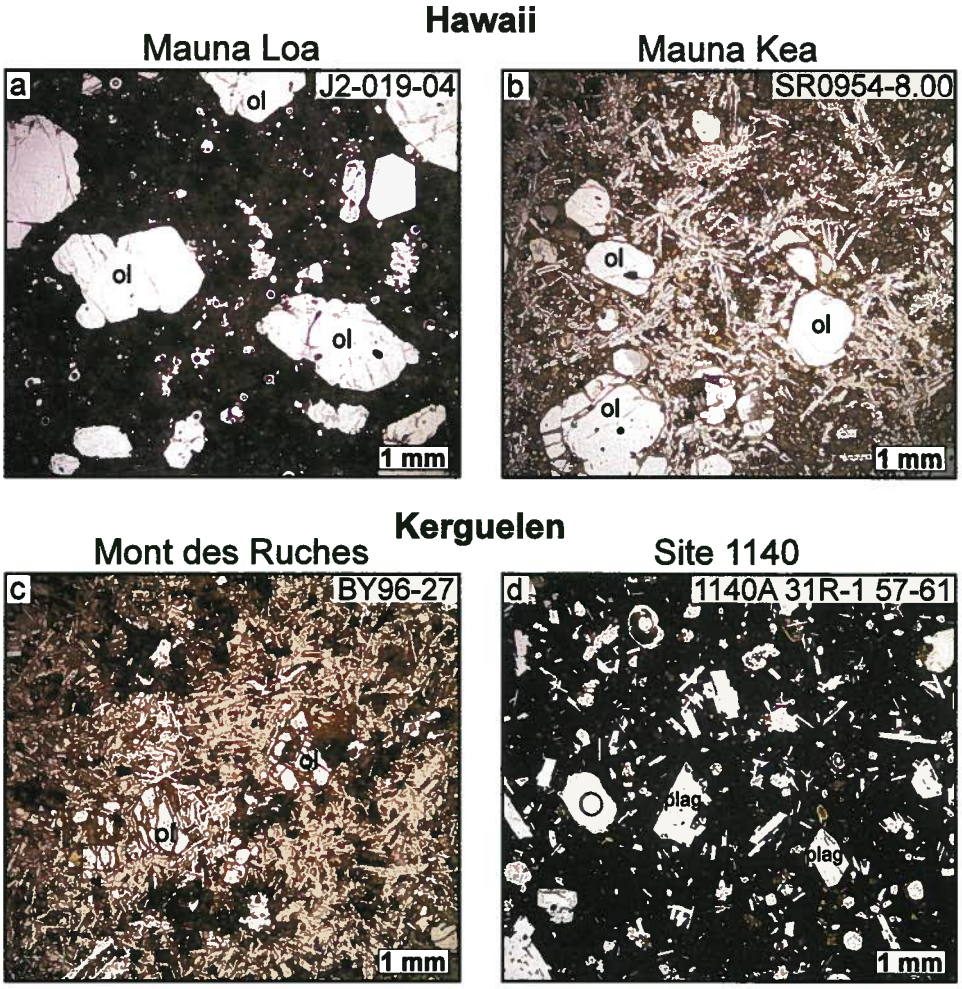

Figure 2.1: Photomicrographs of thin sections showing representative regions of Hawaiian and Kerguelen basalts examined in this study. Photomicrographs in plane-polarized light. Abbreviations: ol = olivine; plag = plagioclase. (**a**) Sample J2-019-04 (Mauna Loa, Hawaii) is characterized by large unaltered olivine phenocrysts in a fine-grained groundmass with trace alteration. (**b**) Sample SR0954-8.00 (Mauna Kea, Hawaii) shows minor alteration of the olivine phenocrysts and moderate alteration of the groundmass (yellow-green patches). (**c**) Sample BY96-27 (Mont des Ruches, Kerguelen Archipelago) contains highly fractured and altered olivine phenocrysts and moderate groundmass alteration. (**d**) Sample 1140A 31R-1 57-61 (Site 1140, Northern Kerguelen Plateau) is dominated by plagioclase phenocrysts set in a fine-grained groundmass. Olivine phenocrysts are small (<0.5 mm) and completely altered. Secondary minerals fill vesicles – see text for description.

belong to the Kerguelen large igneous province in the Southern Indian Ocean. The Kerguelen basalts are significantly older and have a style of alteration that is markedly different from that in the Hawaiian basalts (Table 2.1). The subaerial flood basalts of the Kerguelen Archipelago have been affected by hydrothermal alteration and contain a wide variety of secondary minerals, including carbonates, oxides, sulfides, quartz, clays, epidotes, and zeolites [e.g., *Nougier et al.*, 1982; *Verdier and Natival*, 1988; *Verdier*, 1989]. In contrast, the alteration of submarine basalts from the Northern Kerguelen Plateau does not involve zeolites and most commonly includes smectite (± hydromica), chlorite, and carbonate [*Kurnosov et al.*, 2003].

These basalts represent a sub-selection of samples from the study of *Nobre Silva et al.* (Nobre Silva, I. G., D. Weis, J. Barling, and J. S. Scoates, Leaching systematics for the determination of high-precision Pb isotope compositions of ocean island basalts, manuscript in revision for *Geochemistry Geophysics Geosystems*, 2008; hereinafter referred to as *Nobre Silva et al.*, in revision, 2008). The *Nobre Silva et al.* (in revision, 2008) study identifies changes in the Pb isotope compositions and reproducibility of Hawaiian and Kerguelen basalts via leaching and column chemistry experiments, whereas this study seeks to link these changes to the alteration mineralogy of the samples. The Pb isotope analyses were carried out using whole rock powders of basalt because glass is commonly not available or present in sufficient quantity (especially for older and subaerially erupted basalts). However, to ensure only the freshest material was powdered, surface alteration was first removed from the whole rocks; powders were subsequently prepared using agate and a crushing procedure specifically designed to limit sample exposure to tungsten carbide.

2.3 ANALYTICAL TECHNIQUES

Alteration phases were initially identified based on their morphology and optical properties using conventional optical microscopy, and further characterized by scanning electron microscopy (SEM) and X-ray diffraction (XRD) at the University of British Columbia. Backscattered electron (BSE) imaging and qualitative energy dispersive spectrometry (EDS) on carbon-coated polished petrographic thin sections were carried out on a Phillips XL-30 scanning electron microscope equipped with a Princeton-Gamma-Tech energy-dispersion spectrometer. An operating voltage of 15 Kv was used with a spot diameter of 6 μm and peak count time of 30 s. Whole rock sample powders for XRD were ground under ethanol with an agate mortar-and-pestle, smear-mounted onto glass slides, and then placed in aluminum holders. XRD data were collected over the range 3-80° 2θ using Co*K*α radiation on a Siemens D5000 X-ray powder diffractometer equipped with a diffracted-beam graphite monochromator crystal and operating at 35 Kv and 40 Ma.

After identification of the alteration phases, we carried out acid-leaching experiments on the sample powders to determine how effectively these minerals are removed. The premise of leaching is that any alteration phases or contaminants will be more susceptible to acid attack, leaving behind the more resistant primary (i.e., magmatic) minerals. Due to substantial weight loss during leaching (typically ~30-60%) and to avoid possible "nugget" effects, sufficient whole rock powder for XRD was only available for the two Kerguelen basalts (BY96-27 and 1140A 31R-1 57-61). Following the sequential leaching procedure of *Weis et al.* [2005], sample powders were repeatedly acid-leached in screw-top Teflon® vessels with quartz-distilled 6N HCl in a warm (~50 °C) ultrasonic bath for 20-minute intervals until the supernatant fluid became clear. The use of hot or boiling HCl could

reduce the total leaching time and workload, but significantly increases the likelihood of dissolving primary minerals and is therefore not recommended. Both sample powders required 15 leaching steps and lost ~50% of their initial weight (Table 2.1). Leached powders were rinsed twice with 18 MΩ·cm water to remove any residual traces of acid, taken to dryness, and analyzed by XRD in addition to the unleached powders.

2.4 RESULTS

2.4.1 Characterization of alteration phases

2.4.1.1 Mauna Loa, Hawaii (J2-019-04)

Olivine phenocrysts are unaltered and there is only minor alteration of the groundmass. No secondary minerals were detected by XRD (Figure 2.2a). Manganese-oxides (pyrolusite) fill interstitial voids in the groundmass and display fine compositional banding (Figure 2.3a). Orange-yellow, transparent and birefringent fibro-palagonite [*Zhou and Fyfe*, 1989] lines the walls of originally glassy vesicles (Figure 2.3b) and is likely composed of poorly crystalline smectite [*Zhou et al.*, 1992]. Minor iron-oxides (goethite) and clays (smectite) were also identified in the groundmass.

2.4.1.2 Mauna Kea, Hawaii (SR0954-8.00)

Olivine phenocrysts are altered along rims and fractures to talc, characterized by brownish fibrous aggregates with subparallel alignment and high birefringence (third-order) (Figure 2.4a). Interstitial voids and vesicles are filled with material that occurs as fibrous bundles with lower aggregate birefringence (first-order) and is likely a variety of Mg-rich smectite. The broad peak between 5-10° 2θ that is visible in the original diffractogram

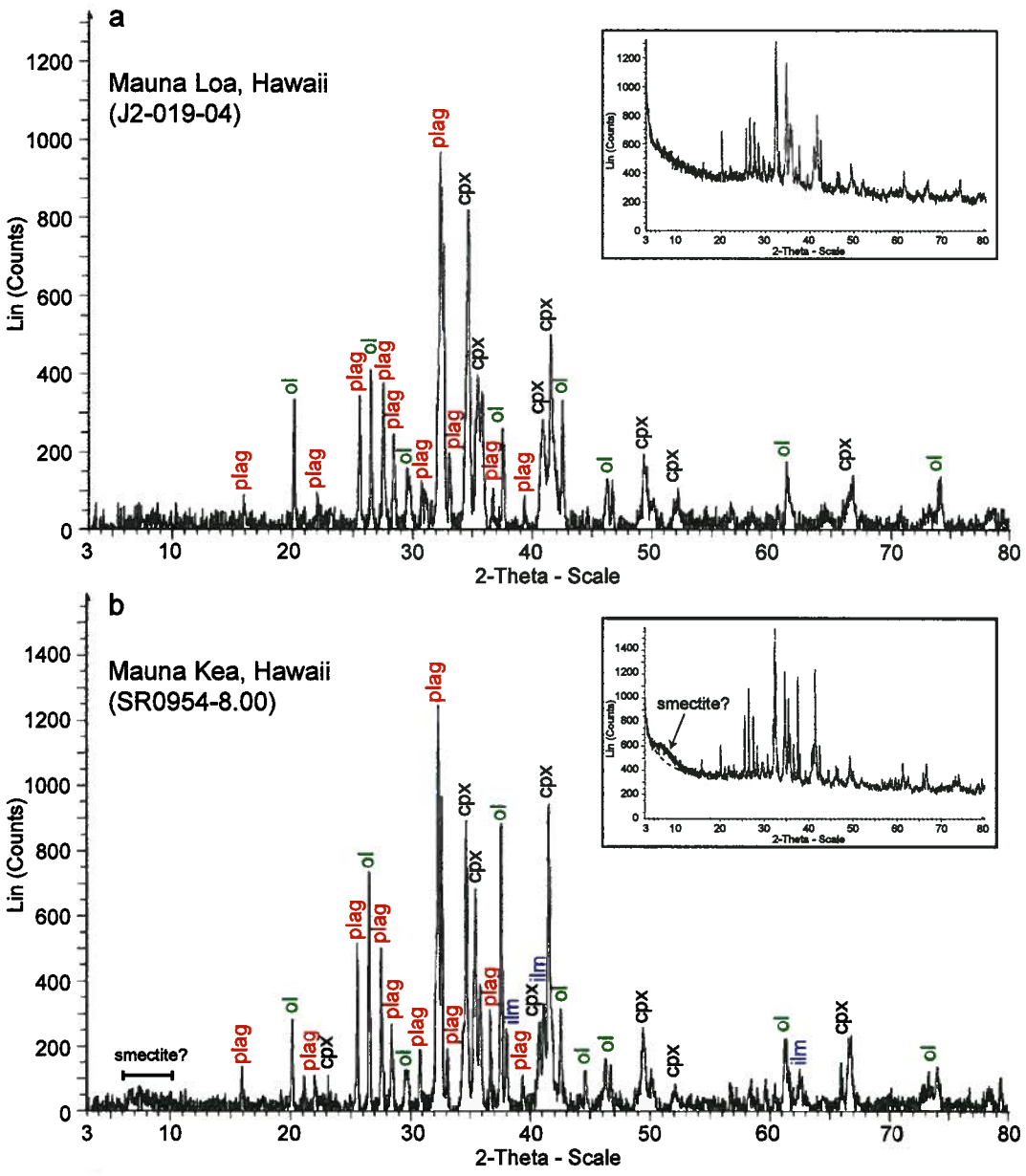
a
Mauna Loa, Hawaii
(J2-019-04)
Lin (Counts)
2-Theta - Scale
plag
ol
cpx
b
Mauna Kea, Hawaii
(SR0954-8.00)
smectite?
ilm

Figure 2.2

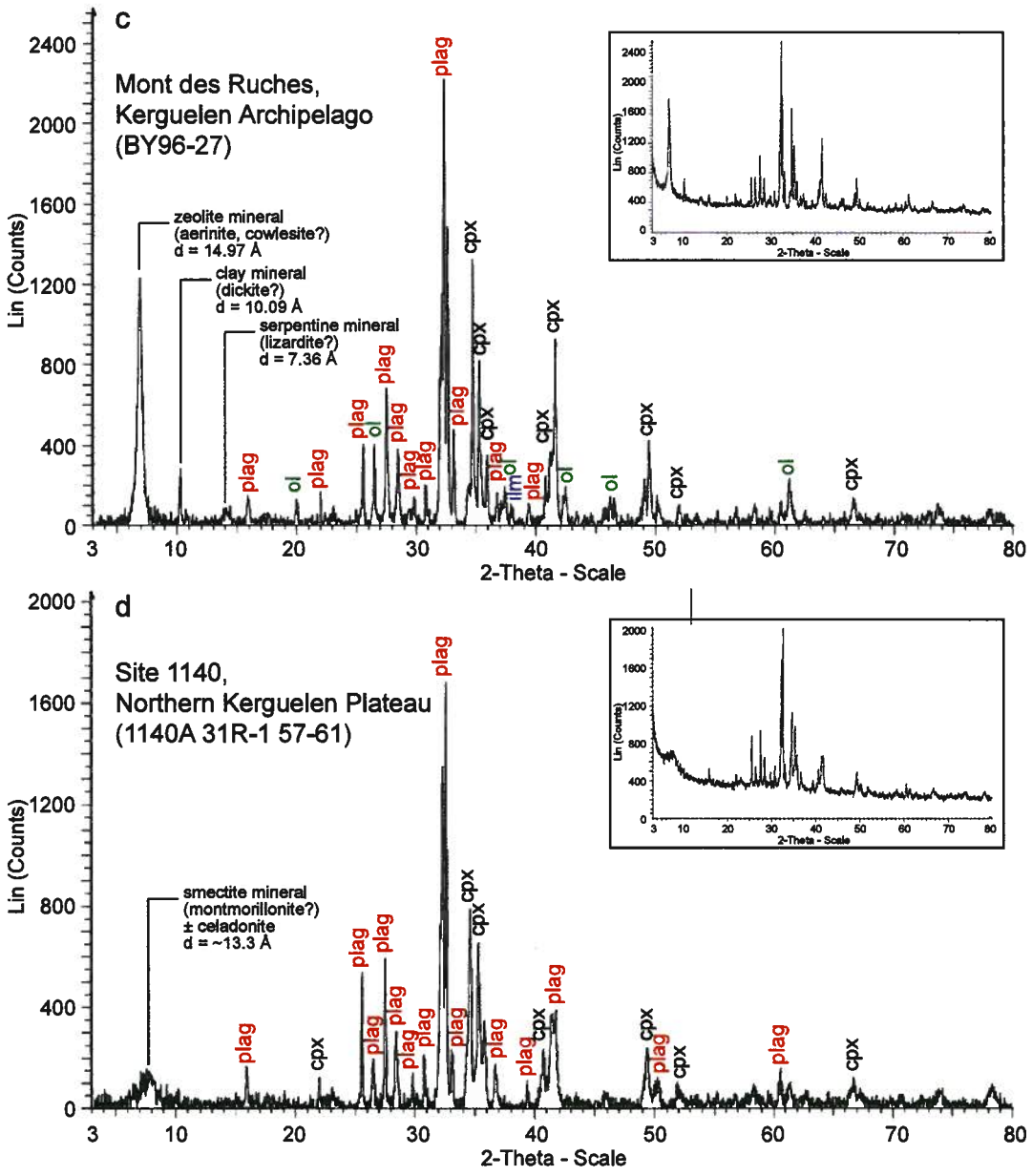

Figure 2.2 (continued)

Figure 2.2: Bulk powder X-ray diffraction patterns for unleached whole rock sample powders showing identified minerals. Inset diagrams: raw X-ray diffraction patterns prior to background subtraction. (**a**) Sample J2-019-04 (Mauna Loa, Hawaii) contains olivine, clinopyroxene, plagioclase, and no alteration minerals. (**b**) Sample SR0954-8.00 (Mauna Kea, Hawaii) contains olivine, clinopyroxene, plagioclase, and ilmenite. The broad hump between 5-10° 2θ likely reflects the presence of clay minerals such as smectite. (**c**) Sample BY96-27 (Mont des Ruches, Kerguelen Archipelago) contains olivine, clinopyroxene, plagioclase, and ilmenite. Additional peaks indicate the presence of zeolite, clay, and serpentine group minerals. (**d**) Sample 1140A 31R-1 57-51 (Site 1140, Northern Kerguelen Plateau) contains clinopyroxene and plagioclase, as well as smectite ± celadonite.

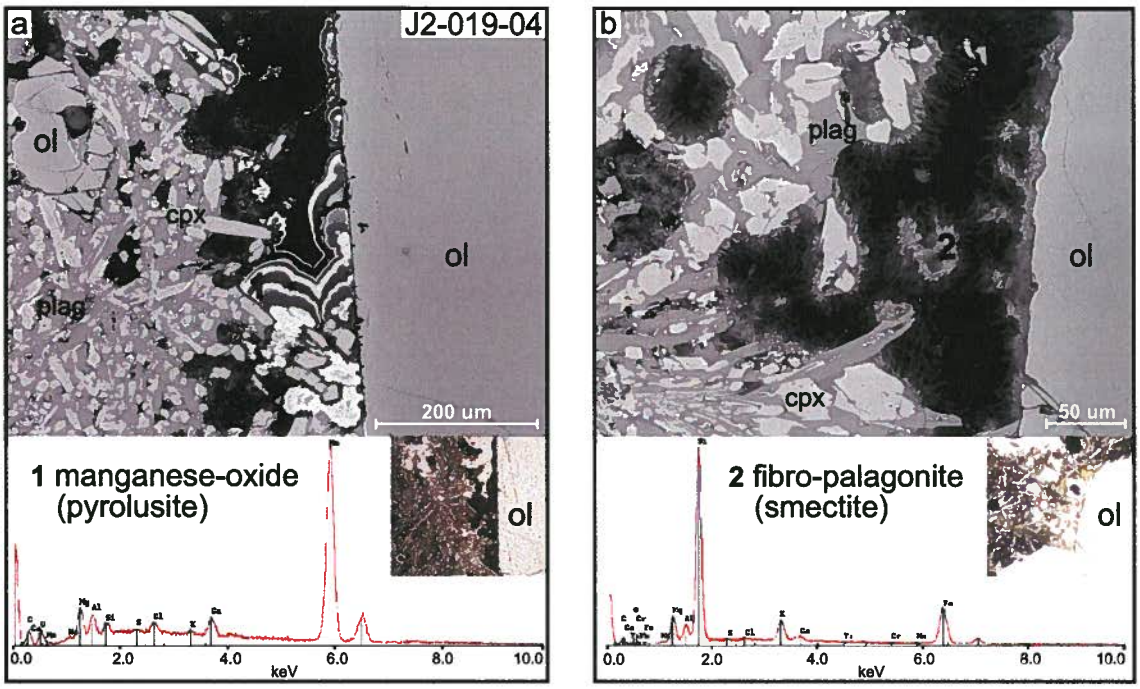

Figure 2.3: Backscattered electron images and qualitative energy-dispersive spectra from regions of basalt sample J2-019-04 (Mauna Loa, Hawaii). Inset photomicrographs in plane-polarized light show the general area (i.e. similar scale) of above BSE images; this applies to all subsequent figures (Figs. 3-5). Abbreviations: ol = olivine; plag = plagioclase; cpx = clinopyroxene. The numbers (**1-2**) indicate the locations of EDS analyses. (**a**) Finely banded manganese-oxide (pyrolusite) in groundmass adjacent to olivine phenocryst. The lighter layers contain a greater proportion of Mn, Mg, and Al. (**b**) Fibro-palagonite (smectite) replacing vesicle-lining glass adjacent to olivine phenocryst.

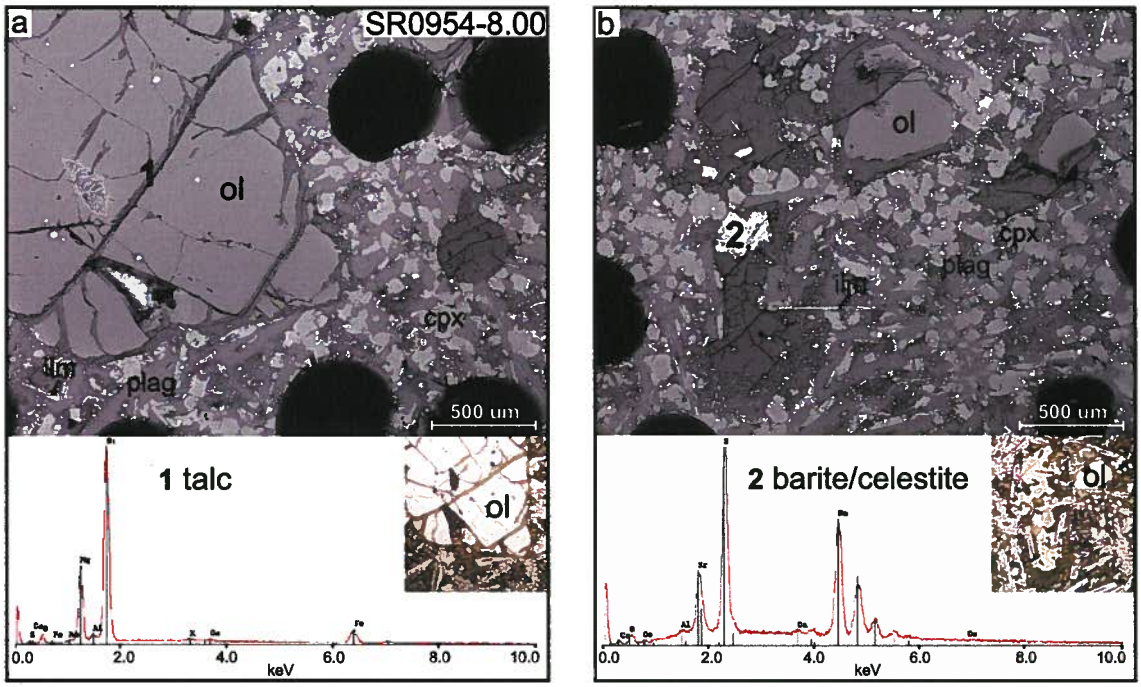

Figure 2.4: Backscattered electron images and qualitative energy-dispersive spectra from regions of basalt sample SR0954-8.00 (Mauna Kea, Hawaii). Black spots are marker points for microprobe traverses. Inset photomicrographs in plane-polarized light. Abbreviations as in Fig. 2; ilm = ilmenite. The numbers (**1-2**) indicate the locations of EDS analyses. (**a**) Talc alteration along fracture within olivine phenocryst. (**b**) Irregularly shaped patches of barite/celestite (bright white regions) within interstitial smectite.

without background subtraction (Figure 2.2b - inset) indicates the presence of poorly-ordered clay minerals such as smectite. Patches of barite/celestite (Figure 2.4b) and minor secondary pyrite occur within the smectite alteration.

2.4.1.3 Mont des Ruches, Kerguelen Archipelago (BY96-27)

Olivine phenocrysts are distinctly altered to red-brown "iddingsite," composed primarily of iron-oxides, smectite and serpentine (Figure 2.5a). Colorless radiating bundles or "flakes" with low birefringence (first-order) are commonly observed and likely composed of zeolite finely intergrown with phyllosilicates (Figure 2.5a). The large well-defined XRD peak with a d-spacing of ~15 Å (Figure 2.2c) confirms the presence of a zeolite mineral, possibly aerinite or cowlesite. Additional XRD peaks occur at d-spacings of ~10.1 Å and ~7.4 Å and reflect the presence of clay and serpentine group minerals such as dickite and lizardite, respectively. The groundmass is characterized by widespread patchy brown alteration that is typically associated with vesicles and is likely altered and devitrified glass. A calcium silicate mineral (apophyllite) was also identified extending into this groundmass alteration along with zeolite (Figure 2.5b).

2.4.1.4 Site 1140, Northern Kerguelen Plateau (1140A 31R-1 57-61)

Plagioclase and clinopyroxene were the only primary minerals identified by XRD (Figure 2.2d). Olivine phenocrysts have been completely replaced by red-brown and yellow-green secondary minerals, including iron-oxides (goethite) and clay minerals (primarily smectite ± chlorite) (Figure 2.6a). Vesicles are typically filled with several smectite layers of varying composition (mostly in Fe, Mg, and Al) and thickness (pore-

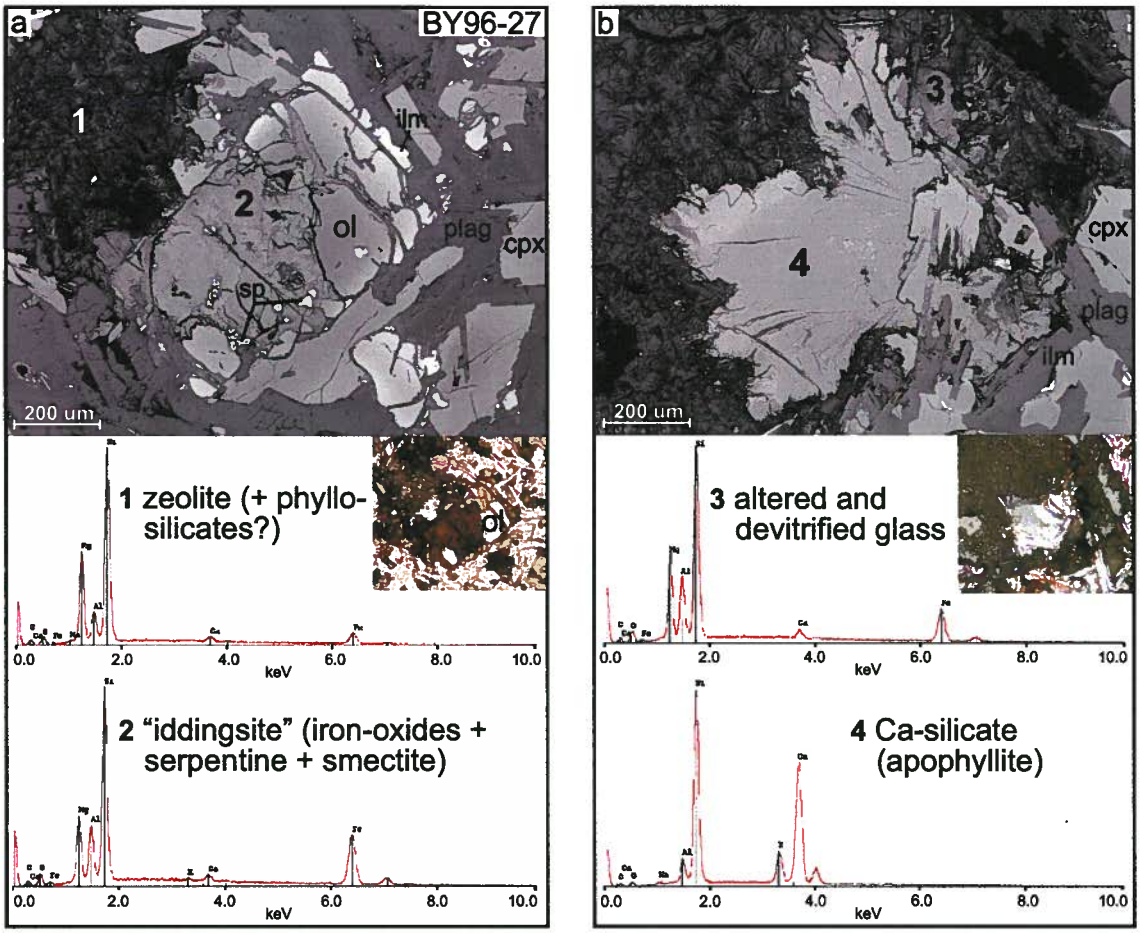

Figure 2.5: Backscattered electron images and qualitative energy-dispersive spectra from regions of basalt sample BY96-27 (Mont des Ruches, Kerguelen Archipelago). Abbreviations as in Fig. 2; ilm = ilmenite; sp = spinel. The numbers (**1-4**) indicate the locations of EDS analyses. (**a**) "Iddingsite" alteration of olivine phenocryst: iron-oxides + serpentine + smectite. Flakes of zeolite (finely intergrown with phyllosilicates?) at upper left. Inset photomicrograph in plane-polarized light. (**b**) Ca-silicate mineral (apophyllite) surrounded by zeolite as well as altered and devitrified glass. Inset photomicrograph in crossed-polars.

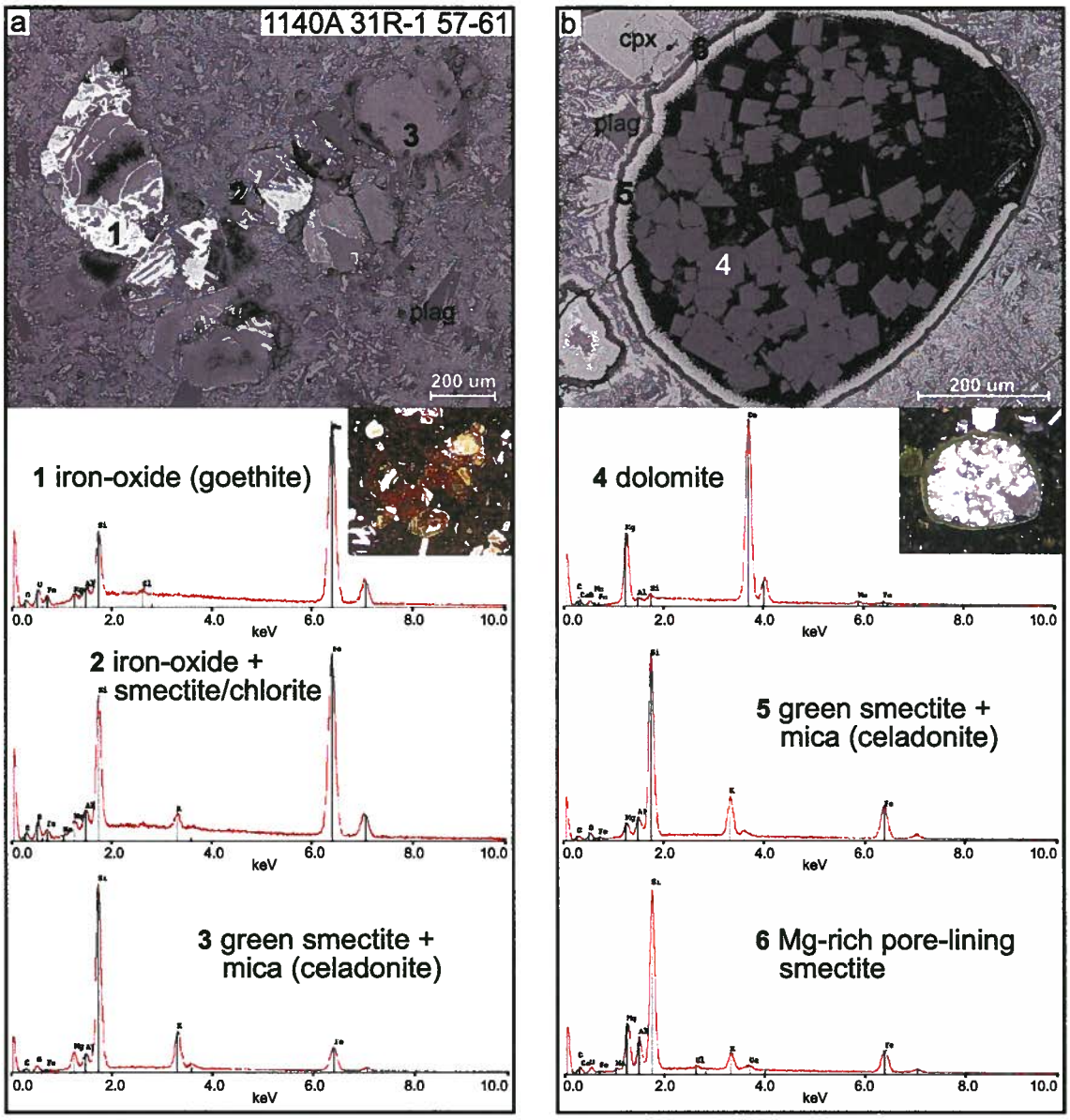
a
1140A 31R-1 57-61
1
2
3
plag
200 um
1 iron-oxide (goethite)
2 iron-oxide + smectite/chlorite
3 green smectite + mica (celadonite)
keV
b
cpx
plag
3
4
5
200 um
4 dolomite
5 green smectite + mica (celadonite)
6 Mg-rich pore-lining smectite
0.0
2.0
4.0
6.0
8.0
10.0

Figure 2.6

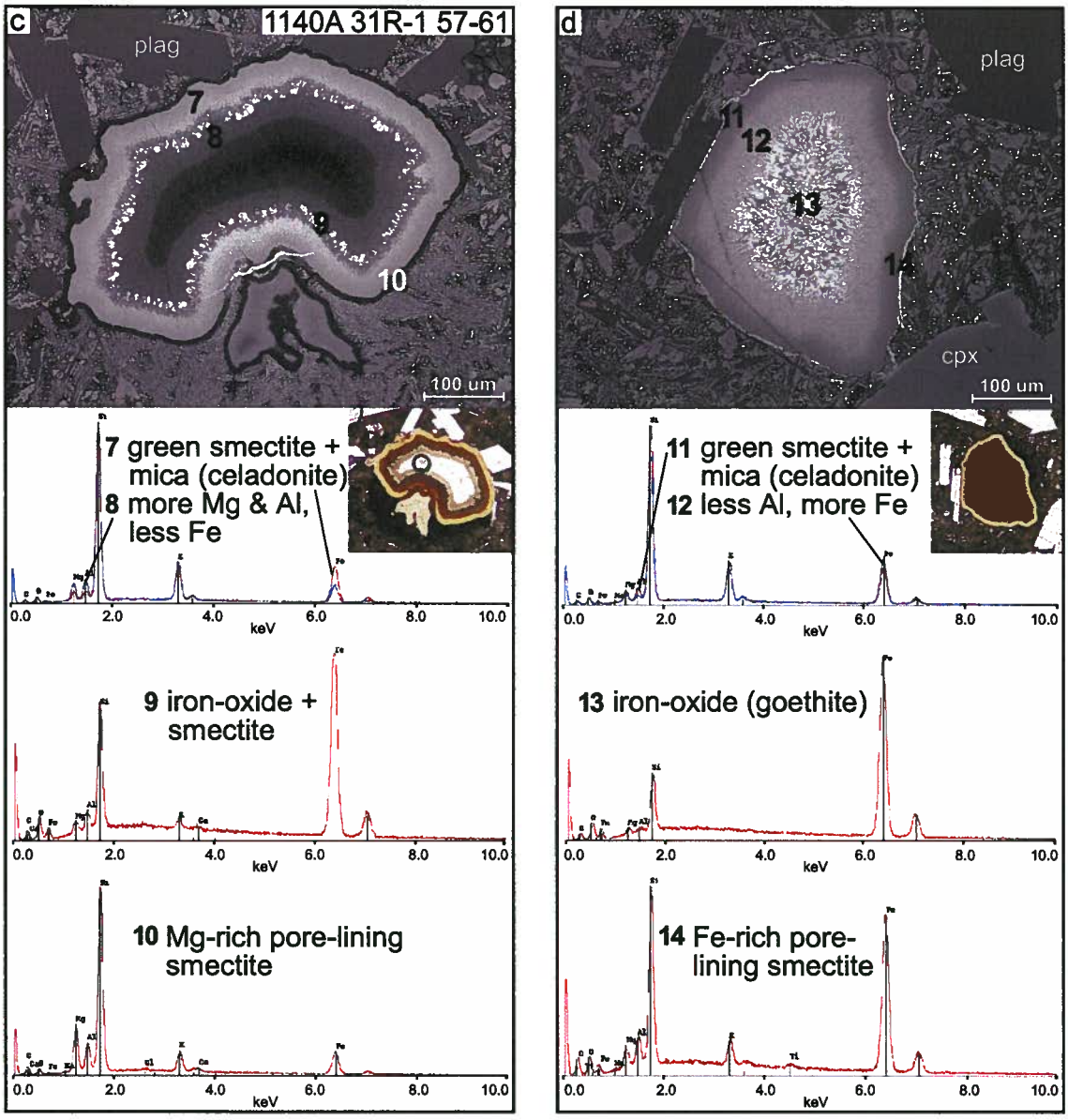

Figure 2.6 (continued)

Figure 2.6: Backscattered electron images and qualitative energy-dispersive spectra from regions of basalt sample 1140A 31R-1 57-61 (Site 1140, Northern Kerguelen Plateau). Abbreviations as in Fig. 2. The numbers (**1-14**) indicate the locations of EDS analyses. (**a**) Complete "iddingsite" replacement of olivine phenocrysts: iron-oxide + chlorite + smectite. Inset photomicrograph in plane-polarized light. (**b**) Vesicle lined with smectite of varying composition and filled with euhedral crystals of dolomite that show zoning due to variable Fe content. Inset photomicrograph in crossed-polars. (**c**) Vesicle filled with smectite and mica (celadonite) layers of varying composition as well as patches of iron-rich material. Inset photomicrograph in plane-polarized light. (**d**) Vesicle lined with smectite and mica (celadonite) layers of varying composition and filled with an iron-rich center dominantly composed of goethite. Inset photomicrograph in plane-polarized light.

lining layers are ~5 μm thick and pore-filling layers are ~50 μm thick) (Figure 2.6b-d). The red-brown variety represents a mixture of iron-oxides and smectite. The presence of appreciable amounts of K, as well as the higher birefringence of the yellow-green variety, suggests that it may contain a mica, which is tentatively identified as celadonite. The broad XRD peak approximately centered at d = ~13.3 Å (Figure 2.2d) reflects the presence of smectite and celadonite that is intergrown/layered, which is common in fine-grained phyllosilicates formed at low grades [*Peacor*, 1992] and expected with members of the celadonite family [*Li et al.*, 1997]. Vesicles also contain dolomite, showing perfect rhombohedral cleavage and compositional zoning (Figure 2.6b), as well as minor disseminated grains of secondary chalcopyrite. Palagonite (partially altered to smectite) lines unfilled glassy vesicles.

2.4.2 Removal of alteration phases by acid-leaching

Comparison of the X-ray diffractograms of unleached and leached whole rock powders for the two Kerguelen basalts allows for identification of the minerals removed by the *Weis et al.* [2005] acid-leaching procedure. For the subaerial Kerguelen basalt from Mont des Ruches (BY96-27), leaching removed the zeolite, clay, and serpentine alteration (Figure 2.7a). An unexpected consequence of the leaching experiment was the disappearance of olivine in the leached powder. The displacement of the leached XRD spectrum to lower intensity (Figure 2.7a – inset) reflects the decreased iron radiation due to removal of iron (in olivine) via leaching. For the submarine Kerguelen basalt from Site 1140 (1140A 31R-1 57-61), the leached and unleached powders show excellent agreement in terms of the primary minerals present (Figure 2.7b). The XRD pattern for the leached

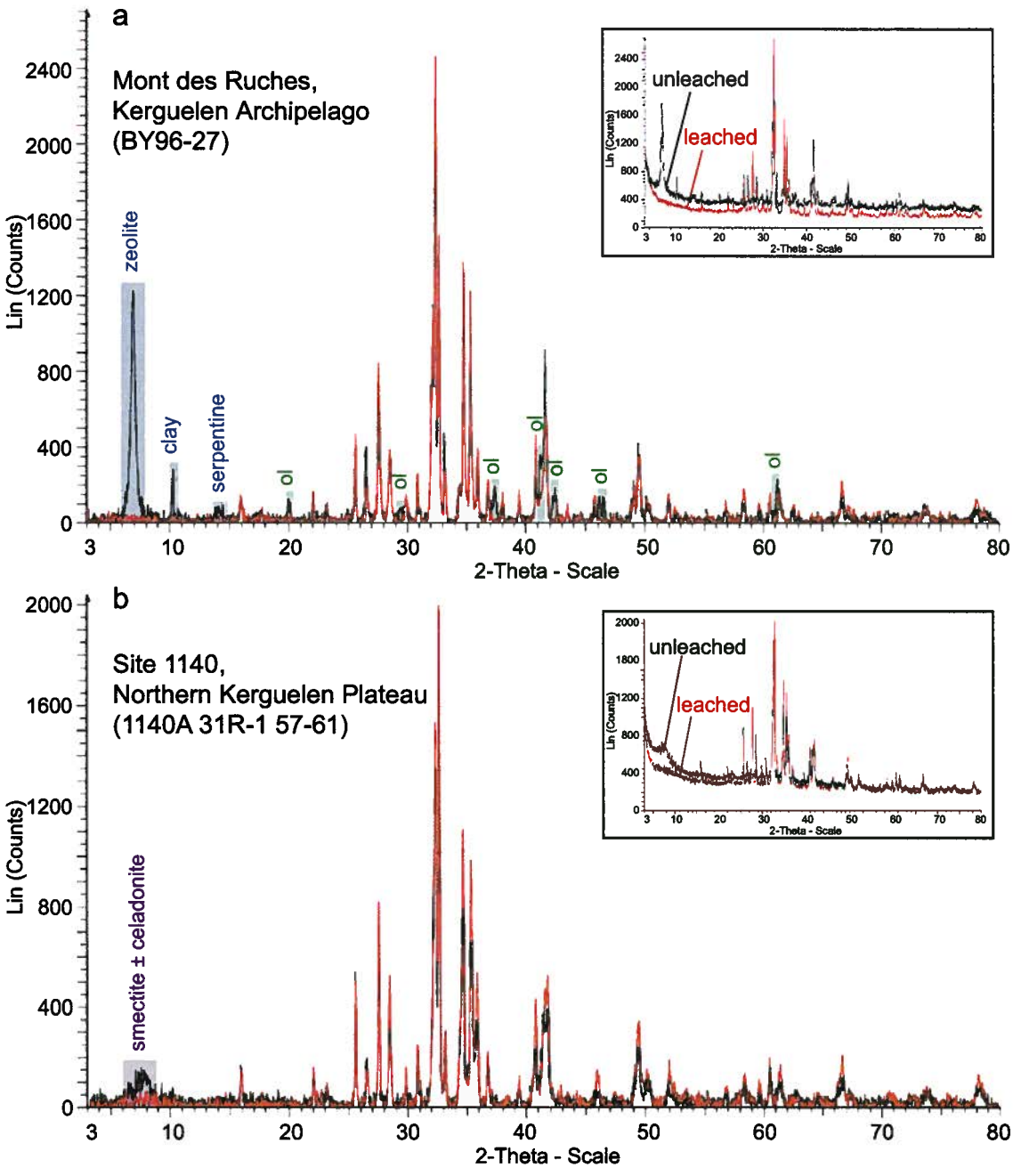
a
Mont des Ruches,
Kerguelen Archipelago
(BY96-27)
unleached
leached
zeolite
clay
serpentine
ol
Lin (Counts)
2-Theta - Scale
b
Site 1140,
Northern Kerguelen Plateau
(1140A 31R-1 57-61)
unleached
leached
smectite ± celadonite
Lin (Counts)
2-Theta - Scale

Figure 2.7

Figure 2.7: Bulk powder X-ray diffraction patterns comparing unleached (black lines) and leached (red lines) whole rock powders for the Kerguelen basalt samples. Inset diagrams: raw X-ray diffraction pattern prior to background subtraction. Minerals that were removed via leaching are highlighted with colored bars. (**a**) Sample BY96-27: leaching effectively removed the zeolites, clays, and serpentine alteration, as well as olivine. (**b**) Sample 1140A 31R-1 57-51: (incomplete?) removal of the smectite ± celadonite alteration.

powder does not show the broad peak caused by the presence of smectite ± celadonite, indicating that this alteration was largely removed through leaching. However, the noise in the leached X-ray diffractogram between 6-9° 2θ (Figure 2.7b) may indicate that not all of the alteration was removed. Microscopic examination of the leached residue revealed the presence of altered grains in varying shades of green, which is characteristic of celadonite.

2.5 DISCUSSION

2.5.1 Alteration phases in oceanic basalts and the effectiveness of acid-leaching

The four Hawaiian and Kerguelen basalts contain a wide variety of secondary minerals (Table 2.2), most commonly clay mineral mixtures (primarily smectite) and iron-oxides. These are typical alteration products of basaltic glass and magnesium silicate minerals resulting from interaction with seawater [e.g., *Böhlke et al.*, 1980; *Giorgetti et al.*, 2001]. The subaerial Kerguelen basalt from Mont des Ruches (BY96-27) also contains zeolite, which is characteristic of hydrothermally altered flood basalts from the Kerguelen Archipelago [e.g., *Natível and Nougier*, 1983; *Natível et al.*, 1994]. The complete removal of the zeolite, clay, and serpentine alteration from this sample (Figure 2.7a) demonstrates the effectiveness of the *Weis et al.* [2005] leaching procedure. The additional removal of olivine was unintended because the leaching procedure is not designed to remove primary minerals. However, the olivine phenocrysts in this basalt were moderately altered, which suggests that the leaching process cannot selectively remove just the alteration from olivine. Despite aggressive leaching (15 steps), the presence of some smectite ± celadonite alteration in the leached residue of the submarine Kerguelen basalt from Site 1140 (1140A 31R-1 57-61) suggests that the *Weis et al.* [2005] leaching procedure may not be effective at

Table 2.2: Summary of alteration phases identified in studied Hawaiian and Kerguelen basalts

	Hawaii		Kerguelen	
Sample	J2-019-04	SR0954-8.00	BY96-27	1140A 31R-1 57-61
Major (>0.5 wt%) alteration phases	none	talc smectite	zeolite smectite serpentine goethite	smectite celadonite chlorite goethite
Minor (<<0.5 wt%) alteration phases	pyrolusite smectite goethite	barite/celestite pyrite	apophyllite	dolomite chalcopyrite

completely removing this type of alteration. This could be due to the abundance or distribution of the alteration phases within this basalt, or because some secondary minerals are not readily soluble in HCl. The incomplete removal of alteration phases, which may have a distinct Pb isotopic signature, has important implications for Pb isotope studies of oceanic basalts.

2.5.2 Effect of alteration phases on Pb isotopes

The external reproducibility of the Pb isotopic compositions of the four Hawaiian and Kerguelen basalts correlates with their degree of alteration (based on extent of phenocryst and matrix alteration, LOI, number of required leaching steps and associated weight loss due to leaching) (Table 2.1). External reproducibility is calculated as the 2 standard deviation on the mean of multiple Pb isotope analyses of separately processed powder aliquots of the same sample. After leaching, the least altered basalt (J2-019-04) has the best $^{206}Pb/^{204}Pb$ reproducibility (2SD/mean x 10^6 = 170 ppm), whereas the most altered basalt (1140A 31R-1 57-61) has the poorest reproducibility (359 ppm) (Table 2.3). The relatively poor reproducibility of the most altered basalt is likely related to the incomplete removal of the smectite ± celadonite alteration from this sample by leaching.

In general, unleached powders have better Pb isotope reproducibility than the leached powders, by a factor of more than two (Table 2.3). This indicates that the alteration phases may be homogeneously distributed throughout the unleached sample powders, but that leaching does not remove these minerals in an entirely reproducible way [*Eisele et al.*, 2003; *Fekiacova et al.*, 2007]. The poorer reproducibility of the leached powders may reflect variable extents of dissolution (between separate powder aliquots) of secondary

Table 2.3: Pb isotopic compositions of studied Hawaiian and Kerguelen basalts[a]

Sample	$^{206}Pb/^{204}Pb$	2σ	$^{207}Pb/^{204}Pb$	2σ	$^{208}Pb/^{204}Pb$	2σ
		Hawaii				
J2-019-04 unL	18.4951	12	15.5703	14	38.4676	42
J2-019-04 L1	18.1796	8	15.4583	8	37.9751	22
J2-019-04 L2	18.1774	7	15.4558	6	37.9677	18
J2-019-04 L mean	18.1785	31 (170)	15.4570	35 (227)	37.9714	106 (278)
SR0954-8.00 unL1	18.6336	14	15.4921	12	38.1946	34
SR0954-8.00 unL2	18.6346	12	15.4921	11	38.1943	33
SR0954-8.00 unL3	18.6323	10	15.4908	11	38.1898	34
SR0954-8.00 unL mean	18.6335	23 (122)	15.4916	15 (98)	38.1929	54 (142)
SR0954-8.00 L1	18.5986	12	15.4811	16	38.1574	43
SR0954-8.00 L2	18.6031	13	15.4832	14	38.1641	50
SR0954-8.00 L3	18.6020	14	15.4804	13	38.1561	41
SR0954-8.00 L mean	18.6012	47 (254)	15.4816	29 (186)	38.1592	86 (225)
		Kerguelen				
BY96-27 unL1	18.2551	6	15.5272	5	38.8273	14
BY96-27 unL2	18.2543	11	15.5273	10	38.8260	29
BY96-27 unL3	18.2534	11	15.5258	11	38.8210	35
BY96-27 unL mean	18.2542	17 (95)	15.5268	17 (110)	38.8248	67 (171)
BY96-27 L1	18.2539	14	15.5201	16	38.7853	55
BY96-27 L2	18.2542	10	15.5211	10	38.7885	31
BY96-27 L3	18.2495	6	15.5167	6	38.7737	21
BY96-27 L mean	18.2525	53 (288)	15.5193	47 (301)	38.7825	156 (402)
1140A 3IR-1 57-61 unL	18.5451	8	15.5619	9	38.9056	29
1140A 3IR-1 57-61 L1	18.5583	12	15.5637	10	38.9384	27
1140A 3IR-1 57-61 L2	18.5519	15	15.5570	15	38.9214	46
1140A 3IR-1 57-61 L3	18.5567	9	15.5631	8	38.9349	23
1140A 3IR-1 57-61 L mean	18.5556	67 (359)	15.5613	74 (475)	38.9316	180 (461)

[a]All Pb isotope data are from *Nobre Silva et al.* (in revision, 2008). Pb isotope ratios were determined by MC-ICP-MS and have been normalized to the NBS981 triple spike values of *Galer and Abouchami* [1998]. Multiple analyses correspond to separate aliquots of unleached (unL) and leached (L) powders. The 2σ error is the absolute error value of an individual sample analysis (internal error) and applies to the last decimal place(s). For the mean values, the error reported is the 2 standard deviation (external error). Numbers in brackets represent the external reproducibility (2SD/mean x 10^6) reported in ppm.

minerals that are not readily soluble in HCl or have differing grain sizes. Alternatively, the poorer reproducibility could reflect discrepancies in the leaching procedure; in particular, the point at which leaching is discontinued (i.e., after how many steps) is based on when a "clear" solution is obtained and is thus inherently subjective. However, such inconsistencies can be greatly reduced if leaching is carried out by the same analyst.

The Pb isotope differences between unleached and leached powders (Figure 2.8) are consistent with the presence of distinct secondary mineral assemblages (e.g., celadonite, Mn-oxides, barite, zeolite). The observed alteration assemblages are unique to each basalt and reflect differences in their eruption environment, age, and sampling method (Table 2.1). The two Kerguelen basalts from Mont des Ruches and Site 1140 exhibit opposite Pb isotope relationships between unleached and leached powders (Figure 2.8), indicating discrete sources of contamination that are likely related to their eruption in subaerial and submarine environments, respectively. Although the Pb isotope differences between unleached and leached powders of these Kerguelen basalts are relatively small, they are resolvable outside of the analytical error (Table 2.3). Despite the significantly younger ages (ka vs. Ma) and lower degrees of alteration of the two Hawaiian basalts, the unleached powders are considerably more radiogenic than the leached powders and indicate contamination by highly radiogenic components (Figure 2.8). For the Mauna Loa basalt, the presence of manganese-oxides (Figure 2.3a) suggests that the source of contamination is likely to be seawater (approximated by Pacific Fe-Mn deposits). Fe-Mn deposits form through precipitation out of seawater and occur widely on the ocean floor, and are thus an important consideration for submarine Hawaiian basalts. For the Mauna Kea basalt, the presence of barite/celestite (Figure 2.4b) indicates that drilling mud is the probable contaminant. Barite

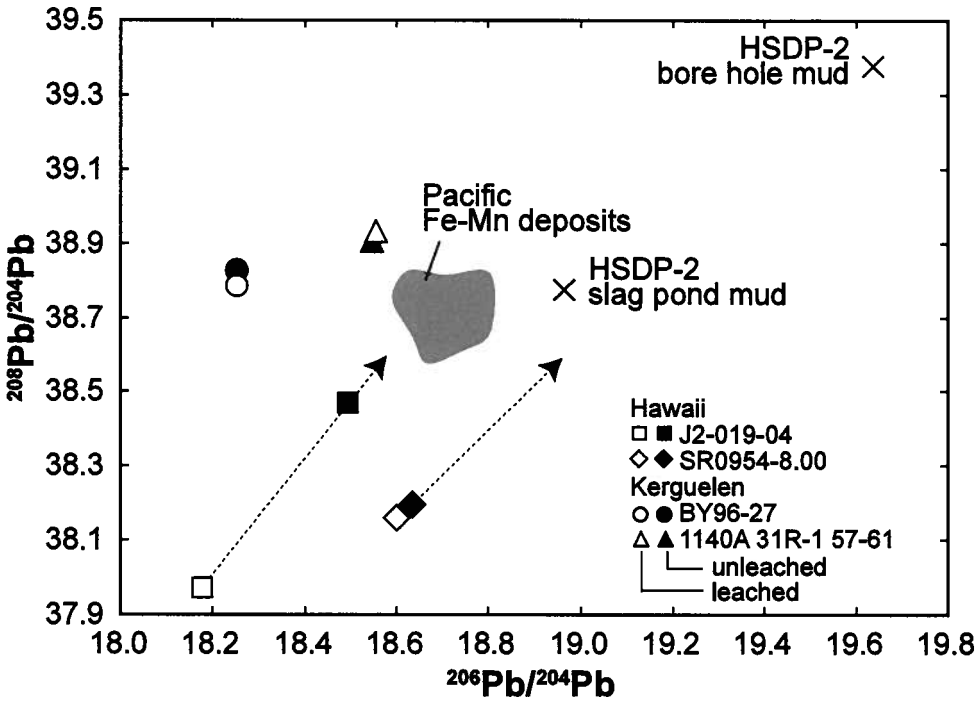

Figure 2.8: Comparison of Pb isotope results from unleached and leached whole rock powders of Hawaiian and Kerguelen basalts examined in this study with potential sources of contamination indicated. Pb isotopic compositions determined by MC-ICP-MS from *Nobre Silva et al.* (in revision, 2008). Unleached compositions are shown with black-filled symbols, leached with white-filled symbols. The ± 2 SD error bars on the mean of multiple analyses are smaller than the symbol sizes. Dashed lines connect the unleached and leached compositions of the same sample and point towards a probable contaminant. Pb isotopic compositions of Pacific Fe-Mn deposits from *Abouchami and Galer* [1998] (field from *Fekiacova et al.* [2007]); HSDP-2 mud compositions from *Eisele et al.* [2003].

is commonly used to add weight to drilling mud, which is a significant source of contamination for samples recovered in the Hawaii Scientific Drilling Project [*Abouchami et al.*, 2000; *Eisele et al.*, 2003]. The least altered basalt (J2-019-04) exhibits the largest difference between leached and unleached Pb isotopic compositions (Figure 2.8), demonstrating that acid-leaching prior to Pb isotopic analysis may be necessary even for basalts that appear to be relatively unaltered.

This study demonstrates the importance of complete removal of alteration phases by acid-leaching for high-precision Pb isotope studies of ocean island basalts. The variable results of the leaching experiment indicate that one leaching procedure may not be effective for all ocean island basalts and that leaching procedures may have to be modified depending of the style of alteration encountered. Therefore, studies analyzing the Pb isotopic compositions of ocean island basalts would benefit from a cursory investigation of the degree and type of alteration of the basalts and evaluation of the effectiveness of the particular leaching procedure. A selection of basalts from each sample suite should be examined both macroscopically and by petrographic methods. Samples that contain celadonitic clay mixtures should be treated with caution, and possibly subjected to a stronger leaching procedure. The leached residues of more altered basalts should also be examined microscopically. Furthermore, we recommend that at least two complete procedural duplicates (separate powder aliquots) be analyzed as part of standard quality control protocols to evaluate the external reproducibility of the Pb isotope ratios. Recent improvements in analytical techniques developed for MC-ICP-MS and TIMS, using either thallium or a double/triple spike to correct for instrumental mass bias, have allowed for increased precision (external reproducibility <100 ppm) of Pb isotope analyses. In

agreement with previous authors [e.g., *Thirlwall et al.*, 2000; *Eisele et al.*, 2003; *Baker et al.*, 2004, 2005; *Albarède et al.*, 2005; *Weis et al.*, 2005], the incomplete removal of alteration phases and contaminants by acid-leaching represents one of the main sources of uncertainty of Pb isotope measurements and may be the ultimate limitation on high-precision Pb isotopic compositions of ocean island basalts.

2.6 ACKNOWLEDGEMENTS

The author would like to thank Inês Garcia Nobre Silva for providing leaching statistics and Pb isotopic data, as well as Mike Garcia and Njoki Gitahi for sending the Hawaiian samples. Sasha Wilson and Mati Raudsepp are thanked for SEM and XRD sample preparation and instrument training. Andrew Greene, Robert Frei, an anonymous reviewer, and *American Mineralogist* associate editor Peter Dahl are thanked for their constructive reviews. D. Hanano was supported by an NSERC Canada Graduate Scholarship (CGS-M). Funding for this research was provided by NSERC Discovery Grants to J. S. Scoates and D. Weis.

2.7 REFERENCES

Abouchami, W., and S.J.G. Galer (1998), The provinciality of Pb isotopes in Pacific Fe-Mn deposits, *Mineralogical Magazine*, *62*A, 1–2.

Abouchami, W., S.J.G. Galer, and A.W. Hofmann (2000), High precision lead isotope systematics of lavas from the Hawaiian Scientific Drilling Project, *Chemical Geology*, *169*, 187–209.

Abouchami, W., A.W. Hofmann, S.J.G. Galer, F.A. Frey, J. Eisele, and M. Feigenson (2005), Lead isotopes reveal bilateral asymmetry and vertical continuity in the Hawaiian mantle plume, *Nature*, *434*, 851-856.

Albarède, F., A. Stracke, V.J.M. Salters, D. Weis, J. Blichert-Toft, P. Telouk, and A. Agranier (2005), Comment to "Pb isotopic analysis of standards and samples using a ^{207}Pb-^{204}Pb double spike and thallium to correct for mass bias with a double-focusing MC-ICP-MS" by Baker et al., *Chemical Geology*, *217*, 171–174.

Alt, J.C., and J. Honnorez (1984), Alteration of the upper oceanic crust, DSDP site 417: mineralogy and chemistry, *Contributions to Mineralogy and Petrology*, *87*, 149–169.

Baker, J., D. Peate, T. Waight, and C. Meyzen (2004), Pb isotopic analysis of standards and samples using a ^{207}Pb-^{204}Pb double spike and thallium to correct for mass bias with a double-focusing MC-ICP-MS, *Chemical Geology*, *211*, 275–303.

Baker, J.A., D.W. Peate, T.E. Waight, and M.F. Thirwall (2005), Reply to the Comment on "Pb isotopic analysis of standards and samples using a ^{207}Pb-^{204}Pb double spike and thallium to correct for mass bias with a double-focusing MC-ICP-MS" by Baker et al., *Chemical Geology*, *217*, 175–179.

Banerjee, N.R., J. Honnorez, and K. Muehlenbachs (2004), Low-temperature alteration of submarine basalts from the Ontong Java Plateau, in *Origin and Evolution of the Ontong Java Plateau*, edited by J.G. Fitton, J.J. Mahoney, P.J. Wallace, and A.D. Saunders, pp. 259–273, Geological Society, Special Publications, London.

Böhlke, J.K., J. Honnorez, and B.-M. Honnorez-Guerstein (1980), Alteration of Basalts From Site 396B, DSDP: Petrographic and Mineralogic Studies, *Contributions to Mineralogy and Petrology*, *73*, 341–364.

Dana, J.D. (1849), Geology, in *United States Exploring Expedition, 1838-1842*, vol. 10, 756 pp., C. Sherman, Philadelphia.

DePaolo, D.J., and E.M. Stolper (1996), Models of Hawaiian volcano growth and plume structure: Implications of results from the Hawaii Scientific Drilling Project, *Journal of Geophysical Research*, *101*(B5), 11643–11654.

Doucet, S., D. Weis, J.S. Scoates, K. Nicolayson, F.A. Frey, and A. Giret (2002), The depleted mantle component in Kerguelen Archipelago basalts: petrogenesis of tholeiitic-transitional basalts from the Loranchet Peninsula, *Journal of Petrology*, *43*, 1341–1366.

Duncan, R.A. (2002), A time frame for construction of the Kerguelen Plateau and Broken Ridge, *Journal of Petrology*, *43*, 1109–1119.

Eisele, J., W. Abouchami, S.J.G. Galer, and A.W. Hofmann (2003), The 320 kyr Pb isotope evolution of Mauna Kea lavas recorded in the HSDP-2 drill core, *Geochemistry Geophysics Geosystems*, *4*, doi:10.1029/2002GC000339.

Fekiacova, Z., W. Abouchami, S.J.G. Galer, M.O. Garcia, and A.W. Hofmann (2007), Origin and temporal evolution of Koolau volcano, Hawaii: Inferences from

isotope data on the Koolau Scientific Drilling Project (KSDP), the Honolulu Volcanics and ODP Site 843, *Earth and Planetary Science Letters, 261*, 65–83.

Garcia, M.O., E.H. Haskins, E.M. Stolper, and M. Baker (2007), Stratigraphy of the Hawaii Scientific Drilling Project core (HSDP2): Anatomy of a Hawaiian shield volcano, *Geochemistry Geophysics Geosystems, 8*, doi:10.1029/2006GC001379.

Giorgetti, G., P. Marescotti, R. Cabella, and G. Lucchetti (2001), Clay mineral mixtures as alteration products in pillow basalts from the eastern flank of Juan de Fuca Ridge: a TEM-AEM study, *Clay Minerals, 36*, 75-91.

Jackson, E.D., E.A. Silver, and G.B. Dalrymple (1972), Hawaiian-Emperor chain and its relation to Cenozoic circum-Pacific tectonics, *Geological Society of America Bulletin, 83*, 601–618.

Kurnosov, V., B. Zolotarev, A. Artamonov, S. Garanina, V. Petrova, V. Eroshchev-Shak, and A. Sokolova (2003), Data Report: Alteration of Basalts from the Kerguelen Plateau, in *Proceedings of the Ocean Drilling Program, Scientific Results,* vol. 183, edited by F.A. Frey, M.F. Coffin, P.J. Wallace, and P.G. Quilty, pp. 1–40, Ocean Drilling Program, College Station, Texas.

Lassiter, J.C., D.J. DePaolo, and M. Tatsumoto (1996), Isotopic evolution of Mauna Kea volcano: Results from the initial phase of the Hawaii Scientific Drilling Project, *Journal of Geophysical Research, 101*(B5), 11769–11780.

Li, G., D.R. Peacor, D.S. Coombs, and Y. Kawachi (1997), Solid solution in the celadonite family: The new minerals ferroceladonite, $K_2Fe^{2+}{}_2Fe^{3+}{}_2Si_8O_{20}(OH)_4$, and ferroaluminoceladonite, $K_2Fe^{2+}{}_2Al_2Si_8O_{20}(OH)_4$, *American Mineralogist, 82*, 503–511.

McDonough, W.F., and C. Chauvel (1991), Sample contamination explains the Pb isotopic composition of some Rurutu island and Sasha seamount basalts, *Earth and Planetary Science Letters, 105*, 397–404.

Nativel, P., and J. Nougier (1983), Les faciès zéolitiques des basalts des plateaux des îles Kerguelen (T.A.A.F.); implications volcanologiques, *Bulletin de la Societé Géologique de France, 6*, 957-961.

Nativel, P., O. Verdier, and A. Giret (1994), Nature et diversité des zéolites de Kerguelen, *Mémoires de la Societé Géologique de France, 166*, 31-45.

Nobre Silva, I. G., D. Weis, J. Barling, and J.S. Scoates (2008), Leaching systematics for the determination of high-precision Pb isotope compositions of ocean island basalts, *Geochemistry Geophysics Geosystems*, paper # 2007GC001891 (in revision).

Nougier, J., R. Ballestracci, and B. Blavoux (1982), Les manifestations post-volcaniques dans les îles Australes françaises (TAAF); zones fumerolliennes et sources thermo-minérales, *Comptes Rendus de l'Academie des Sciences, Paris, 295*, 389–392.

Peacor, D.R. (1992), Diagenesis and low-grade metamorphism of shales and slates, *Reviews in Mineralogy and Geochemistry, 27*, 335-380.

Rhodes, J.M., and M.J. Vollinger (2004), Composition of basaltic lavas sampled by phase-2 of the Hawaii Scientific Drilling Project: Geochemical stratigraphy and magma types, *Geochemistry Geophysics Geosystems, 5*, doi:10.1029/2002GC000434.

Tatsumoto, M. (1978), Isotopic composition of lead in oceanic basalt and implication to mantle evolution, *Earth and Planetary Science Letters, 38*, 63–87.

Thirlwall, M.F. (2000), Inter-laboratory and other errors in Pb isotope analyses investigated using a ^{207}Pb–^{204}Pb double spike, *Chemical Geology*, *163*, 299–322.

Verdier, O., Champs géothermiques et zéolitisation des îles Kerguelen: Implications géologiques (Terres Australes et Antarctiques Françaises, Océan Indien Austral), thèse Doctorat, 271 pp., Université Paris, France, 1989.

Verdier, O., and P. Nativel (1988), Les activités géothermiques des îles Kerguelen (TAAF). Les champs fumerolliens actuels et la zéolitisation, in *Les Îles Océaniques et le Volcanisme des Océans*, pp. 96–100, Colloque France-Danemark, Sp. Pub. Université Paris-Sud, Orsay.

Walton, A.W., and P. Schiffman (2003), Alteration of hyaloclastites in the HSDP 2 Phase 1 Drill Core 1. Description and paragenesis, *Geochemistry Geophysics Geosystems*, *4*, doi:10.1029/2002GC000368.

Weis, D., and F.A. Frey (2002), Submarine basalts of the Northern Kerguelen Plateau: Interaction between the Kerguelen Plume and the Southeast Indian Ridge revealed at ODP site 1140, *Journal of Petrology*, *43*, 1287–1309.

Weis, D., B. Kieffer, C. Maerschalk, W. Pretorius, and J. Barling (2005), High-precision Pb-Sr-Nd-Hf isotopic characterization of USGS BHVO-1 and BHVO-2 reference materials, *Geochemistry Geophysics Geosystems*, *6*, doi:10.1029/2004GC000852.

White, W.M., F. Albarède, and P. Télouk (2000), High-precision analysis of Pb isotope ratios by multi-collector ICP-MS, *Chemical Geology*, *167*, 257–270.

Zhou, Z., and W.S. Fyfe (1989), Palagonitization of basaltic glass from DSDP Site 335, Leg 37: Textures, chemical composition, and mechanisms of formation, *American Mineralogist*, *74*, 1045–1053.

Zhou, Z., W.S. Fyfe, K. Tazaki, and S.J. Vandergaast (1992), The structural characteristics of palagonite from DSDP Site 335, *Canadian Mineralogist*, *30*, 75–81.

CHAPTER 3

TRACE ELEMENT AND ISOTOPE GEOCHEMISTRY OF POST-SHIELD LAVAS FROM MAUNA KEA, KOHALA, AND HUALALAI: EVIDENCE FOR ANCIENT DEPLETED COMPONENTS IN THE HAWAIIAN MANTLE PLUME

3.1 INTRODUCTION[1]

The ~6000 km long Hawaiian-Emperor Seamount Chain represents the surface expression of the Hawaiian mantle plume and is the classic example of intraplate volcanism. The Hawaiian plume is one of the longest-lived and hottest plumes with the largest buoyancy flux [*Sleep*, 1990] and is inferred to have a deep mantle origin [e.g., *Courtillot et al.*, 2003; *Montelli et al.*, 2006]. Volcanoes at the young end (<5 Ma) of the Hawaiian chain define two parallel geographic trends, termed Loa and Kea [*Dana*, 1849; *Jackson et al.*, 1972]. Individual Hawaiian volcanoes evolve through four different growth stages [*Clague and Dalrymple*, 1987]: (1) a small volume (~3%) alkalic pre-shield, (2) the main tholeiitic shield stage during which the majority (95-98%) of the volcano is built, (3) a small volume (~1%) alkalic post-shield, and following 0.5-2.5 myr of quiescence, (4) a volumetrically minor (<<1%) strongly alkalic rejuvenated stage.

The geochemistry of Hawaiian lavas can provide important constraints on the structure and composition of the Hawaiian plume [e.g., *DePaolo et al.*, 2001; *Blichert-Toft et al.*, 2003; *Eisele et al.*, 2003; *Abouchami et al.*, 2005; *Bryce et al.*, 2005; *Marske et al.*, 2007]. In particular, systematic geochemical variations are observed between lavas erupted from the two geographic trends and during different growth stages. These variations are generally explained by inferring that the Hawaiian plume is either concentrically zoned [e.g., *Hauri*, 1996; *Kurz et al.*, 1996; *Lassiter et al.*, 1996] or bilaterally zoned [*Abouchami et al.*, 2005] in cross-section. However, vertical heterogeneities within the upwelling plume are also likely to be an important factor in creating the observed geochemical variability [*Blichert-Toft et al.*, 2003; *Marske et al.*, 2007].

---

[1] A version of this chapter will be submitted for publication. Hanano, D., D. Weis, S. Aciego, J. S. Scoates, and D. J. DePaolo (2008), Geochemistry of post-shield lavas from Mauna Kea, Kohala, and Hualalai: Evidence for ancient depleted components in the Hawaiian plume, *Geochemistry Geophysics Geosystems*.

The compositional range of Hawaiian shield stage lavas is typically accounted for by mixing of at least three isotopically distinct end-members, referred to as Loihi, Kea, and Koolau [e.g., *Staudigel et al.*, 1984; *Stille et al.*, 1986; *West et al.*, 1987; *Eiler et al.*, 1996; *Hauri*, 1996]. However, the depleted isotopic signatures of post-shield and rejuvenated stage lavas require contributions from an additional component that may be intrinsic to the plume [e.g., *Frey et al.*, 2005] or derived at least in part from external sources, including entrained upper mantle and the underlying Pacific lithosphere [e.g., *Chen and Frey*, 1985; *Gaffney et al.*, 2004]. The distribution of heterogeneities in the Hawaiian plume, and in particular the depleted component involved in the post-shield and rejuvenated stages, remains a controversial unresolved aspect of Hawaiian volcanism.

Post-shield lavas occur on many Hawaiian volcanoes including Haleakala, West Maui, East and West Molokai, Waianae, and Kauai. At other Hawaiian volcanoes, the post-shield stage is either minor (e.g., Kahoolawe and Niihau) or absent (e.g., Lanai and Koolau). Post-shield lavas are the target for this research because they are derived from low degrees of partial melting (i.e., a few percent) and can thus provide finer resolution of variation in source composition than shield lavas. The lower magma supply during the post-shield stage (<0.005 km^3/yr; one-tenth to one-hundredth of the rate during the shield stage) prevents a single long-lived conduit from being maintained, and each eruption is likely to be associated with a separate vent and path through the lithosphere [e.g., *Frey et al.*, 1990; *Wolfe et al.*, 1997; *Hieronymus and Bercovici*, 2001]. Assuming that melt can be extracted from small regions (e.g., length scale <10 km) within the melting zone without substantial subsequent chemical modification [*Marske et al.*, 2007], post-shield lavas permit identification of small-scale heterogeneities within the Hawaiian plume. Furthermore, because post-shield lavas

erupt after the volcano has migrated to the periphery of the plume, the geochemistry of these lavas has implications for the large-scale structure of the Hawaiian plume.

We report high-precision trace element concentrations by HR-ICP-MS and Sr, Nd, Pb and Hf isotopic compositions of 32 post-shield lavas from Mauna Kea, Hualalai, and Kohala volcanoes on the island of Hawaii (Figure 3.1; Table 3.1). Systematic temporal trends are identified within these volcanoes as they evolve from the shield to post-shield stage. We then evaluate if the distinct isotopic compositions of the post-shield lavas can be explained by mixing between the shield end-members or by contributions from the underlying Pacific lithosphere, shallow asthenosphere, or components within the plume. The post-shield lavas from this study are compared with late-shield, post-shield, and rejuvenated stage lavas from other Hawaiian volcanoes to determine the extent and origin of depleted components in Hawaiian lavas. Additionally, comparison with Mahukona volcano allows the geochemistry of two consecutive Loa-Kea volcano pairs to be evaluated, which provides both spatial and temporal constraints on the geochemical structure of the Hawaiian plume.

3.2 SAMPLE DESCRIPTION AND GEOLOGIC SETTING

Kohala is the oldest volcano on the island of Hawaii and has completed post-shield activity. Extensive landsliding and erosion have carved deep canyons in the flanks of the volcano, exposing the older stratigraphy of the shield-stage Polulu Volcanics. Three late-shield lavas from the Polulu Volcanics were included in this study, two of which have been dated at 450 ± 40 ka and 375 ± 22 ka (Aciego, S. M., F. Jourdan, D. J. DePaolo, B. M. Kennedy, and P. R. Renne, Combined U-Th/He and $^{40}Ar/^{39}Ar$ geochronology of post-shield

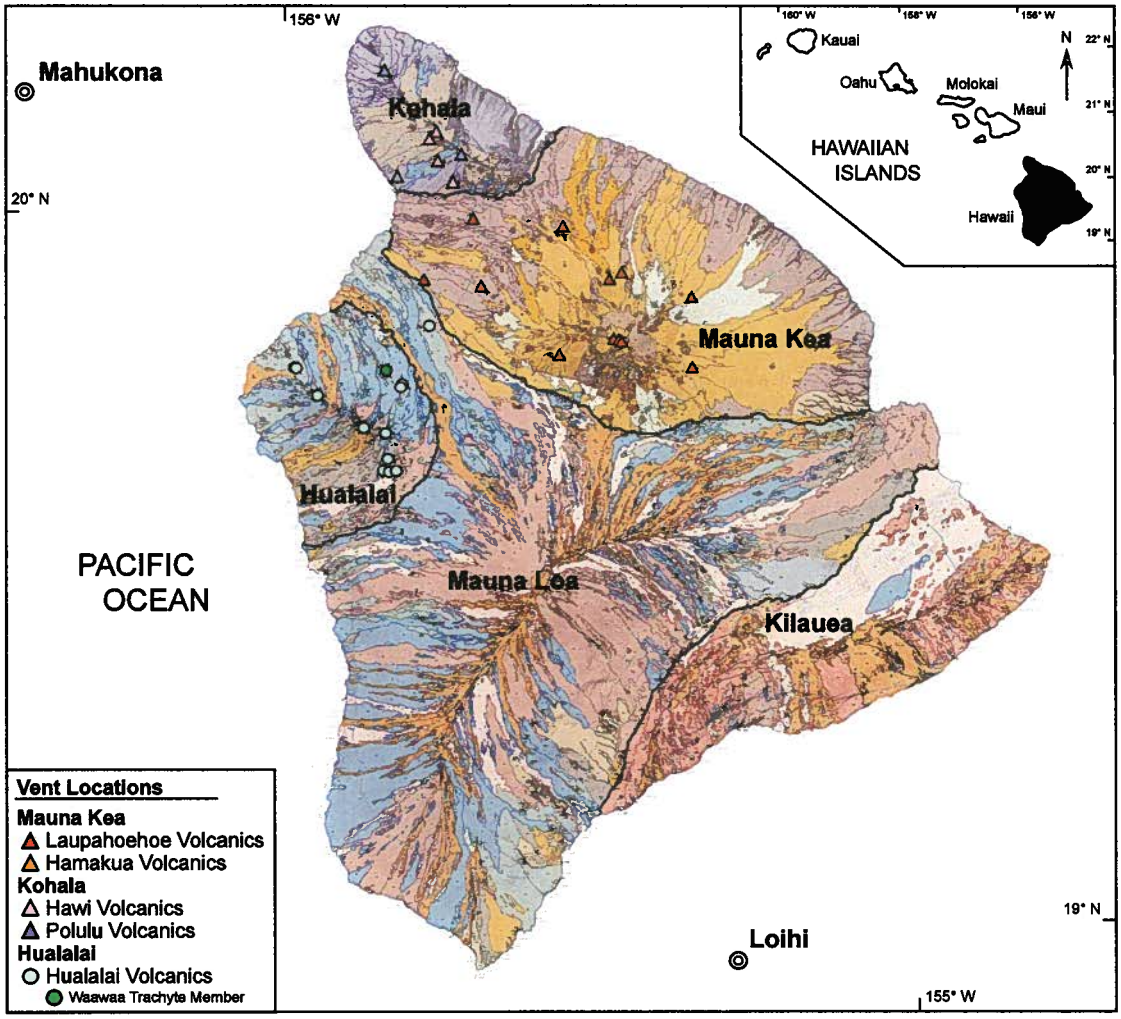

Figure 3.1: Geological map of the island of Hawaii [*Wolfe and Morris*, 1996]. The vent locations of the post-shield samples from Hualalai, Mauna Kea, and Kohala volcanoes are indicated. Different colours and patterns represent distinct lithologic units (mainly lavas flows of varying age). The thick grey lines mark the approximate boundaries between lavas from Kilauea, Mauna Loa, Hualalai, Mauna Kea, and Kohala volcanoes. The approximate locations of the submarine summits of Mahukona and Loihi volcanoes are also shown. The inset map shows the location of the island of Hawaii with respect to the other Hawaiian Islands in the Pacific Ocean.

Table 3.1: Sampling and Vent Locations of Hawaiian Post-shield Lavas[a]

Sample	Vent Name	Age (ka)	Elevation (masl)	Sample		Vent	
				Latitude	Longitude	Latitude	Longitude
			Hualalai Volcano				
02AHU-1	Waha Pele	0.71		19.5692	155.94233	19.64333	155.82833
02AHU-2	Puu Ikaaka	7.25	5428	19.62713	155.8156	19.62713	155.8156
02AHU-3	Poikahi	2.25	6820	19.67532	155.83253	19.68167	155.83253
02AHU-4	no vent	2.29[b]	1352	19.5791	155.94355	*19.62833*	*155.835*
02AHU-5	no vent	12.95[b]	137	19.64175	155.99557	*19.69*	*155.865*
02AHU-6	no vent	2.25	1281	19.553	155.93588	*19.65*	*155.83333*
02AHU-7	unnamed vent	4.7[b]	1979	19.74867	155.97395	19.73333	155.935
02AHU-8	Puu Waawaa	114 ± 3[c]		19.77768	155.83072	19.77768	155.83072
02AHU-9	Kuainiho	7.5	2594	18.83842	155.77017	18.83842	155.77017
02AHU-10	Puu Nahaha	4	372	19.77888	156.01565	19.775	155.975
02AHU-11	Puu Nahaha	4		19.77888	156.01565	19.775	155.975
02AHU-12	unnamed vent	2.25	4100	19.74972	155.81035	19.74972	155.81035
02AHU-13	unnamed vent	2.25	4118	19.74733	155.80987	19.74733	155.80987
			Mauna Kea Volcano				
02AMK-1	Puu o Kauha	45	5923	19.76283	155.57828	19.7975	155.56667
02AMK-2	no vent	160	9913	19.77262	155.4725	*19.82167*	*155.47*
02AMK-3	no vent	155 ± 11[d]	9990	19.77272	155.47212	*19.82333*	*155.47167*
02AMK-4	no vent	30	10068	19.77285	155.47188	*19.825*	*155.47333*
02AMK-5	Puu Io	225	3962	19.98213	155.56375	19.98213	155.56375
02AMK-6	Kaluamakani	45	4866	19.95283	155.50212	19.90417	155.49083
02AMK-7	unnamed vent	123 ± 5[d]	5312	19.94378	155.47448	19.9125	155.47167
02AMK-8	Kalepa	45	5730	19.91	155.34382	19.88	155.36333
02AMK-10	Aahuwela	45	6742	19.7766	155.35068	19.785	155.365
02AMK-11	Puu Hinai	19 ± 4[d]	259	19.94015	155.83792	19.935	155.77667
02AMK-12	Puu Pa	239 ± 84[d]	362	20.00908	155.81372	19.98917	155.70417
02AMK-13	Puu Papapa	142 ± 22[d]	2790	19.90715	155.7051	19.89333	155.68917
			Kohala Volcano				
02AKA-1	Kaiwaiwai	175	302	20.04422	155.73507	20.04422	155.73507
02AKA-2	Puu Pili	190 ± 20[d]	3052	20.11615	155.78838	20.115	155.76
02AKA-3	Puu Honu	175	3250	20.10255	155.77872	20.105	155.76833
02AKA-4	Puu Makela	137 ± 5[e]	3428	20.07263	155.76115	20.07263	155.76115
02AKA-5	no vent	450 ± 40[d]	442	20.04913	155.83075	*20.08333*	*155.71667*
02AKA-6	Puu Kamalii	400	187	20.04182	155.83263	20.04917	155.82167
02AKA-7	Puu o Nale	375 ± 22[d]	1559	20.20917	155.83312	20.20083	155.84333

[a]masl = meters above sea level; latitude and longitude expressed in decimal degrees; 'no vent' indicates that the sample could not be traced back to a specific vent due to overlying flows - the corresponding vent coordinates (in italics) are approximate; where sample and vent coordinates are the same, the sample was taken directly from the vent; ages are approximate and based on the geologic mapping of *Wolfe and Morris* [1996] unless otherwise specified.

[b]*Wolfe and Morris* [1996]. C-14 age.

[c]*Cousens et al.* [2003]. $^{40}Ar/^{39}Ar$ isochron age with analytical uncertainty given at 2σ.

[d]*Aciego et al.* [submitted, 2008]. $^{40}Ar/^{39}Ar$ age with analytical uncertainty given at 2σ.

[e]*McDougall* [1969]. K-Ar age with analytical uncertainty given at 2σ.

lavas from the Mauna Kea and Kohala volcanoes, Hawaii, manuscript submitted to *Earth and Planetary Science Letters*, 2008; hereinafter referred to as *Aciego et al.*, submitted, 2008). Four samples were collected from the overlying lava flows of the post-shield Hawi Volcanics. The majority of the post-shield vents are located along Kohala's northwest rift zone. The post-shield lavas are significantly younger, with ages of samples in this study ranging from 190 ± 20 ka [*Aciego et al.*, submitted, 2008] to 137 ± 5 ka [*McDougall*, 1969].

Mauna Kea is the second largest Hawaiian volcano (after Mauna Loa) and rises to 4205 m above sea level. In contrast to other Hawaiian volcanoes, where vents are largely confined to the rift zones, the post-shield vents at Mauna Kea are scattered over the surface of the volcano. Post-shield volcanism on Mauna Kea is divided into an earlier basaltic substage (Hamakua Volcanics) and a later hawaiitic substage (Laupahoehoe Volcanics) [*Wolfe et al.*, 1997]. Six samples from each sub-stage were selected for this study. The basaltic samples range in age from 239 ± 84 ka to 123 ± 5 ka, and the hawaiitic samples are as young as 19 ± 4 ka [*Aciego et al.*, submitted, 2008].

Hualalai is the youngest of the three volcanoes in this study and is still actively in the post-shield stage, having last erupted in 1801. Most of the surface of the volcano is covered by the post-shield lavas of the Hualalai Volcanics, which form a thin veneer over the shield-stage lavas. The post-shield vents are primarily located along the well-developed northwest rift zone as well as a south-southeast trending rift zone. Thirteen samples were collected, most of which range in age from 13 ka to 2.3 ka [*Wolfe and Morris*, 1996]. One sample is from the young (0.71 ka) Waha Pele flow on the southwestern flank of the volcano, and one sample is from the Puu Waawaa pumice cone (Waawaa Trachyte Member) on the northern slope, dated at 113.5 ± 3.2 ka [*Cousens et al.*, 2003].

A total of 32 subaerial late-shield and post-shield lavas were collected from Kohala, Mauna Kea, and Hualalai volcanoes on the northern part of the island of Hawaii (Figure 3.1). The samples were taken from gulches and road cuts on the flanks of these volcanoes from lava flows that could be traced back to a specific vent (Table 3.1). The collected samples are fresh; olivine phenocrysts are unaltered and there is only rare minor alteration of the groundmass.

3.3 ANALYTICAL TECHNIQUES

Sample preparation of the 32 post-shield lavas was carried out at the Center for Isotope Geochemistry (CIG) at the University of California, Berkeley. Whole rocks were cut using a diamond-embedded saw and then abraded with sandpaper to eliminate saw traces. The samples were coarse-crushed (to ~5 mm diameter) in a hydraulic piston crusher between tungsten carbide (WC) plates and subsequently ground to a fine powder in a WC mill for XRF analyses and an agate mill for ICP-MS and isotope analyses (the effect of WC contamination on trace elements and Pb and Hf isotopes is discussed in Appendix A3). The major element oxides and some trace elements (Co, Ni, Cu, Zn, Ga, Ge, As, Rb, Sr, Y, Zr, Nb, Mo, Ba, La, Ce, Pr, Nd, Sm, Pb, Th and U) were determined by X-ray fluorescence (XRF) using a Philips PW2400 spectrometer at the CIG, University of California, Berkeley. Measurements were calibrated against USGS reference materials AGV, BHVO, and BCR. The major elements were measured on glass discs (fused with lithium tetraborate flux) and the trace elements were measured on pressed powder pellets. XRF compositions are the mean of duplicate analyses and are reported in Table 3.2.

Complete trace element characterization by high-resolution inductively coupled

Table 3.2: Major and Trace Element Abundances of Hawaiian Post-shield Lavas[a]

	Hualalai Volcano							
	02AHU-1	02AHU-2	02AHU-3[b]	02AHU-4	02AHU-5	02AHU-6	02AHU-7	02AHU-8
Major elements (wt%)								
SiO_2	46.74	45.39	49.46	47.51	47.33	46.63	47.35	62.20
TiO_2	1.99	1.53	2.45	1.82	2.03	2.25	2.90	0.39
Al_2O_3	13.63	9.76	14.99	12.61	12.70	13.49	14.41	17.28
Fe_2O_3*	13.90	13.29	12.65	13.13	13.03	13.67	14.06	4.54
MnO	0.18	0.18	0.18	0.18	0.18	0.18	0.19	0.31
MgO	10.55	16.74	6.30	12.00	10.36	9.30	5.80	0.49
CaO	10.39	10.08	8.42	10.43	11.38	10.06	9.87	0.88
Na_2O	2.76	1.93	3.76	2.45	2.48	2.93	3.38	7.26
K_2O	0.81	0.55	1.40	0.68	0.69	0.93	1.15	4.91
P_2O_5	0.26	0.19	0.45	0.21	0.23	0.29	0.38	0.15
Total	101.21	99.65	100.07	101.02	100.40	99.73	99.49	98.42
mg-number	0.63	0.73	0.52	0.67	0.64	0.60	0.48	0.19
A.I.	0.71	0.12	1.29	-0.02	0.09	1.04	1.44	3.59
Trace elements (ppm)								
Sc^{ICP}	25.4	28.9	18.8	27.0	31.0	25.6	22.4	6.2
V^{ICP}	301	278	250	279	316	299	377	0.68
Cr^{ICP}	470	1513	163	778	644	385	100	0.23
Co^{ICP}	60.4	80.6	40.6	62.4	65.5	57.5	46.2	0.14
Ni^{XRF}	252	648	96	362	240	208	76	4
Zn^{XRF}	99	95	103	96	90	105	114	180
Ga^{XRF}	21	15	21	18	20	21	23	26
Cs^{ICP}	0.131	0.052	0.294	0.039	0.115	0.213	0.258	1.109
Rb^{ICP}	19.2	10.5	33.9	13.2	15.4	21.6	27.6	115.5
Sr^{XRF}	427	319	549	364	382	488	508	37
Ba^{ICP}	249	183	443	224	213	304	370	281
Y^{XRF}	21.1	16.8	29.6	19.2	20.8	23.5	27.8	58.7
Zr^{XRF}	125	101	209	109	114	140	181	960
Hf^{ICP}	2.77	2.28	4.55	2.44	2.69	3.25	4.06	20.23
Nb^{XRF}	20.9	16.1	39.3	18.3	19.7	24.0	32.4	139.8
Ta^{ICP}	0.93	0.83	1.80	0.74	0.69	1.16	1.49	4.78
W^{ICP}	0.22	0.14	0.45	0.17	0.28	0.53	0.52	2.69
La^{ICP}	15.0	12.0	28.4	12.8	13.8	18.7	21.6	57.5
Ce^{ICP}	33.6	26.9	60.7	28.5	31.3	42.1	47.7	116.8
Pr^{ICP}	4.27	3.42	7.38	3.57	3.95	5.11	6.11	12.51
Nd^{ICP}	17.8	14.6	29.8	15.2	16.7	21.4	25.6	42.4
Sm^{ICP}	4.06	3.30	6.26	3.53	3.90	4.81	5.75	8.06
Eu^{ICP}	1.36	1.10	2.03	1.22	1.31	1.63	1.92	1.89
Gd^{ICP}	4.01	3.26	5.90	3.55	3.83	4.68	5.42	6.55
Tb^{ICP}	0.61	0.49	0.88	0.56	0.61	0.71	0.84	1.20
Dy^{ICP}	3.68	2.98	5.24	3.43	3.62	4.19	4.86	7.64
Ho^{ICP}	0.70	0.58	1.01	0.65	0.67	0.79	0.91	1.55
Er^{ICP}	1.80	1.46	2.57	1.69	1.73	2.02	2.34	4.61
Yb^{ICP}	1.44	1.16	2.14	1.36	1.46	1.69	1.96	5.18
Lu^{ICP}	0.213	0.165	0.308	0.199	0.215	0.248	0.283	0.818
Pb^{ICP}	1.38	1.02	2.23	1.23	1.16	4.48	1.70	7.15
Th^{ICP}	1.44	1.03	2.74	1.15	1.17	1.59	1.94	8.37
U^{ICP}	0.396	0.281	0.759	0.303	0.282	0.458	0.585	2.458

Table 3.2 (continued)

						Mauna Kea Volcano		
	02AHU-9	02AHU-10	02AHU-11	02AHU-12	02AHU-13	02AMK-1	02AMK-2	02AMK-3
Major elements (wt%)								
SiO_2	47.12	47.50	45.33	47.06	47.09	48.37	47.92	47.96
TiO_2	2.05	1.87	2.19	2.23	2.18	2.93	3.17	3.30
Al_2O_3	13.10	12.60	12.33	14.13	14.10	16.59	14.09	14.17
Fe_2O_3*	12.71	13.26	13.38	13.77	13.72	12.04	13.75	14.54
MnO	0.18	0.18	0.18	0.19	0.19	0.20	0.18	0.19
MgO	9.60	11.95	11.65	8.72	9.05	4.48	5.92	5.74
CaO	11.58	10.67	10.61	10.58	10.59	7.16	10.85	10.77
Na_2O	2.48	2.45	2.53	2.81	2.78	4.53	2.88	2.94
K_2O	0.73	0.68	0.81	0.94	0.91	1.74	0.81	0.80
P_2O_5	0.23	0.22	0.26	0.27	0.27	0.76	0.38	0.41
Total	99.78	101.39	99.27	100.70	100.88	98.80	99.95	100.83
mg-number	0.62	0.66	0.66	0.58	0.59	0.45	0.49	0.46
A.I.	0.21	-0.01	1.00	0.77	0.70	2.80	0.39	0.42
Trace elements (ppm)								
Sc^{ICP}	29.3	29.0	28.0	27.6	25.5	9.9	23.9	25.7
V^{ICP}	318	296	327	304	302	109	280	298
Cr^{ICP}	555	701	689	338	372	4.5	30	34
Co^{ICP}	55.2	67.2	63.5	55.6	55.7	18.4	42.5	46.2
Ni^{XRF}	228	343	328	173	195	13	74	64
Zn^{XRF}	101	97	100	104	106	124	118	127
Ga^{XRF}	21	20	20	22	22	26	26	26
Cs^{ICP}	0.066	0.081	0.176	0.199	0.226	0.252	0.110	0.105
Rb^{ICP}	14.0	13.4	18.4	20.5	20.2	29.8	11.8	12.1
Sr^{XRF}	375	347	436	443	439	1287	565	573
Ba^{ICP}	226	205	268	269	257	533	209	231
Y^{XRF}	21.8	19.8	19.8	24.1	23.4	46.3	33.0	35.0
Zr^{XRF}	122	109	129	153	146	396	230	241
Hf^{ICP}	2.92	2.56	3.03	3.52	3.36	8.11	4.75	5.23
Nb^{XRF}	18.7	18.8	24.8	24.7	24.0	55.9	25.0	29.0
Ta^{ICP}	0.98	0.99	1.22	1.14	1.20	2.69	2.62	1.41
W^{ICP}	0.34	0.69	0.63	0.70	0.70	1.26	0.79	0.73
La^{ICP}	14.3	12.9	16.5	18.6	17.4	39.2	19.1	22.4
Ce^{ICP}	32.4	28.4	36.6	41.5	38.7	92.9	45.4	52.3
Pr^{ICP}	4.06	3.78	4.57	5.22	4.94	12.07	6.10	7.02
Nd^{ICP}	17.3	15.9	19.4	21.7	20.3	51.9	26.4	31.1
Sm^{ICP}	4.10	3.68	4.35	4.84	4.56	11.65	6.61	7.28
Eu^{ICP}	1.38	1.27	1.47	1.56	1.50	3.74	2.19	2.38
Gd^{ICP}	4.06	3.71	4.24	4.62	4.39	10.37	6.45	6.93
Tb^{ICP}	0.63	0.58	0.63	0.73	0.69	1.44	0.97	1.04
Dy^{ICP}	3.74	3.39	3.54	4.04	3.99	7.96	5.23	5.92
Ho^{ICP}	0.71	0.65	0.68	0.80	0.75	1.41	0.98	1.05
Er^{ICP}	1.83	1.71	1.76	2.16	2.02	3.55	2.54	2.68
Yb^{ICP}	1.53	1.41	1.40	1.75	1.58	2.66	1.98	2.07
Lu^{ICP}	0.222	0.198	0.198	0.255	0.240	0.378	0.279	0.297
Pb^{ICP}	1.19	1.10	1.33	1.57	1.55	2.32	1.22	1.28
Th^{ICP}	1.20	1.13	1.46	1.56	1.52	3.13	1.49	1.65
U^{ICP}	0.272	0.273	0.399	0.434	0.434	0.886	0.469	0.519

Table 3.2 (continued)

	02AMK-4	02AMK-5	02AMK-6	02AMK-7[b]	02AMK-8[b]	02AMK-10	02AMK-11	02AMK-12
Major elements (wt%)								
SiO_2	49.85	46.60	50.31	46.54	50.96	48.91	49.66	46.72
TiO_2	2.71	2.20	2.52	3.79	2.46	2.60	2.76	1.82
Al_2O_3	16.76	11.27	16.92	13.80	17.08	16.76	16.86	10.09
Fe_2O_3*	11.61	12.47	11.28	14.43	11.22	11.52	11.86	11.84
MnO	0.21	0.17	0.21	0.19	0.21	0.21	0.21	0.16
MgO	4.22	13.35	3.94	5.88	3.79	3.94	4.27	15.95
CaO	6.98	11.13	6.80	9.61	6.68	6.75	6.98	11.19
Na_2O	4.83	1.97	4.89	3.39	4.98	4.66	4.86	1.80
K_2O	1.86	0.53	1.96	1.27	2.02	1.86	1.85	0.44
P_2O_5	0.83	0.26	0.94	0.64	0.98	0.88	0.81	0.20
Total	99.85	99.94	99.77	99.54	100.38	98.09	100.11	100.22
mg-number	0.44	0.70	0.43	0.47	0.43	0.43	0.44	0.75
A.I.	2.68	-0.31	2.67	1.87	2.57	2.85	2.77	-0.62
Trace elements (ppm)								
Sc^{ICP}	9.2	30.7	8.3	21.3	8.2	8.9	10.0	32.7
V^{ICP}	102	227	88	289	80	86	83	221
Cr^{ICP}	8.9	818	18	166	0.87	1.9	0.75	1271
Co^{ICP}	15.9	61.0	15.2	45.2	14.1	16.2	17.2	70.9
Ni^{XRF}	14	451	14	91	5	8	12	539
Zn^{XRF}	126	97	130	139	133	141	115	88
Ga^{XRF}	25	19	26	26	25	26	25	16
Cs^{ICP}	0.300	0.067	0.215	0.143	0.097	0.120	0.286	0.063
Rb^{ICP}	33.1	9.4	32.8	21.1	33.3	29.3	32.6	7.7
Sr^{XRF}	1279	458	1271	724	1255	1246	1295	377
Ba^{ICP}	564	180	578	378	610	573	556	135
Y^{XRF}	48.8	21.2	52.1	40.1	52.6	49.0	47.2	17.8
Zr^{XRF}	422	149	461	341	478	442	416	120
Hf^{ICP}	8.83	3.69	9.56	7.35	10.23	9.48	8.75	2.97
Nb^{XRF}	58.2	19.6	61.4	45.0	65.5	61.3	57.5	14.7
Ta^{ICP}	3.41	0.92	3.13	1.76	3.04	3.03	2.53	0.91
W^{ICP}	1.75	0.54	1.53	0.99	1.23	1.74	5.03	0.65
La^{ICP}	43.6	16.5	49.0	36.1	52.9	46.9	45.1	12.9
Ce^{ICP}	103.3	38.6	115.7	81.2	121.8	104.2	103.3	28.4
Pr^{ICP}	13.38	4.99	14.64	10.45	15.53	13.96	13.44	3.91
Nd^{ICP}	56.7	21.8	61.9	44.1	66.5	60.0	57.8	17.4
Sm^{ICP}	12.62	5.08	13.60	9.69	14.14	13.07	12.65	4.18
Eu^{ICP}	3.98	1.69	4.18	3.08	4.48	4.20	4.09	1.41
Gd^{ICP}	11.16	4.95	11.78	8.99	12.53	11.52	11.34	4.12
Tb^{ICP}	1.59	0.71	1.69	1.29	1.78	1.60	1.63	0.60
Dy^{ICP}	8.59	4.01	9.05	7.19	9.54	8.77	8.80	3.44
Ho^{ICP}	1.52	0.72	1.62	1.28	1.71	1.57	1.56	0.63
Er^{ICP}	3.81	1.86	4.10	3.19	4.28	3.81	3.86	1.56
Yb^{ICP}	2.90	1.45	3.16	2.42	3.32	2.95	2.97	1.19
Lu^{ICP}	0.405	0.193	0.444	0.339	0.466	0.405	0.420	0.161
Pb^{ICP}	2.46	0.96	2.64	1.95	2.92	2.86	2.58	0.79
Th^{ICP}	3.46	1.26	3.84	2.96	4.04	3.61	3.49	1.00
U^{ICP}	1.091	0.398	1.236	0.892	1.252	1.127	1.073	0.297

Table 3.2 (continued)

		Kohala Volcano						
	02AMK-13	02AKA-1[b]	02AKA-2	02AKA-3	02AKA-4[b]	02AKA-5[b]	02AKA-6	02AKA-7
Major elements (wt%)								
SiO_2	47.15	46.88	50.69	49.04	58.02	46.90	49.63	48.42
TiO_2	2.96	2.85	2.18	2.54	1.02	3.17	2.81	3.32
Al_2O_3	15.11	15.64	16.67	16.51	17.84	13.06	14.11	14.04
Fe_2O_3*	13.55	12.92	10.92	12.17	7.13	13.31	13.25	13.34
MnO	0.18	0.22	0.23	0.23	0.23	0.18	0.18	0.17
MgO	5.80	4.34	3.55	3.86	1.48	7.75	5.89	4.78
CaO	11.46	7.36	6.10	6.77	2.86	10.65	10.33	9.85
Na_2O	2.76	4.84	5.38	4.89	6.90	2.78	2.77	3.15
K_2O	0.75	1.54	1.99	1.80	2.90	0.80	0.61	0.85
P_2O_5	0.36	2.15	1.60	1.83	0.68	0.49	0.38	0.50
Total	100.08	98.74	99.31	99.64	99.06	99.10	99.97	98.41
mg-number	0.49	0.42	0.42	0.41	0.31	0.56	0.49	0.44
A.I.	0.49	3.46	3.04	2.98	2.76	0.66	-0.55	0.51
Trace elements (ppm)								
Sc^{ICP}	28.4	8.1	6.2	7.3	2.5	26.9	29.8	27.5
V^{ICP}	291	77	36	62	3.2	240	278	317
Cr^{ICP}	139	0.30	0.24	0.17	0.44	385	78	89
Co^{ICP}	46.0	15.5	9.8	13.4	2.1	47.5	42.3	42.7
Ni^{XRF}	75	14	10	10	7	180	81	63
Zn^{XRF}	108	129	128	123	115	120	118	125
Ga^{XRF}	25	20	22	21	21	25	24	28
Cs^{ICP}	0.116	0.251	0.337	0.236	0.243	0.065	0.112	0.124
Rb^{ICP}	13.6	24.1	33.3	31.9	75.9	9.1	11.7	11.6
Sr^{XRF}	609	1832	1954	1734	1319	504	439	536
Ba^{ICP}	233	553	689	623	933	258	176	260
Y^{XRF}	29.6	62.3	60.3	58.0	44.9	38.2	36.0	38.2
Zr^{XRF}	203	320	424	376	626	269	223	264
Hf^{ICP}	5.21	6.62	8.64	7.98	11.14	5.77	4.82	5.91
Nb^{XRF}	25.4	54.0	69.6	61.3	86.6	28.9	22.0	33.1
Ta^{ICP}	1.35	2.60	2.49	3.27	3.62	1.22	0.99	1.48
W^{ICP}	0.96	2.94	0.80	1.95	1.15	0.86	0.97	1.18
La^{ICP}	22.5	51.2	65.2	57.3	81.0	25.3	20.5	25.6
Ce^{ICP}	51.4	123.7	148.9	133.5	163.2	58.3	46.2	57.3
Pr^{ICP}	6.75	17.06	19.18	17.63	17.48	7.83	6.36	7.72
Nd^{ICP}	29.4	77.4	82.0	77.6	68.6	34.5	28.1	33.8
Sm^{ICP}	7.02	17.40	16.80	16.70	12.55	8.13	6.88	8.15
Eu^{ICP}	2.30	5.51	5.17	5.21	4.05	2.57	2.28	2.71
Gd^{ICP}	6.73	15.57	14.13	14.79	9.26	7.91	6.75	7.88
Tb^{ICP}	0.97	2.08	1.95	1.99	1.39	1.16	1.05	1.19
Dy^{ICP}	5.51	10.90	10.41	10.61	8.23	6.72	6.22	6.74
Ho^{ICP}	0.98	1.95	1.88	1.88	1.48	1.25	1.16	1.26
Er^{ICP}	2.50	4.60	4.63	4.52	3.96	3.11	2.96	3.18
Yb^{ICP}	1.88	3.24	3.39	3.25	3.41	2.47	2.32	2.51
Lu^{ICP}	0.263	0.457	0.481	0.450	0.493	0.348	0.325	0.358
Pb^{ICP}	1.24	1.94	2.64	2.40	4.37	1.37	1.19	1.36
Th^{ICP}	1.75	2.85	3.89	3.74	8.00	1.85	1.37	1.80
U^{ICP}	0.568	0.891	1.073	1.242	2.258	0.506	0.454	0.662

[a]Major element abundances were determined by XRF; trace element abundances were determined by either XRF or HR-ICP-MS (denoted as ICP); Fe_2O_3* is total Fe; mg-number = $(Mg/Mg+Fe^{2+})$; A.I. (Alkalinity Index) = $(Na_2O+K_2O)-0.37*SiO_2+14.43$.

[b]ICP-MS abundances are the mean of duplicate or replicate analyses.

plasma mass spectrometry (HR-ICP-MS) was carried out at the Pacific Centre for Isotopic and Geochemical Research (PCIGR), University of British Columbia. Comprehensive sample preparation and analytical procedures are described in *Pretorius et al.* [2006]. Sample powders were digested in a mixture of concentrated HF and HNO_3 in sealed Teflon® vessels and subsequently diluted (with 1% HNO_3 and 1 ppb In) to 1000 and 3000 times for the rare earth element (REE) and high field strength element (HFSE) analyses, respectively. Indium (In), which was used as an internal standard, was spiked at 1 ppb in all blank, standard, and sample solutions. The solutions were analysed on a Thermo Finnigan Element2 HR-ICP-MS using external calibration. The REE were measured in high resolution, whereas U, Pb and Th were measured in low resolution. The majority of the HFSE were measured in medium resolution, except for Sr, Zr and Ba, which were measured in high resolution to avoid overloading the detector. Trace element abundances by HR-ICP-MS are reported in Table 3.2 (see Appendix A1 for a comparison of XRF and HR-ICP-MS values). For most elements, values of the USGS reference materials BCR-2 and AGV-2, reported in Appendix A2, are within 2σ error of literature and recommended values (Tables A1 and A2). Procedural duplicates and replicate measurements show excellent agreement, with relative standard deviations (RSD) less than 5% for most elements. Procedural blank values for the REE and most other elements are in the parts-per-trillion (ppt) range, and are considered negligible in comparison to the sample concentrations, which are in the parts-per-million (ppm) range. Column blanks for Sr, Nd, Pb and Hf isotope chemistry (discussed below) were also negligible (<<1 ng).

Sr and Nd isotopic compositions were determined at the CIG, University of California, Berkeley and are reported in Table 3.3. Sample powders were leached in a

Table 3.3: Hf, Sr, and Nd Isotopic Compositions of Hawaiian Post-shield Lavas[a]

Sample	Volcanic Series	$^{176}Hf/^{177}Hf$	2σ	$^{87}Sr/^{86}Sr$	2σ	$^{143}Nd/^{144}Nd$	2σ
		Hualalai Volcano					
02AHU-1	Hualalai	0.283144	4	0.703578	8	0.512944	10
02AHU-2	Hualalai	0.283135	6	0.703556	13	0.512934	6
02AHU-3	Hualalai	0.283108	5			0.512935	4
		0.283119	5				
02AHU-4	Hualalai	0.283129	6	0.703564	11	0.512945	5
02AHU-5	Hualalai	0.283134	5	0.703537	11	0.512915	6
02AHU-6	Hualalai	0.283127	5	0.703532	10	0.512954	5
02AHU-7	Hualalai	0.283130	5	0.703568	10	0.512958	5
02AHU-8	Hualalai[b]	0.283093	4	0.703713	35	0.512904	6
02AHU-9	Hualalai	0.283123	5	0.703570	14	0.512936	4
02AHU-10	Hualalai	0.283112	5	0.703636	10	0.512949	6
02AHU-11	Hualalai	0.283128	6	0.703511	10	0.512964	6
02AHU-12	Hualalai	0.283113	6	0.703587	12	0.512941	6
02AHU-13	Hualalai	0.283110	4	0.703597	10	0.512928	4
		0.283113	4				
		Mauna Kea Volcano					
02AMK-1	Laupahoehoe	0.283130	4	0.703432	11	0.513003	6
02AMK-2	Hamakua	0.283126	4	0.703551	20	0.512980	4
02AMK-3	Hamakua	0.283127	4	0.703488	17	0.512979	4
02AMK-4	Laupahoehoe	0.283133	5	0.703455	8	0.512969	5
02AMK-5	Hamakua	0.283127	7	0.703512	14	0.513003	8
02AMK-6	Laupahoehoe	0.283134	5	0.703463	10	0.513015	5
02AMK-7	Hamakua	0.283124	5	0.703517	8	0.513009	9
02AMK-8	Laupahoehoe	0.283126	4	0.703454	11	0.512987	4
		0.283127	4				
02AMK-10	Laupahoehoe	0.283133	6	0.703449	8	0.512996	6
02AMK-11	Laupahoehoe	0.283135	3	0.703488	11	0.513012	8
02AMK-12	Hamakua	0.283131	6	0.703562	8	0.512987	6
02AMK-13	Hamakua	0.283132	4	0.703530	10	0.512996	4
		Kohala Volcano					
02AKA-1	Hawi	0.283133	4	0.703520	8	0.512986	6
		0.283133	5				
02AKA-2	Hawi	0.283139	4	0.703534	10	0.512987	5
02AKA-3	Hawi	0.283136	4	0.703513	10	0.512988	6
02AKA-4	Hawi	0.283141	4	0.703525	10	0.513008	4
02AKA-5	Polulu	0.283116	4	0.703647	7	0.512993	7
02AKA-6	Polulu	0.283119	5	0.703654	9	0.512996	4
02AKA-7	Polulu	0.283119	4	0.703633	10	0.512969	4

[a]All Hf isotopic ratios were determined by MC-ICP-MS and have been normalized to JMC 475 $^{176}Hf/^{177}Hf = 0.282160$ [*Vervoort and Blichert-Toft*, 1999]. All Sr and Nd isotopic ratios were determined by TIMS; Sr data were normalized to SRM 987 $^{87}Sr/^{86}Sr = 0.710248$; Nd data were normalized to the Berkeley Ames standard $^{143}Nd/^{144}Nd = 0.510939$. The 2σ error is the absolute error value of an individual sample analysis (internal error) and applies to the last decimal place(s). Additional analyses for the same sample represent procedural duplicates using separate powder aliquots.

[b]Waawaa Trachyte Member

boiling mixture of strong HCl and HNO_3 to remove non-magmatic Sr resulting from diagenetic processes. Sr was purified on chromatographic ion exchange columns using Eichrom Sr spec resin following the procedures of *Horwitz et al.* [1991] and loaded in Ta_2O_5 on rhenium filaments. Nd was purified using a three-column procedure following the methods outlined in *Luo et al.* [1997] and *DePaolo* [1978] and loaded in 5 N HNO_3 on rhenium filaments. Nd was run as NdO^+ with an oxygen pressure of $\sim 10^{-6}$ mbar. Sr and Nd isotopic measurements were made on a VG Sector 54 multicollector thermal ionization mass spectrometer operating in dynamic mode. Analytical procedures were similar to those described in *DePaolo and Daley* [2000]. Sr and Nd isotopic ratios were normalized to $^{86}Sr/^{88}Sr = 0.1194$ and $^{146}Nd/^{142}Nd = 0.636151$, respectively, to correct for within-run fractionation. Nd data were further corrected for oxygen isotopes assuming that $^{17}O/^{16}O = 0.000387$ and $^{18}O/^{16}O = 0.00211$. The average $^{87}Sr/^{86}Sr$ of the SRM 987 Sr standard was 0.710281 ± 0.000015 (2sd; n = 140) during the course of the post-shield analyses. Mean values of the Berkeley Ames standard gave 0.510977 ± 0.000006 (2sd; n = 86) and BCR-1 gave $^{143}Nd/^{144}Nd = 0.511876 \pm 0.000005$ (2sd; n = 10). All measured Sr and Nd isotopic ratios were normalized to SRM 987 $^{87}Sr/^{86}Sr = 0.710248$ and Berkeley Ames standard $^{143}Nd/^{144}Nd = 0.510939$, respectively.

Pb and Hf isotopic compositions were determined at the PCIGR, University of British Columbia and are reported in Tables 3.3 and 3.4. All of the sample powders were acid-leached to remove alteration phases prior to isotopic analysis, following the sequential leaching procedure of *Weis et al.* [2005]. Leached sample powders were digested in a mixture of concentrated HF and HNO_3 in sealed Teflon® vessels and processed on chromatographic ion exchange columns. A thorough review of sample dissolution, isotopic

Table 3.4: Pb Isotopic Compositions of Hawaiian Post-shield Lavas[a]

Sample	Volcanic Series	$^{208}Pb/^{204}Pb$	2σ	$^{207}Pb/^{204}Pb$	2σ	$^{206}Pb/^{204}Pb$	2σ
		Hualalai Volcano					
02AHU-1	Hualalai	37.6779	21	15.4459	7	17.8913	9
02AHU-2	Hualalai	37.7063	27	15.4471	10	17.9356	12
02AHU-3	Hualalai	37.7444	18	15.4515	6	17.9690	8
02AHU-4	Hualalai	37.7532	27	15.4479	10	17.9784	11
02AHU-5	Hualalai	37.7442	18	15.4473	6	17.9802	6
		37.7470	16	15.4483	6	17.9805	5
02AHU-6	Hualalai	37.7285	19	15.4549	7	17.9572	7
02AHU-7	Hualalai	37.7134	14	15.4505	5	17.9702	6
02AHU-8	Hualalai[b]	37.7291	19	15.4456	7	17.9578	8
02AHU-9	Hualalai	37.7392	36	15.4449	13	17.9544	17
02AHU-10	Hualalai	37.7621	24	15.4578	10	17.9992	10
02AHU-11	Hualalai	37.7483	16	15.4524	6	18.0114	7
02AHU-12	Hualalai	37.7472	24	15.4590	9	18.0059	11
02AHU-13	Hualalai	37.7119	16	15.4500	6	17.9426	6
		37.7092	18	15.4491	7	17.9417	7
		Mauna Kea Volcano					
02AMK-1	Laupahoehoe	37.9365	40	15.4743	7	18.3437	7
02AMK-2	Hamakua	38.0072	15	15.4857	5	18.4210	6
02AMK-3	Hamakua	37.9894	15	15.4806	6	18.4070	6
02AMK-4	Laupahoehoe	37.9259	13	15.4708	5	18.3431	6
02AMK-5	Hamakua	37.9603	31	15.4787	12	18.3712	12
02AMK-6	Laupahoehoe	37.9328	18	15.4720	7	18.3495	8
02AMK-7	Hamakua	37.9718	20	15.4771	7	18.3782	9
02AMK-8	Laupahoehoe	37.9310	13	15.4711	4	18.3500	5
02AMK-10	Laupahoehoe	37.9377	17	15.4741	6	18.3517	6
02AMK-11	Laupahoehoe	37.9244	29	15.4717	10	18.3411	9
		37.9268	23	15.4717	8	18.3411	9
02AMK-12	Hamakua	37.9608	18	15.4788	6	18.3496	6
02AMK-13	Hamakua	37.9796	12	15.4784	6	18.4080	6
		Kohala Volcano					
02AKA-1	Hawi	38.0041	17	15.4843	5	18.4393	7
02AKA-2	Hawi	37.9908	41	15.4823	15	18.4258	18
02AKA-3	Hawi	37.9865	17	15.4780	7	18.4378	7
02AKA-4	Hawi	37.9949	13	15.4808	5	18.4394	6
		37.9994	17	15.4824	6	18.4410	6
02AKA-5	Polulu	37.9045	21	15.4762	8	18.2863	8
02AKA-6	Polulu	37.8989	19	15.4728	8	18.2482	8
02AKA-7	Polulu	37.9233	14	15.4763	5	18.3134	6

[a]All Pb isotopic ratios were determined by MC-ICP-MS on acid-leached sample powders; Pb data were corrected for fractionation by Tl spiking and then normalized to the NBS 981 triple spike values of *Galer and Abouchami* [1998] using the standard bracketing method. The 2σ error is the absolute error value of an individual sample analysis (internal error) and applies to the last decimal place(s). Additional analyses for the same sample represent procedural duplicates using separate powder aliquots.

[b]Waawaa Trachyte Member

likely related to accumulated apatite, whereas the low values in the benmoreite and trachyte reflect apatite fractionation.

There are systematic variations in incompatible trace elements with Nb concentration, which ranges between 15-70 ppm for most of the post-shield lavas (Figure 3.4). Abundances of incompatible trace elements are generally well-correlated with Nb, although some subtle differences exist between the transitional/alkalic basalts and alkalic lavas as well as between lavas from each volcano. For example, the Ba and Rb abundances of basalts from Hualalai define a separate, steeper trend than the other post-shield lavas. The alkalic lavas from Kohala are also distinct, being shifted to slightly lower Zr and higher La and Ce concentrations. The elevated Y and Sr concentrations (~60 ppm Y; ~1800 ppm Sr) in the three of these lavas from Kohala are consistent with accumulated apatite. The trachyte from Hualalai (140 ppm Nb) has anomalous trace element contents, including extremely low Sr (37 ppm) and Ba (281 ppm) concentrations that are indicative of extensive feldspar (+ apatite) fractionation.

Chondrite-normalized rare earth element (REE) patterns for the post-shield lavas are smooth with relatively steep slopes (La_N/Yb_N = 6.0-16.2), reflecting enrichment in the light REE (Figure 3.5). The overall patterns are similar, but show variations in the REE concentrations between samples from each volcano. The alkalic lavas from Kohala have the highest REE abundances (e.g., La = 215-340 times chondrites), and the transitional/alkalic basalts from Mauna Kea and Hualalai have the lowest abundances (e.g., La = 50-95 times chondrites). The REE pattern of the trachyte from Hualalai is distinctive, showing enrichment in the light and heavy REE relative to the middle REE, and a small negative Eu anomaly.

3.4 RESULTS

3.4.1 Major and trace elements

The post-shield lavas from Hualalai, Mauna Kea, and Kohala range widely in composition from basalt to trachyte (Figure 3.2). At Mauna Kea, the earlier substage of post-shield volcanism (Hamakua Volcanics) is characterized by transitional to alkalic basalts, whereas the later substage (Laupahoehoe Volcanics) contains hawaiites and mugearites. At Kohala, the late-shield lavas (Polulu Volcanics) are dominated by transitional to alkalic basalts and the post-shield lavas (Hawi Volcanics) have compositions ranging from hawaiite to benmoreite. In contrast, at Hualalai there is a large compositional gap between the alkalic basalts and trachytes of the post-shield stage (Hualalai Volcanics). For most samples (31 of 32) $K_2O/P_2O_5 > 1$, indicating that they have not undergone significant post-eruptive alteration, which results in a preferential loss of K relative to P [e.g., *Feigenson et al.*, 1983; *Chen and Frey*, 1985; *Frey et al.*, 1994].

The major element variations of the post-shield lavas can be divided into two groups, transitional/alkalic basalts and alkalic lavas (hawaiite to trachyte). The MgO contents of the post-shield lavas range widely from ~0.5-17 wt% (Figure 3.3). For lavas with >5 wt% MgO (transitional/alkalic basalts), Ni is strongly correlated with MgO, which is consistent with the combined effects of olivine fractionation and olivine accumulation (lavas with MgO > 10 wt% have abundant olivine phenocrysts). For lavas with <5 wt% MgO (alkalic lavas), CaO and Sc abundances decrease strongly with decreasing MgO, indicating an important role for clinopyroxene fractionation. Abundances of Fe_2O_3 and TiO_2 also decrease below 5 wt% MgO in the alkalic lavas, which signals the effect of fractionation of Fe-Ti oxides. The anomalously higher P_2O_5 contents (1.6-2.2 wt%) of three alkalic lavas from Kohala are

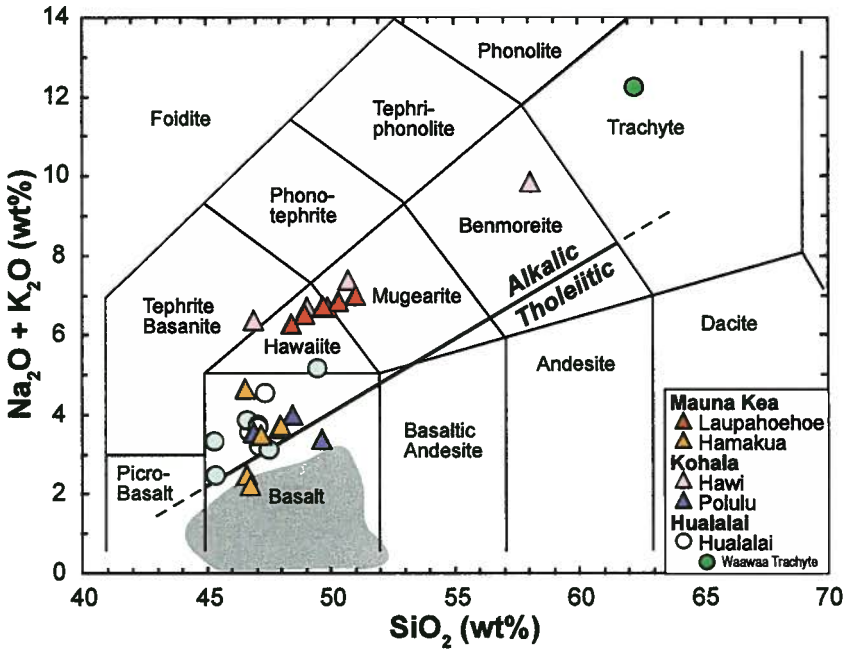

Figure 3.2: Total alkalis vs. silica classification diagram (modified from *Le Bas et al.* [1986]) showing the range in composition of the post-shield lavas from basalt to trachyte. The tholeiitic-alkalic dividing line is from *Macdonald and Katsura* [1964]. The shaded field represents the compositions of shield tholeiites from Hualalai, Mauna Kea, and Kohala. The majority of the post-shield lavas in this study are alkalic basalts and hawaiites.

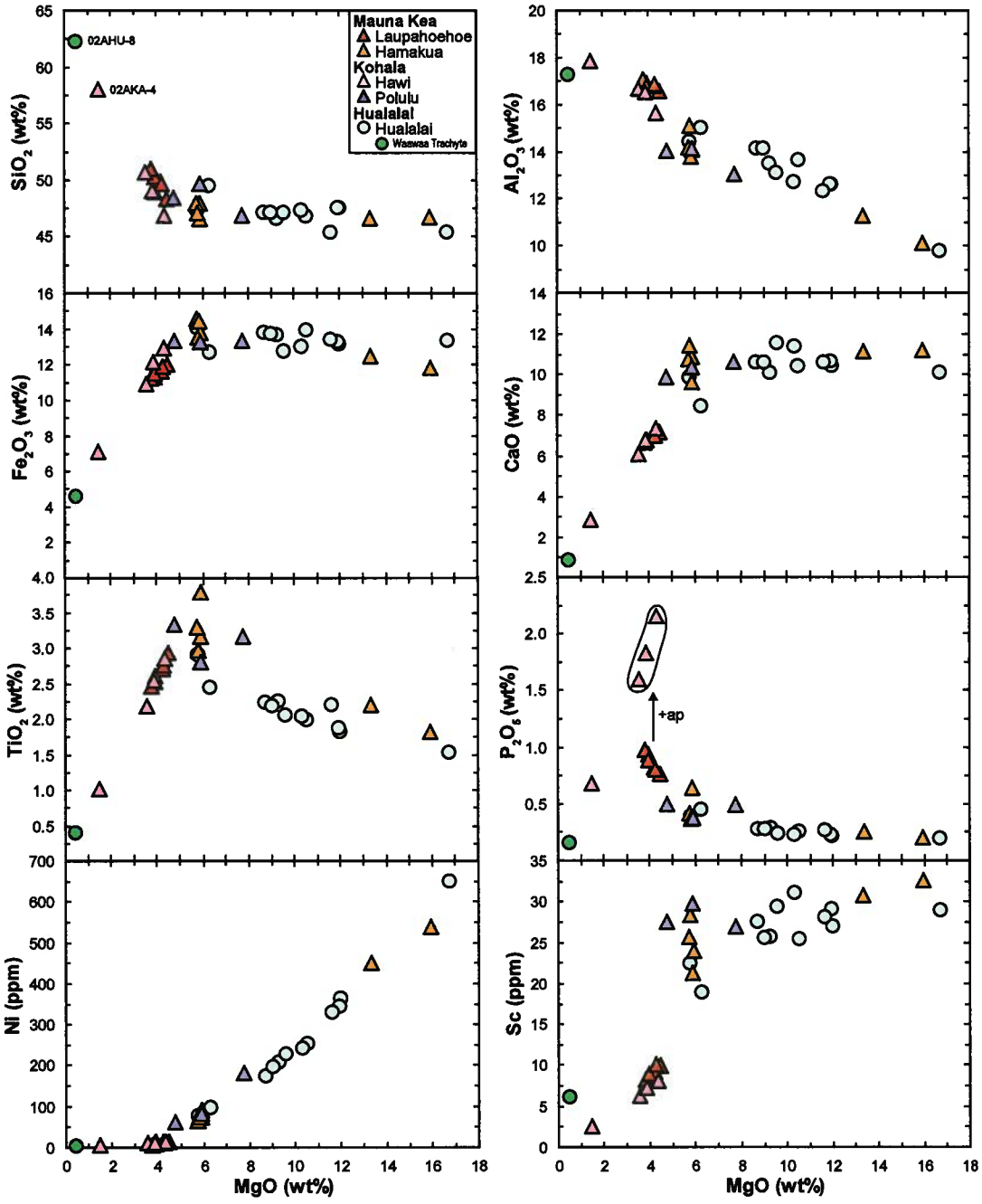

Figure 3.3: MgO variation diagrams of selected major element oxides and compatible trace elements for the Hawaiian post-shield lavas. The transitional/alkalic basalts and alkalic lavas exhibit marked differences in their major element chemistry. The anomalously high P_2O_5 contents of three lavas from the Kohala Hawi Volcanics likely reflect the effects of apatite accumulation.

likely related to accumulated apatite, whereas the low values in the benmoreite and trachyte reflect apatite fractionation.

There are systematic variations in incompatible trace elements with Nb concentration, which ranges between 15-70 ppm for most of the post-shield lavas (Figure 3.4). Abundances of incompatible trace elements are generally well-correlated with Nb, although some subtle differences exist between the transitional/alkalic basalts and alkalic lavas as well as between lavas from each volcano. For example, the Ba and Rb abundances of basalts from Hualalai define a separate, steeper trend than the other post-shield lavas. The alkalic lavas from Kohala are also distinct, being shifted to slightly lower Zr and higher La and Ce concentrations. The elevated Y and Sr concentrations (~60 ppm Y; ~1800 ppm Sr) in the three of these lavas from Kohala are consistent with accumulated apatite. The trachyte from Hualalai (140 ppm Nb) has anomalous trace element contents, including extremely low Sr (37 ppm) and Ba (281 ppm) concentrations that are indicative of extensive feldspar (+ apatite) fractionation.

Chondrite-normalized rare earth element (REE) patterns for the post-shield lavas are smooth with relatively steep slopes (La_N/Yb_N = 6.0-16.2), reflecting enrichment in the light REE (Figure 3.5). The overall patterns are similar, but show variations in the REE concentrations between samples from each volcano. The alkalic lavas from Kohala have the highest REE abundances (e.g., La = 215-340 times chondrites), and the transitional/alkalic basalts from Mauna Kea and Hualalai have the lowest abundances (e.g., La = 50-95 times chondrites). The REE pattern of the trachyte from Hualalai is distinctive, showing enrichment in the light and heavy REE relative to the middle REE, and a small negative Eu anomaly.

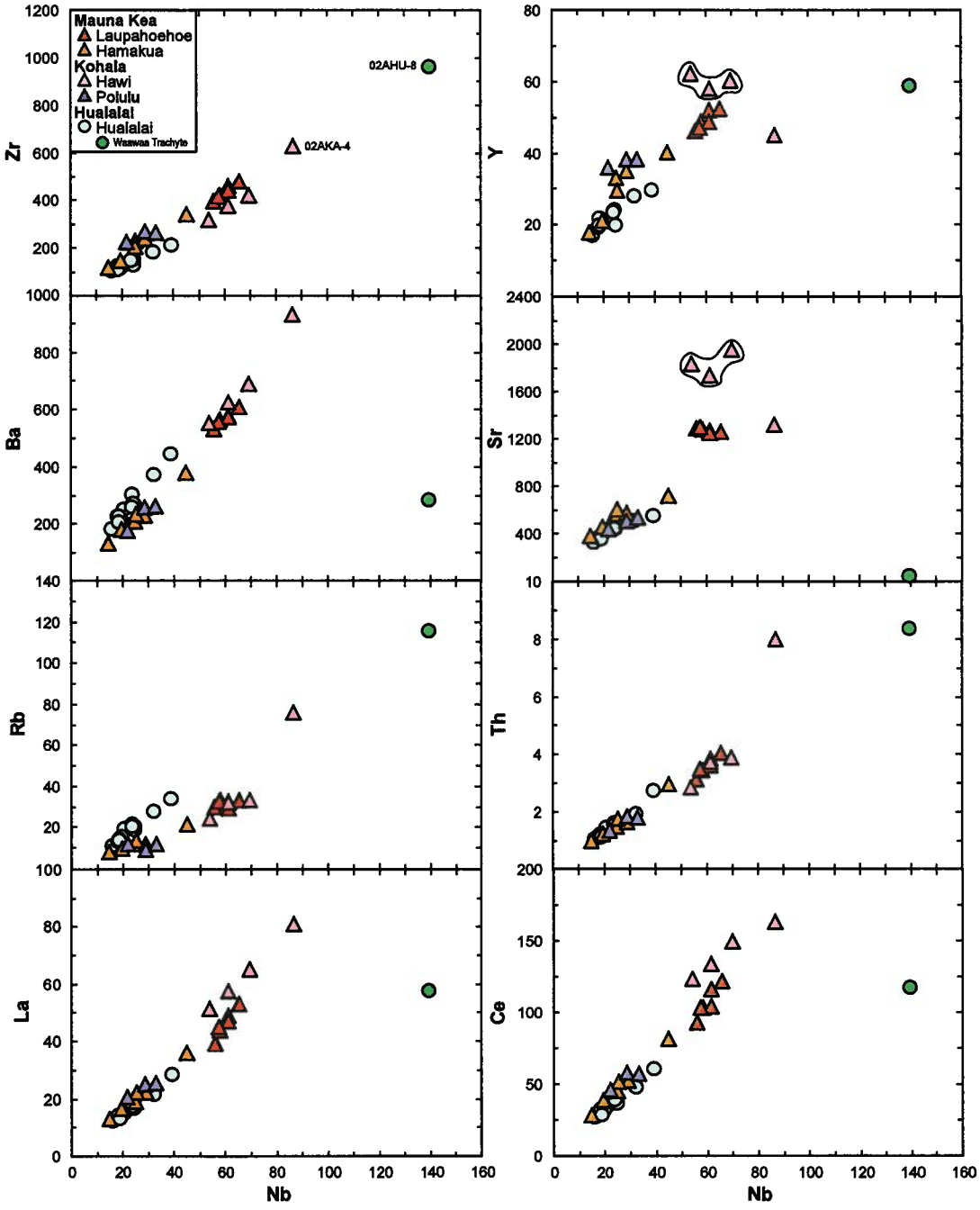

Figure 3.4: Nb variation diagrams of selected trace elements (in ppm) for the Hawaiian post-shield lavas. Positive correlations with Nb are observed, as well as subtle variations in lavas from Hualalai and Kohala. The three Kohala lavas with elevated Y and Sr concentrations have accumulated apatite.

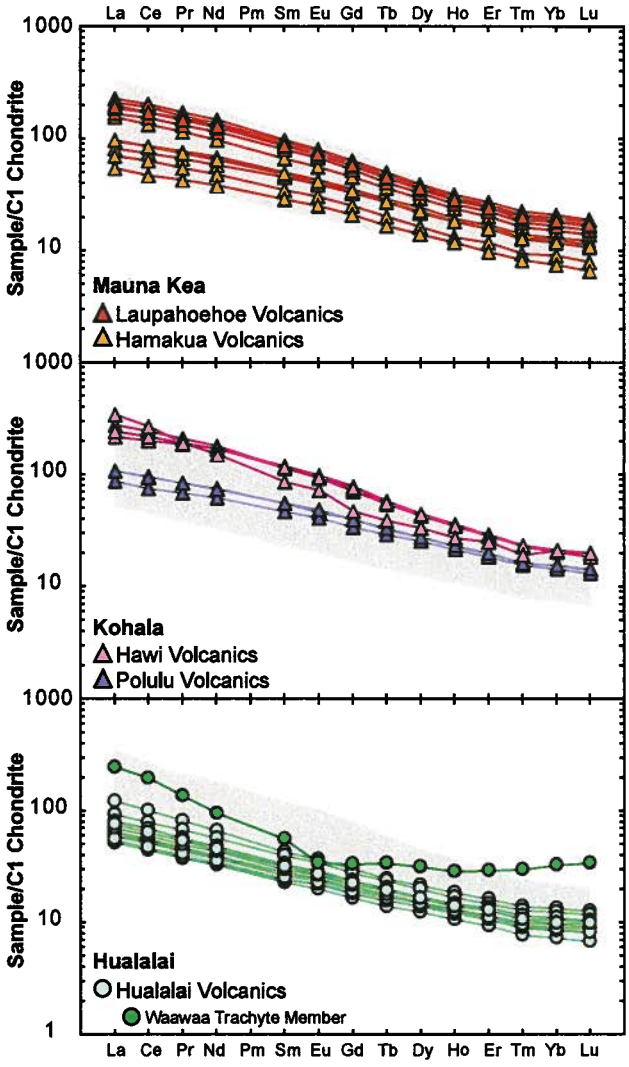

Figure 3.5: Chondrite-normalized rare earth element abundances of the Hawaiian post-shield lavas. Normalizing values from *McDonough and Sun* [1995]. The shaded field in each panel encompasses the range of values from all three volcanoes (excluding the trachyte from Hualalai).

Primitive mantle-normalized patterns for the post-shield lavas show a prominent negative Pb anomaly, as well as enrichment in the light REE and high field strength elements, but with a distinctive convex-down shape defined by lower U, Th, and especially Cs (Figure 3.6). The positive Rb anomaly and the negative Ba, Sr, and Eu anomalies in the trachyte from Hualalai reflect the effects of extensive feldspar (+ apatite) fractionation. The trachyte also has elevated Zr and Hf abundances signalling the presence of accumulated zircon. At Mauna Kea, the alkalic lavas from the late post-shield sub-stage (Laupahoehoe Volcanics) have higher trace element abundances than basalts from the early post-shield sub-stage (Hamakua Volcanics). Similarly, at Kohala, the post-shield alkalic lavas (Hawi Volcanics) are more enriched than the late-shield basalts (Polulu Volcanics). Collectively, the post-shield lavas are significantly more enriched in incompatible trace elements relative to typical shield-stage tholeiites (Figure 3.6), and demonstrate a systematic trend of trace element enrichment as each volcano evolves though the shield and post-shield stages.

3.4.2 Sr-Nd-Hf-Pb isotopic compositions

The majority of the post-shield lavas are characterized by a relatively limited range of Sr, Nd, and Hf isotopic compositions ($^{87}Sr/^{86}Sr$ = ~0.70345-0.70365; $^{143}Nd/^{144}Nd$ = ~0.51292-0.51302; $^{176}Hf/^{177}Hf$ = ~0.28311-0.28314) (Figure 3.7). In contrast, the Pb isotopic compositions of the post-shield lavas range to a greater extent (e.g., $^{206}Pb/^{204}Pb$ = ~17.9-18.45) and show a clear separation between the Kea-trend (Mauna Kea and Kohala) and Loa-trend (Hualalai) volcanoes. The transitional/alkalic basalts and alkalic lavas from Mauna Kea and Kohala, which are clearly distinguished by their major and trace element chemistry, also exhibit differences in their Sr and Pb isotopic compositions (Figure 3.7).

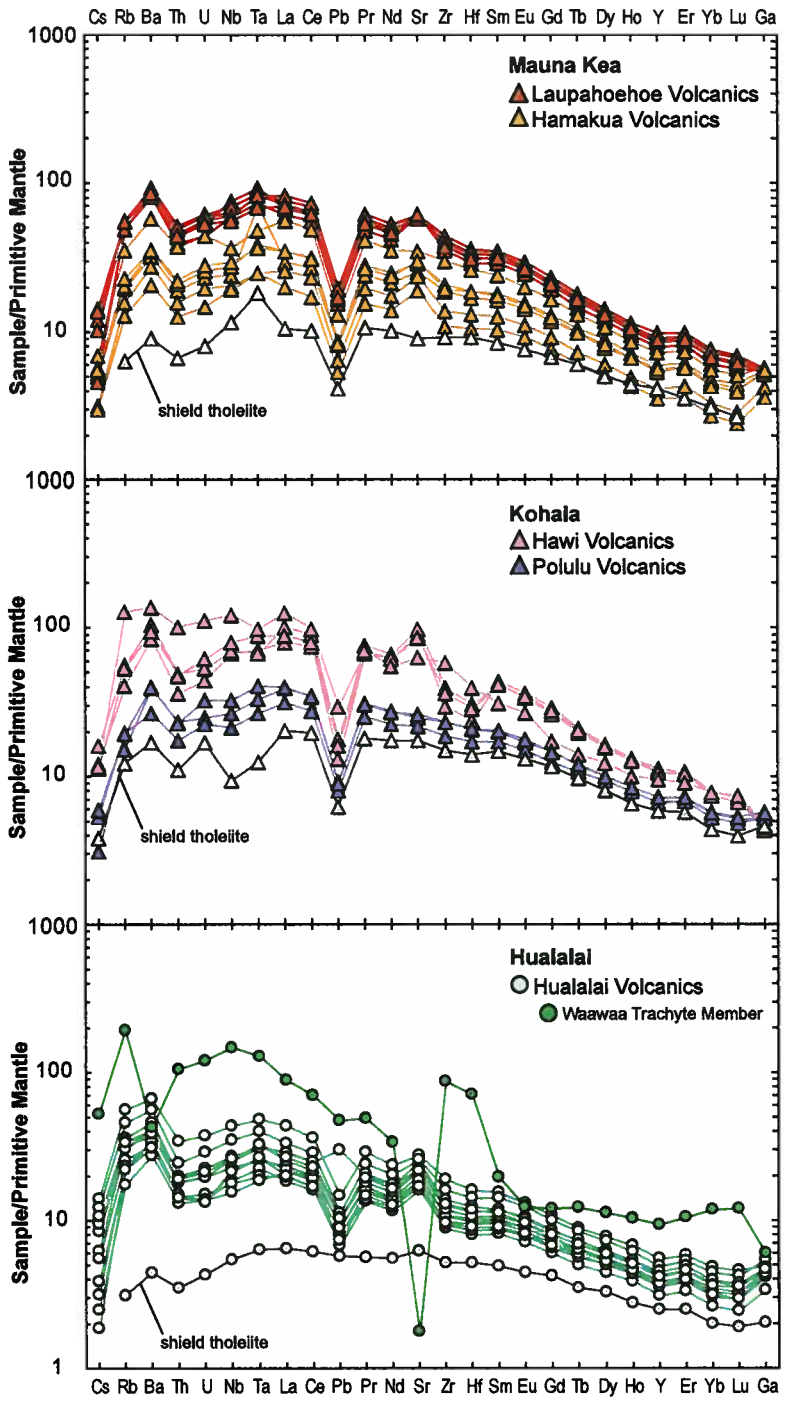

Figure 3.6: Primitive mantle-normalized incompatible trace element abundances of the Hawaiian post-shield lavas. Element compatibility increases from left to right and the normalizing values are from *McDonough and Sun* [1995]. The post-shield lavas are more enriched in incompatible trace elements compared to representative shield-stage tholeiitic basalts from each volcano: Mauna Kea tholeiite, *Huang and Frey* [2005]; Kohala and Hualalai tholeiites, this study.

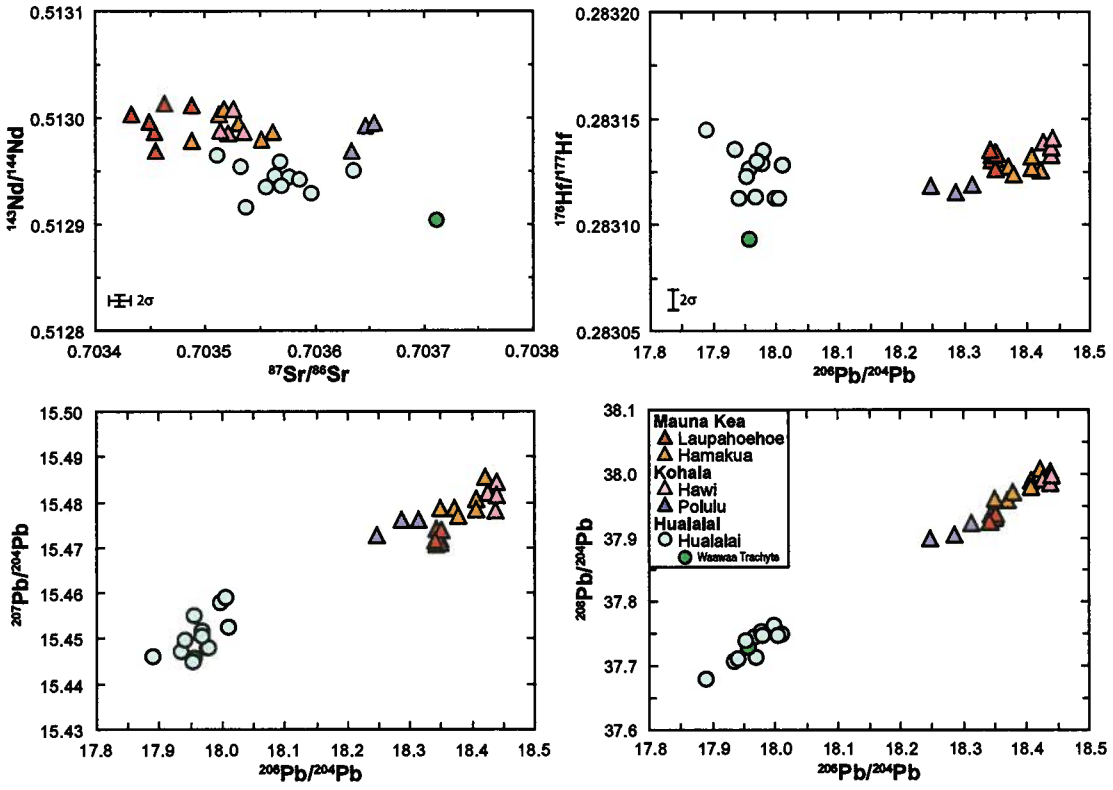

Figure 3.7: Isotopic (Sr-Nd-Pb-Hf) co-variation diagrams of the Hawaiian post-shield lavas. Representative 2σ error bars for Sr, Nd, and Hf are indicated; for Pb, the error bars are smaller than the symbol sizes. The samples are characterized by a limited range of Sr, Nd, and Hf isotopic compositions, but vary widely with respect to Pb. The post-shield lavas from Hualalai have distinctly less radiogenic Pb isotope ratios than those from Mauna Kea and Kohala. Despite overlapping Nd and Hf isotopic compositions, the younger lavas from Mauna Kea and Kohala can be distinguished from older lavas from each volcano by their Sr and Pb isotopic compositions.

The trachyte from Hualalai has higher Sr and slightly lower Nd and Hf isotopic compositions ($^{87}Sr/^{86}Sr = 0.70371$; $^{143}Nd/^{144}Nd = 0.51290$; $^{176}Hf/^{177}Hf = 0.28309$) than the other post-shield lavas, but does not have a distinctive Pb isotopic composition. The youngest sample in this study (710 years; Waha Pele, Hualalai) has the highest Hf and lowest Pb isotopic compositions of the post-shield lavas.

The post-shield lavas as a group lie towards the more depleted (i.e., low $^{87}Sr/^{86}Sr$, high $^{143}Nd/^{144}Nd$, high $^{176}Hf/^{177}Hf$) end of the Hawaiian array in Nd-Sr and Hf-Nd diagrams (Figure 3.8). Post-shield lavas from Mauna Kea and Kohala have Sr, Nd, and Hf isotopic compositions that are consistent with shield stage lavas from Mauna Kea, Kilauea, and West Maui. In contrast, post-shield lavas from Hualalai are shifted to slightly lower $^{87}Sr/^{86}Sr$ and higher $^{176}Hf/^{177}Hf$ compared to other Loa-trend volcanoes (e.g., Mauna Loa), having values more similar to Kea-trend volcanoes and plotting above the ε_{Hf}–ε_{Nd} Hawaiian array.

Post-shield lavas from Hualalai have some of the least radiogenic Pb isotopic compositions ($^{208}Pb/^{204}Pb = 37.67$; $^{206}Pb/^{204}Pb = 17.89$) observed in recent (<5 Ma) Hawaiian lavas and do not overlap with any Loa- or Kea- trend volcano in Hf-Pb and Sr-Pb diagrams (Figures 3.9 and 3.10). Shield and late-shield lavas from Kohala have the least radiogenic Pb isotopic compositions of any Kea-trend volcano, whereas the post-shield lavas have higher $^{206}Pb/^{204}Pb$ values that are more characteristically Kea-like, consistent with shield lavas from Mauna Kea, Kilauea, and West Maui. Post-shield lavas from Mauna Kea extend to less radiogenic $^{206}Pb/^{204}Pb$ and $^{87}Sr/^{86}Sr$ than most shield lavas from Kea-trend volcanoes, similar to the trend observed in lavas from West Maui.

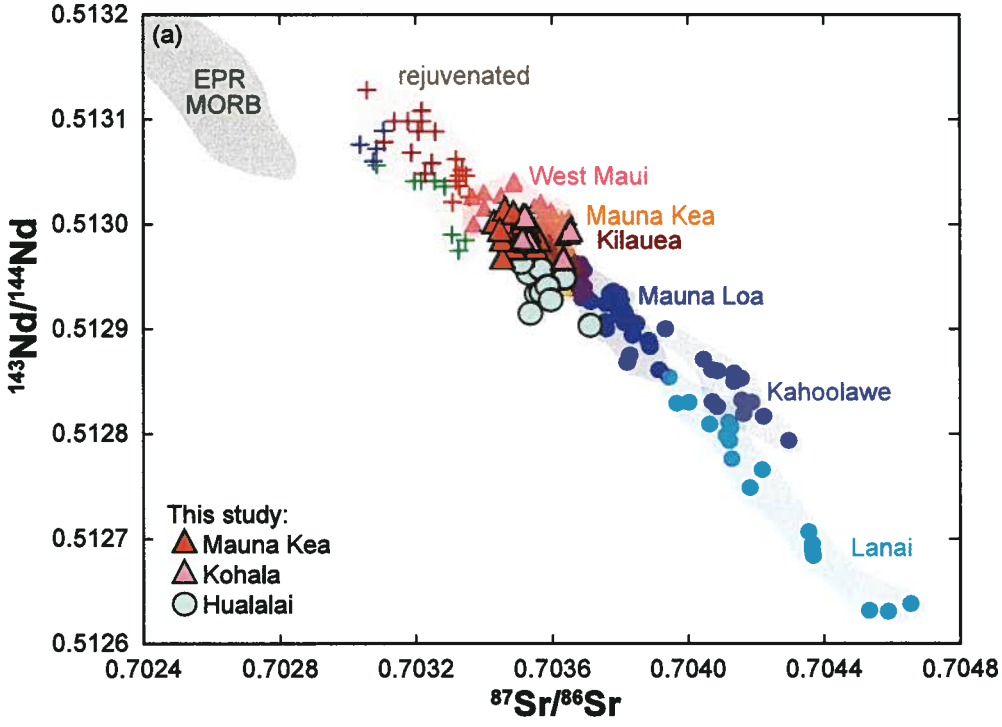
(a)
EPR MORB
rejuvenated
West Maui
Mauna Kea
Kilauea
Mauna Loa
Kahoolawe
Lanai
This study:
Mauna Kea
Kohala
Hualalai
0.5132
0.5131
0.5130
0.5129
0.5128
0.5127
0.5126
143Nd/144Nd
0.7024
0.7028
0.7032
0.7036
0.7040
0.7044
0.7048
87Sr/86Sr

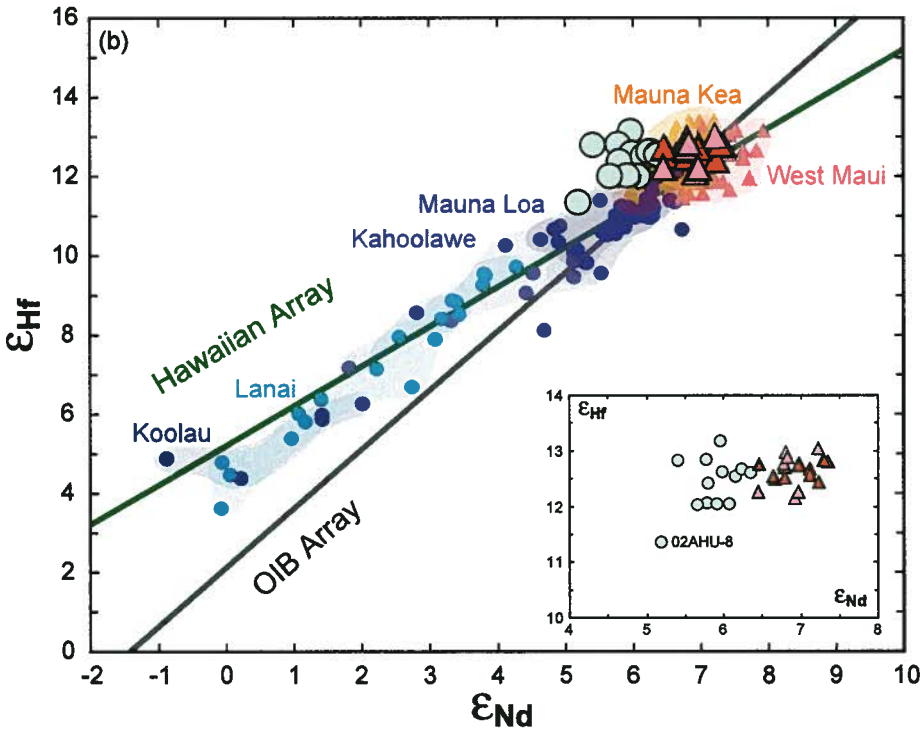
(b)
Mauna Kea
West Maui
Mauna Loa
Kahoolawe
Hawaiian Array
Lanai
Koolau
OIB Array
02AHU-8
εHf
εNd
16
14
12
10
8
6
4
2
0
-2
-1
0
1
2
3
4
5
6
7
8
9
10

Figure 3.8

Figure 3.8: (a) $^{143}Nd/^{144}Nd$ vs. $^{87}Sr/^{86}Sr$ and (b) ε_{Hf} vs. ε_{Nd} for the post-shield lavas from Mauna Kea, Kohala, and Hualalai compared to selected Hawaiian shield stage lavas. Loa-trend volcanoes are represented by circles and Kea-trend volcanoes are represented by triangles. The 2σ error bars are smaller than the symbol sizes. Also shown in (a) are fields for Hawaiian rejuvenated stage lavas (Haleakala, West Maui, East Molokai, Oahu, Kauai, North Arch) and East Pacific Rise mid-ocean ridge basalts (EPR MORB). The Hawaiian and OIB arrays in (b) are from *Blichert-Toft et al.* [1999]. Data sources: Loihi - *Blichert-Toft et al.* [1999], *Abouchami et al.* [2005]; Mauna Loa - *Blichert-Toft et al.* [2003], D. Weis, unpublished data; Hualalai - D. Weis, unpublished data; Kahoolawe - *Blichert-Toft et al.* [1999], *Abouchami et al.* [2005], *Huang et al.* [2005]; Lanai - *Abouchami et al.* [2005], *Gaffney et al.* [2005]; Koolau - *Blichert-Toft et al.* [1999], *Abouchami et al.* [2005]; Kilauea - *Blichert-Toft et al.* [1999], *Abouchami et al.* [2005]; Mauna Kea - *Blichert-Toft et al.* [2003], *Eisele et al.* [2003], *Bryce et al.* [2005]; Kohala - *Feigenson et al.*, 1983, *Abouchami et al.* [2005], M. Garcia, unpublished data, D. Weis, unpublished data; Haleakala - *West and Leeman* [1987], *Chen et al.* [1990], *Chen et al.* [1991], *Blichert-Toft et al.* [1999]; West Maui - *Gaffney et al.* [2004]; East Molokai - *Xu et al.* [2005]; Oahu - *Reiners and Nelson* [1998]; Kauai - *Reiners and Nelson* [1998], *Lassiter et al.* [2000]; North Arch - *Frey et al.* [2000]; EPR MORB - *Niu et al.* [1999], *Regelous et al.* [1999], *Castillo et al.* [2000].

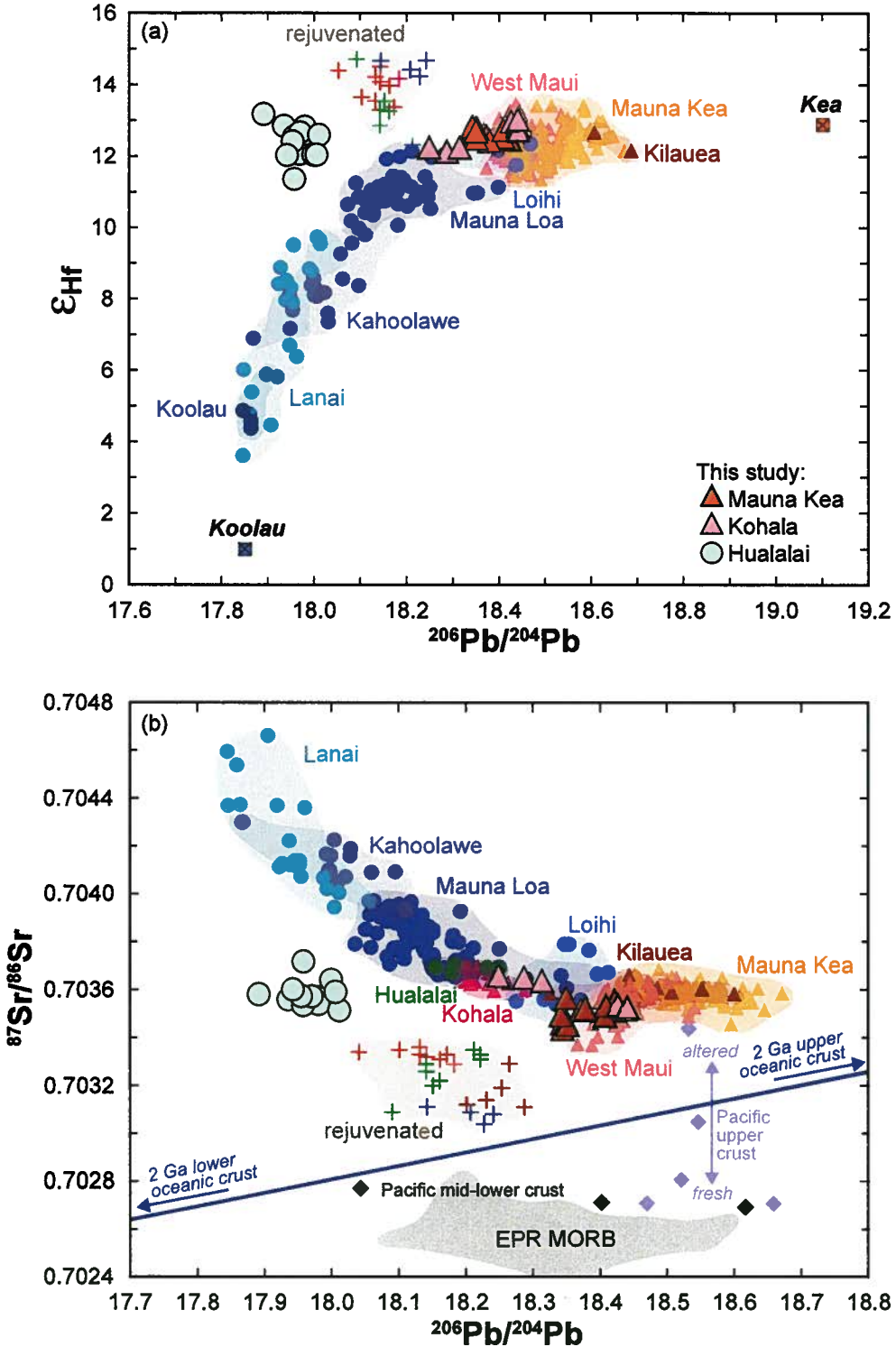
(a)
rejuvenated
West Maui
Mauna Kea
Kea
Kilauea
Loihi
Mauna Loa
Kahoolawe
Lanai
Koolau
Koolau
This study:
Mauna Kea
Kohala
Hualalai
εHf
206Pb/204Pb
(b)
Lanai
Kahoolawe
Mauna Loa
Loihi
Kilauea
Mauna Kea
Hualalai
Kohala
West Maui
altered
2 Ga upper oceanic crust
rejuvenated
Pacific upper crust
2 Ga lower oceanic crust
Pacific mid-lower crust
fresh
EPR MORB
87Sr/86Sr
206Pb/204Pb

Figure 3.9

Figure 3.9: (a) ε_{Hf} vs. $^{206}Pb/^{204}Pb$ and (b) $^{87}Sr/^{86}Sr$ vs. $^{206}Pb/^{204}Pb$ for the post-shield lavas from Mauna Kea, Kohala, and Hualalai compared to Hawaiian shield and rejuvenated stage lavas. The hypothetical Kea and Koolau end members in (a) are from *Blichert-Toft et al.* [1999]. In (b) the field for EPR MORB and isotopic compositions of the Pacific mid-lower crust (gabbroic xenoliths, Hualalai: *Lassiter and Hauri* [1998]) and Pacific upper crust (fresh to altered basalts, ODP Site 843: *King et al.* [1993]) are shown for comparison. For the Pacific crust, unleached and measured isotopic ratios were used. The blue line in (b) represents a mixing line between the 2 Ga lower and upper oceanic crust end-members from *Gaffney et al.* [2004]. Symbols and data sources are the same as in Figure 3.8.

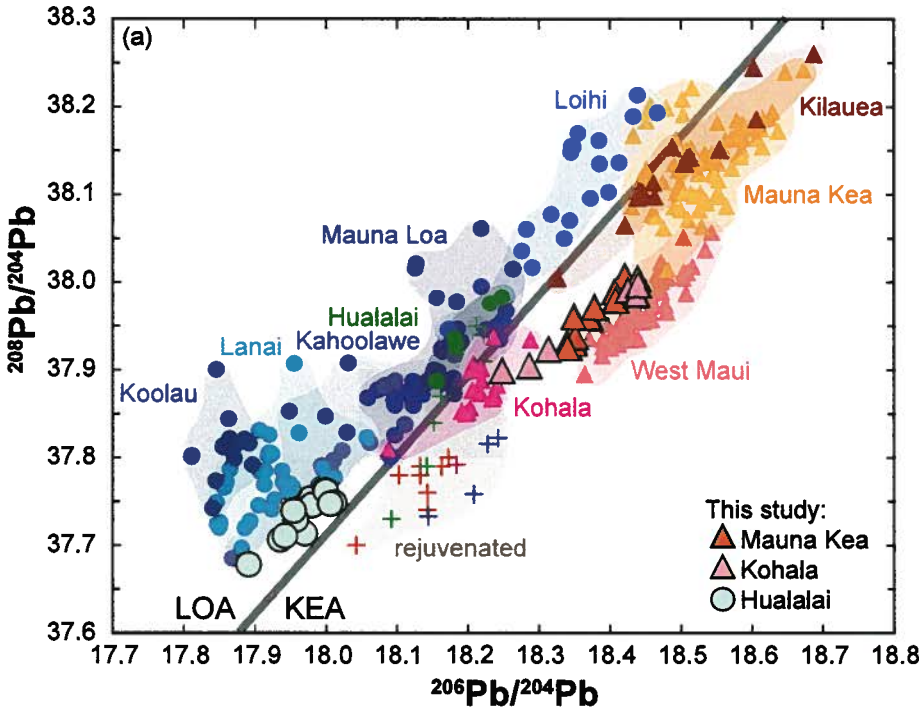
(a)
Loihi
Kilauea
Mauna Kea
Mauna Loa
Hualalai
Kahoolawe
Lanai
Koolau
West Maui
Kohala
rejuvenated
LOA
KEA
This study:
Mauna Kea
Kohala
Hualalai
$^{208}Pb/^{204}Pb$
$^{206}Pb/^{204}Pb$
38.3
38.2
38.1
38.0
37.9
37.8
37.7
37.6
17.7
17.8
17.9
18.0
18.1
18.2
18.3
18.4
18.5
18.6
18.7
18.8

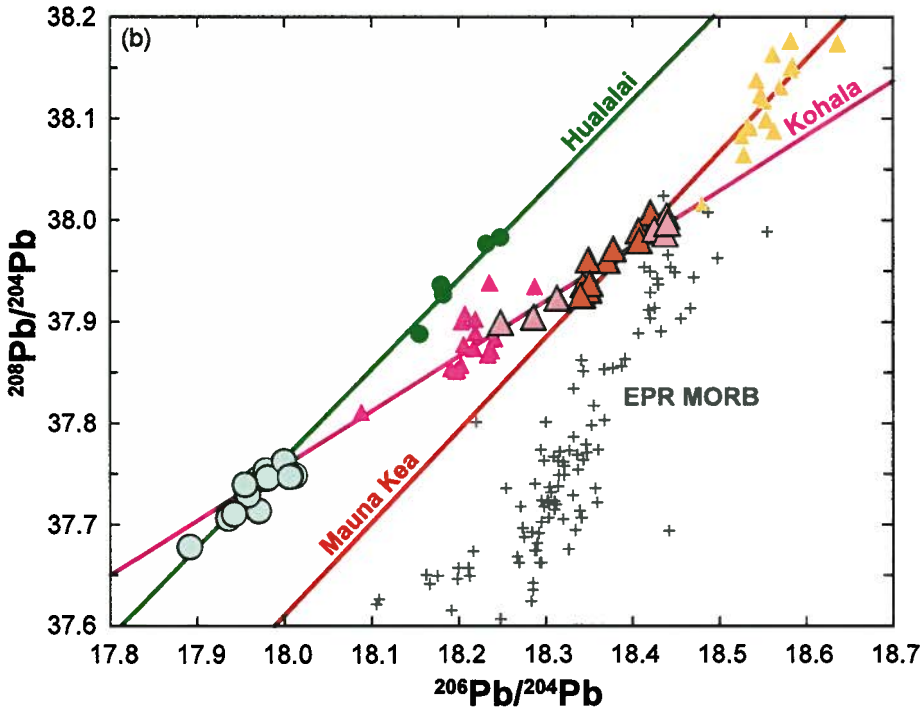
(b)
Hualalai
Kohala
EPR MORB
Mauna Kea
$^{208}Pb/^{204}Pb$
$^{206}Pb/^{204}Pb$
38.2
38.1
38.0
37.9
37.8
37.7
37.6
17.8
17.9
18.0
18.1
18.2
18.3
18.4
18.5
18.6
18.7

Figure 3.10

Figure 3.10: $^{208}Pb/^{204}Pb$ vs. $^{206}Pb/^{204}Pb$ for the post-shield lavas from Mauna Kea, Kohala, and Hualalai compared to Hawaiian shield and rejuvenated stage lavas. The thick grey line in (a) represents the Loa-Kea Pb isotopic division defined by *Abouchami et al.* [2005]. In (b) the isotopic compositions of EPR MORB and shield stage lavas from Mauna Kea, Kohala, and Hualalai are shown for comparison. For Mauna Kea, only shield stage samples from to the "lo8" array of HSDP-2 [*Eisele et al.*, 2003] are included. The thin lines in (b) are regression lines through shield and post-shield lavas from the same volcano. Symbols and data sources are the same as in Figure 3.8.

3.5 DISCUSSION

3.5.1 Sr-Nd-Pb-Hf isotope systematics of Hawaiian lavas

The isotopic variability observed within individual Hawaiian volcanoes and between volcanoes on the scale of the entire Hawaiian chain is used to infer the compositional characteristics of their mantle source region. Specifically, the change in the isotopic compositions of lavas during the critical transition from the shield to post-shield stage, and the relationship of the post-shield lavas to the inferred isotopic mixing trends defined by shield lavas, provides constraints on the geochemical structure of the plume and the sources of Hawaiian lavas. Pb isotopes in particular are one of the most powerful isotopic tracers and have a demonstrated ability in identifying heterogeneities and source components associated with the Hawaiian plume [e.g., *Eisele et al.*, 2003; *Abouchami et al.*, 2005; *Fekiacova et al.*, 2007; *Marske et al.*, 2007].

3.5.1.1 Shield to post-shield transition

Lavas erupted during different growth stages (i.e., pre-shield, shield, post-shield, rejuvenated) of a Hawaiian volcano have distinct geochemical characteristics. Post-shield alkalic capping lavas at Haleakala volcano have higher incompatible element abundance ratios (e.g., Ba/La, Nb/La, La/Yb) than underlying shield tholeiites, as well as higher $^{143}Nd/^{144}Nd$ and lower $^{87}Sr/^{86}Sr$ [*Chen and Frey*, 1985]. Geochemical changes associated with the transition to the post-shield stage have also been documented at other Hawaiian volcanoes, including East and West Molokai [*Xu et al.*, 2005; *Xu et al.*, 2007] and Kauai [*Swinnard et al.*, in preparation, 2008].

At Mauna Kea, Hualalai, and Kohala, the enriched trace element characteristics of post-shield lavas compared to their respective shield lavas (Section 3.4.1) are accompanied by slightly lower $^{87}Sr/^{86}Sr$ as well as by marked changes in Pb isotopic compositions (Figures 3.9b and 3.11). Lavas from Mauna Kea show a systematic shift from their most radiogenic Pb isotope ratios during the shield stage to less radiogenic values during the early basaltic post-shield substage to the lowest values yet observed at Mauna Kea ($^{208}Pb/^{204}Pb$ = 37.93; $^{206}Pb/^{204}Pb$ = 18.34) during the late hawaiitic post-shield substage. Similarly, post-shield lavas from Hualalai are significantly less radiogenic in Pb than the shield tholeiites. In contrast, at Kohala, late-shield lavas are more radiogenic in Pb than most shield tholeiites, and the post-shield lavas have distinctly more radiogenic Pb isotopic compositions.

Shield and post-shield lavas from the same volcano form linear correlations in Pb-Pb isotope diagrams (Figure 3.10b). Given that these linear arrays are best interpreted as binary mixing lines (rather than isochrons) [e.g., *Abouchami et al.*, 2000; *Eisele et al.*, 2003; *Abouchami et al.*, 2005], this indicates that shield and post-shield lavas may be derived from common source components mixed in variable proportions. Therefore, with respect to Pb, a greater contribution from a less radiogenic end-member is required during the post-shield stage at Mauna Kea and Hualalai, whereas at Kohala, a more radiogenic end-member dominates the post-shield stage (Figure 3.11). However, the Pb-Pb arrays of Mauna Kea and Hualalai are sub-parallel and suggest that two separate unradiogenic (lower $^{208}Pb/^{204}Pb$ and $^{206}Pb/^{204}Pb$) end-members are required. The temporal Pb isotope variations, combined with the distinct Sr, Nd, and Hf isotopic compositions of the post-shield lavas, correspond to a systematic change in the proportions of discrete components sampled by each volcano during the post-shield stage.

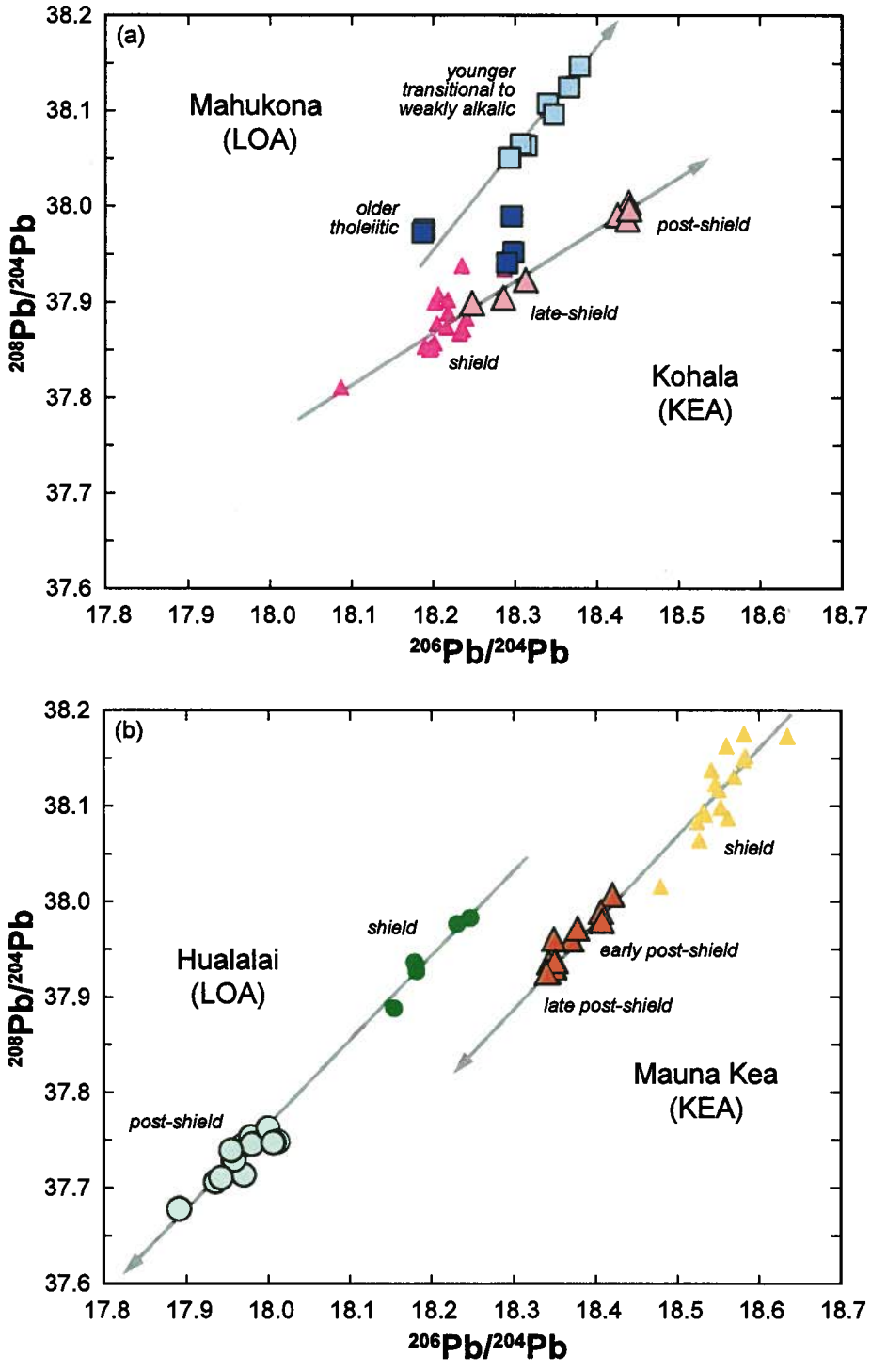
(a)
Mahukona
(LOA)
younger
transitional to
weakly alkalic
older
tholeiitic
post-shield
late-shield
shield
Kohala
(KEA)
(b)
Hualalai
(LOA)
shield
post-shield
shield
early post-shield
late post-shield
Mauna Kea
(KEA)
208Pb/204Pb
206Pb/204Pb
38.2
38.1
38.0
37.9
37.8
37.7
37.6
17.8
17.9
18.0
18.1
18.2
18.3
18.4
18.5
18.6
18.7

Figure 3.11

Figure 3.11: $^{208}Pb/^{204}Pb$ vs. $^{206}Pb/^{204}Pb$ for shield and post-shield lavas from consecutive pairs of Hawaiian volcanoes: (a) Mahukona and Kohala and (b) Hualalai and Mauna Kea. For Mauna Kea, only shield stage samples from to the "lo8" array of HSDP-2 [*Eisele et al.*, 2003] are included. The grey arrows show the temporal geochemical trend from the shield to post-shield stage and point towards a hypothetical end-member. Symbols and data sources are the same as in Figure 3.8, except for Mahukona [Appendix B1; *Garcia et al.*, in preparation, 2008].

3.5.1.2 Mixing relationships

The compositional variability in Hawaiian shield stage lavas requires the existence of at least three isotopically distinct components, referred to as Loihi, Koolau, and Kea [e.g., *Staudigel et al.*, 1984; *Stille et al.*, 1986; *West et al.*, 1987; *Eiler et al.*, 1996; *Hauri*, 1996]. However, principal component analysis of Sr, Nd, Pb, He, and O isotope ratios in Hawaiian shield lavas indicates that almost 90% of the variation can be explained by mixing between the Koolau and Kea end-members [*Eiler et al.*, 1996]. The Koolau end-member has the highest $^{87}Sr/^{86}Sr$, and lowest $^{143}Nd/^{144}Nd$, $^{176}Hf/^{177}Hf$, and Pb isotope ratios and is best expressed in lavas from Koolau and other Loa-trend volcanoes. The Koolau source is thought to contain recycled oceanic crust and pelagic sediments [e.g., *Lassiter and Hauri*, 1998; *Blichert-Toft et al.*, 1999]. In contrast, the Kea end-member is characterized by the lowest $^{87}Sr/^{86}Sr$, and highest $^{143}Nd/^{144}Nd$, $^{176}Hf/^{177}Hf$, and Pb isotope ratios and is best expressed in lavas from Mauna Kea and other Kea-trend volcanoes. The origin of the Kea component is not as well characterized, and has been variously interpreted to be assimilated Pacific Ocean lithosphere, entrained asthenosphere (i.e., MORB-source mantle), or recycled oceanic crust [e.g., *Eiler et al.*, 1996; *Lassiter et al.*, 1996; *Lassiter and Hauri*, 1998]. An important question is whether mixing between the Koolau and Kea end-members can produce the range of isotopic compositions observed in post-shield lavas from Mauna Kea, Hualalai, and Kohala.

In ε_{Hf} – $^{206}Pb/^{204}Pb$ and $^{87}Sr/^{86}Sr$ – $^{206}Pb/^{204}Pb$ diagrams (Figure 3.9), Hawaiian shield lavas form strongly concave hyperbolic mixing trends between the Kea and Koolau end-members, which are thus inferred to have very different Hf/Pb and Sr/Pb abundance ratios [*Blichert-Toft et al.*, 1999; *Huang et al.*, 2005]. Importantly, both late- and post-shield lavas

from Kohala lie within the Hawaiian shield mixing hyperbola. In contrast, post-shield lavas from Hualalai are displaced to higher $^{176}Hf/^{177}Hf$ and lower $^{87}Sr/^{86}Sr$ and $^{206}Pb/^{204}Pb$ than expected from mixing between the Koolau and Kea end-members, and do not lie within the mixing hyperbola. Post-shield lavas from Mauna Kea deviate slightly from the Sr-Pb hyperbola, showing a weakly positive correlation that is oblique to the shield trend and extends towards less radiogenic Sr and Pb isotopic compositions (Figure 3.9b).

The isotopic compositions of post-shield lavas from Hualalai and Mauna Kea therefore cannot be explained by binary mixing between the Koolau and Kea end-members. Specifically, the unradiogenic Pb isotopic compositions of post-shield Hualalai lavas and the positive Sr-Pb correlation defined by post-shield Mauna Kea lavas preclude their generation from these two end-members. In addition, the Nd and Hf isotopic compositions of the post-shield lavas define a separate trend with a shallower slope than either the OIB or Hawaiian arrays (Figure 3.8b), indicating a source with higher $^{176}Hf/^{177}Hf$ for a given $^{143}Nd/^{144}Nd$. The observed isotope systematics require a contribution from at least one additional source component with relatively unradiogenic $^{87}Sr/^{86}Sr$ and $^{206}Pb/^{204}Pb$ (and possibly also more radiogenic $^{176}Hf/^{177}Hf$) that is not expressed in Hawaiian shield stage lavas.

3.5.2 Constraints on the origin and extent of depleted components in Hawaiian lavas

Most ocean island basalts are characterized by enriched geochemical signatures, but some also commonly contain trace element abundances and isotope ratios with compositional similarities to MORB (i.e., $La/Sm_N < 1$; high $^{143}Nd/^{144}Nd$ and $^{176}Hf/^{177}Hf$, and low $^{87}Sr/^{86}Sr$ compared to primitive mantle). These depleted signatures have been observed in a number of hotspot settings, including Iceland, Kerguelen, Galapagos, and Hawaii [e.g.,

Blichert-Toft and White, 2001; *Doucet et al.*, 2002; *Fitton et al.*, 2003; *Mukhopadhyay et al.*, 2003; *Frey et al.*, 2005]. In Hawaii, however, lavas with depleted isotope ratios are associated with enriched rather than depleted trace element abundances. In particular, the combination of low $^{87}Sr/^{86}Sr$ and high $^{143}Nd/^{144}Nd$ with high Rb/Sr and low Sm/Nd is a paradox that remains largely unresolved.

3.5.2.1 The role of oceanic lithosphere: Ambient Pacific crust or recycled plume component?

The origin of depleted components in Hawaiian lavas and at other ocean islands is the subject of continued debate. The depleted isotopic compositions are commonly attributed to assimilation of the underlying oceanic crust or entrained shallow asthenosphere (i.e., MORB-source mantle) [e.g., *Chen and Frey*, 1985; *Gaffney et al.*, 2004]. To explain the enrichment in trace elements, these models generally invoke a source recently enriched (i.e., metasomatized) in incompatible trace elements [e.g., *Yang et al.*, 2003; *Shafer et al.*, 2005] or very small degree melts (0.1-1%) of a depleted source [e.g., *Chen and Frey*, 1985]. In contrast, other studies argue that the depleted signatures are derived from within the plume itself or from entrained mantle material [e.g., *Frey et al.*, 2005; *Fekiacova et al.*, 2007]. In these models, the depleted material is ancient oceanic lithosphere (and sediments) that have been subducted, stored at the base of the mantle, and recycled into the upwelling plume. We investigate whether any of these sources could serve as a suitable end-member for the low-$^{87}Sr/^{86}Sr$, low-$^{206}Pb/^{204}Pb$ compositions observed in post-shield lavas from Hualalai and Mauna Kea.

Basalts from ODP Site 843, located 320 km west of the island of Hawaii, are representative of the ambient ~110 Ma Pacific upper oceanic crust [*King et al.*, 1993]. Gabbroic xenoliths from the 1800-1801 Kaupuhuehue flow on Hualalai are inferred to represent the Pacific mid-lower oceanic crust [*Lassiter and Hauri*, 1998]. Fresh Pacific upper crust, Pacific mid-lower crust, and EPR MORB have the low $^{87}Sr/^{86}Sr$ required of an end-member (Figure 3.9b). However, the $^{206}Pb/^{204}Pb$ of these sources, especially the Pacific upper crust, is too radiogenic to be a plausible depleted end-member for the Hualalai post-shield lavas. Linear Pb-Pb trendlines from Hualalai and Mauna Kea are parallel to and do not intersect the EPR MORB field (Figure 3.10b), providing further evidence against assimilation of MORB-related lithosphere or asthenosphere.

The depleted component sampled by the post-shield lavas is distinct from the depleted MORB source and must therefore be closely related to the Hawaiian plume, either as material within the plume core, or as mantle material that is thermally accreted to the sides of the plume during ascent. Suitable candidates for this depleted source material include ancient recycled oceanic lithosphere and sediments. Preferential removal of the mobile elements U and Rb during subduction dehydration may lead to low U/Pb and Rb/Sr and the development of unradiogenic $^{206}Pb/^{204}Pb$ and $^{87}Sr/^{86}Sr$ [*McCulloch and Gamble*, 1991; *Weaver*, 1991]. Forward modelling of the composition of 2 Ga oceanic lithosphere shows that gabbroic lower oceanic crust evolves to unradiogenic $^{206}Pb/^{204}Pb$ and $^{87}Sr/^{86}Sr$ over time [*Gaffney et al.*, 2004], and could thus account for the Sr and Pb isotopic compositions of the post-shield lavas (Figure 3.9b). Similarly, pelagic sediments develop unradiogenic $^{206}Pb/^{204}Pb$ because of long-term evolution with low U/Pb. The presence of pelagic sediments, which have high Lu/Hf [e.g., *Patchett et al.*, 1984; *Vervoort et al.*, 1999],

could also explain the Hf-Nd isotope systematics of the post-shield lavas (Figure 3.8b). These observations are consistent with the recycling model and provide evidence for ancient lower oceanic crust and sediments in the mantle source of the post-shield lavas.

3.5.2.2 Identification of depleted signatures at other Hawaiian volcanoes

The extent to which depleted components are sampled varies considerably between different volcanoes and is mainly restricted to lavas erupted after the volcano has migrated away from the plume center following the main shield-building stage. The low degrees of partial melting from which such lavas are derived correspond to small volumes within the melting region and may allow for these isotopic signatures to be more readily identified. The trend to low $^{87}Sr/^{86}Sr$ and low $^{206}Pb/^{204}Pb$ observed in post-shield lavas from Mauna Kea has also been found for late-shield and post-shield lavas from West Maui [*Gaffney et al.*, 2004], East Molokai [*Xu et al.*, 2005] and Haleakala [*Chen et al.*, 1991]. The presence of this isotopic signature at four consecutive Kea-trend volcanoes indicates that this depleted component is a persistent feature of the Kea source [*Xu et al.*, 2005]. The isotopic compositions of post-shield lavas from Hualalai represent the first example of a low-$^{87}Sr/^{86}Sr$, low-$^{206}Pb/^{204}Pb$ signature at a Loa-trend volcano. This demonstrates that depleted components are also present in the Loa source and are therefore more widely distributed within the plume than previously thought.

Rejuvenated stage lavas from East Molokai, Oahu, Kauai, and the North Arch Volcanic Field, which have the highest $^{143}Nd/^{144}Nd$ and $^{176}Hf/^{177}Hf$ and lowest $^{87}Sr/^{86}Sr$ of all Hawaiian lavas, have also sampled a depleted component [e.g., *Frey et al.*, 2000; *Lassiter et al.*, 2000; *Xu et al.*, 2005; *Fekiacova et al.*, 2007; *Swinnard et al.*, in preparation, 2008].

However, rejuvenated stage lavas are characterized by a relatively limited range of isotopic compositions and plot almost exclusively on the Kea side of the Pb isotopic boundary [e.g., *Fekiacova et al.*, 2007] (Figure 3.10a). Late-shield lavas from West Maui were interpreted to have a distinct source from Hawaiian rejuvenated lavas [*Gaffney et al.*, 2004], whereas at East Molokai, late-shield/post-shield and rejuvenated lavas were found to contain variable amounts of the same depleted component [*Xu et al.*, 2005]. Post-shield lavas from Mauna Kea trend towards the field for rejuvenated lavas and may thus share a common depleted component. Given that rejuvenated lavas erupt considerably later (~0.25-2 Myr) than post-shield lavas and at a distance significantly further from the plume centre, this depleted component is inferred to be a relatively long-lived feature of the plume. In contrast, post-shield lavas from Hualalai are Loa-like and have Pb isotopic compositions that are too unradiogenic to share a source with the rejuvenated lavas. This indicates sampling of source material at Hualalai that is not expressed at any other Hawaiian volcano and implies that more than one depleted component is present within the plume.

A depleted component is required to explain the isotopic variability observed in shield lavas from Kauai, and may also be present in varying proportion and to a lesser degree at other Hawaiian volcanoes [*Mukhopadhyay et al.*, 2003]. Despite proximity of the plume to a spreading ridge axis, the depleted component that contributed to lavas from the 76-81 Ma Detroit Seamount at the northern end of the Emperor seamount chain is thought to be intrinsic to the Hawaiian plume [*Frey et al.*, 2005]. Thus, the sampling of depleted components is not solely restricted to the late-stages (late-shield/post-shield and rejuvenated) of volcanism or to the recent (<5 Ma) volcanoes of the Hawaiian chain. Instead, these depleted components represent a fundamental part of the Hawaiian plume that

may only be sampled under specific melting conditions or in certain geodynamic settings. For example, melting of a depleted plume component could be facilitated under thin lithosphere [*Regelous et al.*, 2003] or, alternatively, in a secondary melting zone [*Ribe and Christensen*, 1999] or by flexural arch decompression [*Bianco et al.*, 2005], as has been proposed to explain Hawaiian rejuvenated volcanism.

3.5.3 Spatial distribution of heterogeneities in the Hawaiian plume

The geochemical differences between lavas erupted along the Loa and Kea spatial trends are typically explained by two different models for the geochemical structure of the plume beneath Hawaii (Figure 3.12). The concentrically zoned model [e.g., *Hauri*, 1996; *Kurz et al.*, 1996; *Lassiter et al.*, 1996] proposes a plume core with enriched (Loa-type) compositions and an outer margin with more depleted (Kea-type) compositions. In contrast, the Pb isotope systematics of Hawaiian lavas suggest that the plume is bilaterally zoned [*Abouchami et al.*, 2005] into southwest and northeast halves that correspond to Loa and Kea source regions, respectively. Pb isotopes are one of the most reliable discriminants between lavas from the two trends, with Loa volcanoes having higher $^{208}Pb/^{204}Pb$ for a given $^{206}Pb/^{204}Pb$ than Kea volcanoes [*Tatsumoto*, 1978; *Abouchami et al.*, 2005].

3.5.3.1 Horizontal zoning: Constraints from the shield to post-shield transition

The geochemistry of the shield to post-shield transition provides the opportunity to discriminate between the concentrically and bilaterally zoned plume models (Figure 3.12). During the time period corresponding to shield and post-shield volcanism, individual volcanoes traverse the plume conduit from a more central to peripheral location due to the

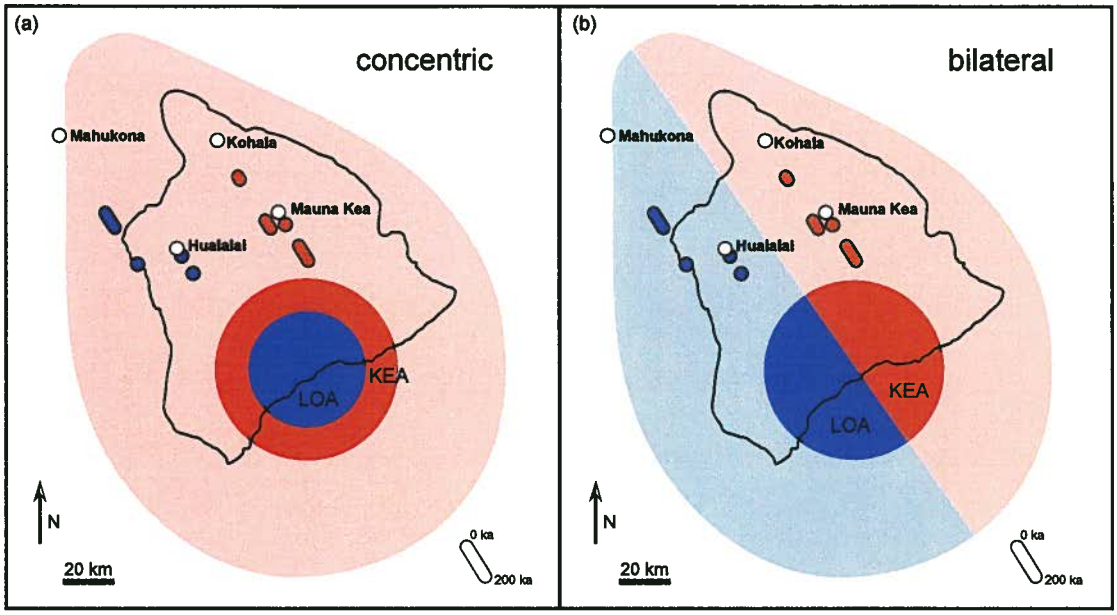

Figure 3.12: Schematic comparison of the two main models for the spatial distribution of Loa and Kea source compositions in the Hawaiian plume: (a) concentric and (b) bilateral zonation. The map of the plume melting region (coloured areas) beneath the island of Hawaii is after *DePaolo et al.* [2001], based on the melt supply models of *DePaolo and Stolper* [1996] and *Ribe and Christensen* [1999]. The outer field represents the lateral extent of the primary melting zone; the darker inner circle corresponds to a melt supply rate of >0.05 cm/yr. In the concentric model (a), Loa source material (blue) is in the core of the plume and Kea source material (red) is restricted to the plume margin [e.g., *Hauri*, 1996; *Kurz et al.*, 1996; *Lassiter et al.*, 1996], whereas in the bilateral model (b), Loa and Kea source material is divided into southwest and northeast sides of the plume, respectively [*Abouchami et al.*, 2005]. Superimposed on the map are the outline of the island of Hawaii and the current summits of Mahukona, Kohala, Hualalai, and Mauna Kea (white circles). Also shown are the summit locations of these volcanoes at the time of eruption of the post-shield lavas (sample/vent locations are omitted for clarity), assuming a Pacific plate velocity of 9 cm/yr. The colour of the paleo-summits corresponds to the isotopic signature of the lavas (blue = Loa-like; red = Kea-like) and show that the post-shield lavas are consistent with a bilaterally zoned plume (b).

motion of the Pacific lithosphere. In a concentrically zoned plume, where Loa-trend volcanoes are inferred to sample the plume centre and Kea-trend volcanoes sample the plume edge, both Loa- and Kea-trend shield volcanoes are predicted to be Kea-like during the post-shield stage. In contrast, in a bilaterally zoned plume, Loa- and Kea-trend volcanoes will retain their initial Loa- and Kea-like geochemical characteristics, respectively.

Post-shield lavas from the Kea-trend volcanoes, Mauna Kea and Kohala, are Kea-like, and post-shield lavas from the Loa-trend Hualalai are Loa-like in their Pb isotopic compositions (Figure 3.10a). Transitional to weakly alkalic basalts from Mahukona, a submerged Hawaiian shield volcano located ~50 km west of Kohala on the Loa spatial trend, likely belong to the early post-shield stage of this volcano and are also Loa-like [Appendix B1; *Garcia et al.*, in preparation, 2008]. The persistence of the Kea and Loa Pb signatures from the shield to post-shield stage at these four Hawaiian volcanoes is inconsistent with the concentric model and strongly supports a bilateral plume zonation (Figure 3.12). However, these observations could also be explained by a concentrically zoned plume that has been distorted in the downstream direction by the movement of the over-riding Pacific lithosphere [*DePaolo et al.*, 2001; *Bryce et al.*, 2005].

Information from the southwest side of the plume is required to differentiate between these two models; Loa-like isotopic compositions to the southwest would support the bilateral model, whereas Kea-like compositions would support the distorted concentric model. Basalts from Penguin Bank, which lies west of the main Hawaiian Ridge (Figure B1), have Loa-like Sr, Nd, and Hf isotopic compositions and Pb isotopic compositions that lie along the Loa-Kea Pb isotopic division [Appendix B2; *Xu et al.*, 2007]. The dominantly

Loa-like isotopic compositions of lavas from Penguin Bank are consistent with a bilateral plume zonation. However, the possibility that an exclusively Kea-like volcano exists further to the southwest (Kaula?) cannot be ruled out.

The oblique Pb-Pb trend of Kohala that crosses the Pb isotopic division (Figure 3.10) reflects sampling of Loa source material by a Kea-trend volcano and indicates that the division between Loa and Kea sources in most plume zoning models is oversimplified. The presence of both Loa and Kea geochemical characteristics within a single Hawaiian volcano has been documented at Mauna Kea [*Eisele et al.*, 2003], Haleakala [*Ren et al.*, 2006], Kilauea [*Marske et al.*, 2007], West Molokai [*Xu et al.*, 2007] and Mahukona [Appendix B1; *Garcia et al.*, in preparation, 2008]. These observations may be explained by the presence of a "mixed" zone within the plume conduit that contains both Loa and Kea source material, or if the division between the two sources fluctuates with time.

3.5.3.2 Vertical heterogeneity: Constraints from consecutive volcano pairs

The previous discussion has assumed a time-invariant geochemical cross-section of the plume conduit. However, the geochemical variability observed in Hawaiian lavas may also be related to vertical heterogeneities within the upwelling plume. Due to the high upwelling velocities (e.g., >1 m/yr) predicted for the Hawaiian plume, the vertical component of heterogeneity cannot be ignored [*Blichert-Toft et al.*, 2003; *Marske et al.*, 2007]. Rather than investigating the temporal evolution of a single volcano, which mainly records a horizontal geochemical gradient across the plume conduit, we compare post-shield lavas from two consecutive pairs of Hawaiian volcanoes: Mahukona-Kohala and Hualalai-Mauna Kea.

Lavas from the older Mahukona and Kohala volcanoes initially have similar isotopic compositions and become more radiogenic in Pb with time (Figure 3.11a). In contrast, lavas from the younger Hualalai and Mauna Kea volcanoes become less radiogenic in Pb during the post-shield stage (Figure 3.11b). Mahukona and Kohala were thus sampling a more enriched (high $^{208}Pb/^{204}Pb$ and $^{206}Pb/^{204}Pb$) source that was present in the melting region of the plume at that time. As these volcanoes migrated away from the plume axis, the mantle continued to rise and was replaced by relatively depleted (low $^{208}Pb/^{204}Pb$ and $^{206}Pb/^{204}Pb$) source material that was subsequently sampled by Hualalai and Mauna Kea. The sampling of isotopically similar source material at another pair of neighbouring volcanoes, Mauna Loa and Kilauea, is thought to have been caused by the passage of a small-scale heterogeneity (either a single body or the plume matrix itself) through their melting regions [*Marske et al.*, 2007]. Although for Mahukona-Kohala and Hualalai-Mauna Kea, the Pb-Pb arrays do not converge to a common composition, the observed Pb isotope systematics provide compelling evidence for a significant component of vertical heterogeneity within the upwelling Hawaiian plume.

3.6 CONCLUSIONS

High-precision trace element concentrations and Sr, Nd, Pb and Hf isotopic compositions of Hawaiian post-shield lavas from Mauna Kea, Kohala, and Hualalai show that the shield to post-shield transition was accompanied by systematic changes in the types and proportions of discrete components sampled by each volcano. The unradiogenic Pb isotopic compositions at Hualalai, positive Sr-Pb correlation at Mauna Kea, and the shallow ε_{Hf}–ε_{Nd} trend preclude generation of these lavas from mixing between the Kea and Koolau

end-members. These lavas require a contribution from at least one additional source component with relatively unradiogenic $^{87}Sr/^{86}Sr$ and $^{206}Pb/^{204}Pb$, as well as more radiogenic $^{176}Hf/^{177}Hf$, that is not expressed in Hawaiian shield lavas. This depleted isotopic signature cannot be explained by assimilation of the underlying Pacific oceanic crust or shallow entrained asthenosphere. Basalts from ODP Site 843 and gabbroic xenoliths from Hualalai do not have sufficiently unradiogenic Pb isotopic compositions and Pb-Pb trendlines for post-shield lavas from Mauna Kea and Hualalai do not intersect the EPR MORB field.

The Sr, Nd, Pb, and Hf isotopic compositions of the post-shield lavas reflect sampling of an intrinsic plume component and are consistent with the presence of ancient lower oceanic crust and sediments in their source. Post-shield lavas from Mauna Kea trend to low $^{87}Sr/^{86}Sr$ and $^{206}Pb/^{204}Pb$ towards compositions characteristic of Hawaiian rejuvenated stage lavas; this trend is observed at four consecutive Kea-trend volcanoes and indicates that this depleted component is characteristic of the Kea source and is a long-lived feature of the Hawaiian plume. A different low-$^{87}Sr/^{86}Sr$, low-$^{206}Pb/^{204}Pb$ component is sampled by post-shield lavas from Hualalai, which indicates that several depleted components may be present in the Hawaiian plume and that they are widely distributed in both the Kea and Loa sources. The post-shield lavas retain their characteristic Loa- and Kea-like Pb isotope signatures and are consistent with a bilateral or distorted concentric model of plume zonation. The Pb-Pb array for Kohala crosses the Loa-Kea Pb isotopic division and indicates that the boundary between Loa and Kea source material within the plume may fluctuate with time or that a mixed zone is present. The contrasting Pb isotope systematics of the consecutive pairs of volcanoes, in which Mahukona and Kohala become more radiogenic and Hualalai and Mauna Kea become less radiogenic, imply that the vertical component of heterogeneity is

significant and also contributes to the observed geochemical variation observed in Hawaiian lavas.

3.7 ACKNOWLEDGEMENTS

The author would like to thank Don DePaolo and Sarah Aciego for the opportunity to work on the post-shield samples. Jane Barling, Rich Friedman, Bruno Kieffer, Claude Maerschalk, Bert Mueller, and Wilma Pretorius are thanked for their help with sample processing and HR-ICP-MS, TIMS, and MC-ICP-MS analyses at the Pacific Centre for Isotopic and Geochemical Research, University of British Columbia. D. Hanano was supported by an NSERC Canada Graduate Scholarship (CGS-M). Funding for this research was provided by NSERC Discovery Grants to J. S. Scoates and D. Weis.

3.8 REFERENCES

Abouchami, W., S. J. G. Galer, and A. W. Hofmann (2000), High precision lead isotope systematics of lavas from the Hawaiian Scientific Drilling Project, *Chemical Geology, 169*, 187-209.

Abouchami, W., A. W. Hofmann, S. J. G. Galer, F. A. Frey, J. Eisele, and M. Feigenson (2005), Lead isotopes reveal bilateral asymmetry and vertical continuity in the Hawaiian mantle plume, *Nature, 434*, 851-856.

Bianco, T. A., G. Ito, J. M. Becker, and M. O. Garcia (2005), Secondary Hawaiian volcanism formed by flexural arch decompression, *Geochemistry Geophysics Geosystems, 6*(Q08009), doi:10.1029/2005GC000945.

Blichert-Toft, J., C. Chauvel, and F. Albarède (1997), Separation of Hf and Lu for high-precision isotope analysis of rock samples by magnetic sector-multiple collector ICP-MS, *Contributions to Mineralogy and Petrology, 127*, 248-260.

Blichert-Toft, J., F. A. Frey, and F. Albarède (1999), Hf isotope evidence for pelagic sediments in the source of Hawaiian basalts, *Science, 285*, 879-882.

Blichert-Toft, J., D. Weis, C. Maerschalk, A. Agranier, and F. Albarède (2003), Hawaiian hot spot dynamics as inferred from the Hf and Pb isotope evolution of Mauna Kea volcano, *Geochemistry Geophysics Geosystems, 4*(2), doi:10.1029/2002GC000340.

Blichert-Toft, J., and W. M. White (2001), Hf isotope geochemistry of the Galapagos Islands, *Geochemistry Geophysics Geosystems, 2*, doi:10.1029/2000GC000138.

Bryce, J. G., D. J. DePaolo, and J. C. Lassiter (2005), Geochemical structure of the Hawaiian plume: Sr, Nd, and Os isotopes in the 2.8 km HSDP-2 section of Mauna Kea volcano, *Geochemistry Geophysics Geosystems, 6*(9), doi:10.1029/2004GC000809.

Castillo, P., E. Klein, J. Bender, C. Langmuir, S. Shirley, R. Batiza, and W. White (2000), Petrology and Sr, Nd, and Pb isotope geochemistry of mid-ocean ridge basalt glasses from the 11°45'N to 15°00'N segment of the East Pacific Rise, *Geochemistry, Geophysics, Geosystems, 1*(11), doi:10.1029/1999GC000024.

Chen, C. Y., and F. A. Frey (1985), Trace element and isotopic geochemistry of lavas from Haleakala volcano, East Maui, Hawaii: Implications for the origin of Hawaiian basalts, *Journal of Geophysical Research, 90*, 8743-8768.

Chen, C. Y., F. A. Frey, and M. O. Garcia (1990), Evolution of alkalic lavas at Haleakala volcano, East Maui, Hawaii, *Contributions to Mineralogy and Petrology, 105*, 197-218.

Chen, C.-Y., F. A. Frey, M. O. Garcia, G. B. Dalrymple, and S. R. Hart (1991), The tholeiitic to alkalic basalt transition at Haleakala volcano, Maui, Hawaii, *Contributions to Mineralogy and Petrology, 106*, 183-200.

Clague, D. A., and G. B. Dalrymple (1987), The Hawaiian-Emperor volcanic chain, Part 1: Geologic evolution, in *Volcanism in Hawaii*, edited by R.W. Decker, T.L. Wright, and P.H. Stauffer, pp. 1667, US Geological Survey Professional Paper 1350, Denver.

Courtillot, V., A. Davaille, J. Besse, and J. Stock (2003), Three distinct types of hotspots in the Earth's mantle, *Earth and Planetary Science Letters, 205*, 295-308.

Cousens, B. L., D. A. Clague, and W. D. Sharp (2003), Chronology, chemistry, and origin of trachytes from Hualalai Volcano, Hawaii, *Geochemistry Geophysics Geosystems*, *4*(9), 1078, doi:10.1029/2003GC000560.

Dana, J. D. (1849), Geology, in *United States Exploring Expedition, 1838-1842*, vol. 10, pp. 756, C. Sherman, Philadelphia.

DePaolo, D. J., Study of magma sources, mantle structure and the differentiation of the earth using variations of $^{143}Nd/^{144}Nd$ in igneous rocks, Ph.D. dissertation thesis, California Institute of Technology, Pasadena, 1978.

DePaolo, D. J., J. G. Bryce, A. Dodson, D. L. Shuster, and B. M. Kennedy (2001), Isotopic evolution of Mauna Loa and the chemical structure of the Hawaiian plume, *Geochemistry Geophysics Geosystems*, *2*, doi: 10.1029/2000GC000139.

DePaolo, D. J., and E. E. Daley (2000), Neodymium isotopes in basalts of the southwest basin and range and lithospheric thinning during continental extension, *Chemical Geology*, *169*, 157-185.

DePaolo, D. J., and E. M. Stolper (1996), Models of Hawaiian volcano growth and plume structure: Implications from the Hawaii Scientific Drilling Project, *Journal of Geophysical Research*, *101*, 11,643-11,655.

Doucet, S., D. Weis, J. S. Scoates, K. Nicolaysen, F. A. Frey, and A. Giret (2002), The depleted mantle component in Kerguelen Archipelago basalts: Petrogenesis of the tholeiitic - transitional basalts from the Loranchet Peninsula, *Journal of Petrology*, *43*(7), 1341-1366.

Eiler, J. M., K. A. Farley, J. W. Valley, A. W. Hofmann, and E. M. Stolper (1996), Oxygen isotope constraints on the sources of Hawaiian volcanism, *Earth and Planetary Science Letters*, *144*, 453-468.

Eisele, J., W. Abouchami, S. J. G. Galer, and A. W. Hofmann (2003), The 320 kyr Pb isotopic evolution of Mauna Kea lavas recorded in the HSDP-2 drill core, *Geochemistry Geophysics Geosystems*, *4*(5), doi: 10.1029/2002GC000339.

Feigenson, M. D., A. W. Hofmann, and F. J. Spera (1983), Case studies on the origin of basalt: II The transition from tholeiitic to alkalic volcanism on Kohala volcano, Hawaii, *Contributions in Mineralogy and Petrology*, *84*, 390-405.

Fekiacova, Z., W. Abouchami, S. J. G. Galer, M. O. Garcia, and A. W. Hofmann (2007), Origin and temporal evolution of Koolau volcano, Hawaii: Inferences from isotope data on the Koolau Scientific Drilling Project (KSDP), the Honolulu Volcanics and ODP Site 843, *Earth and Planetary Science Letters*, *261*, 65-83.

Fitton, J. G., A. D. Saunders, P. D. Kempton, and B. S. Hardarson (2003), Does depleted mantle form an intrinsic part of the Iceland plume? , *Geochemistry Geophysics Geosystems*, *4*(3), doi:10.1029/2002GC000424.

Frey, F., D. Clague, J. Mahoney, and J. Sinton (2000), Volcanism at the edge of the Hawaiian plume: Petrogenesis of submarine alkalic lavas from the North Arch Volcanic Field, *Journal of Petrology*, *41*, 667-691.

Frey, F. A., M. O. Garcia, and M. F. Roden (1994), Geochemical characteristics of Koolau Volcano: Implications of intershield geochemical differences among Hawaiian volcanoes, *Geochimica et Cosmochimica Acta*, *58*(5), 1441-1462.

Frey, F. A., S. Huang, J. Blichert-Toft, M. Regelous, and M. Boyet (2005), Origin of depleted components in basalt related to the Hawaiian hot spot: Evidence from

isotopic and incompatible element ratios, *Geochemistry Geophysics Geosystems*, *6*(1), doi: 10.1029/2004GC000757.

Frey, F. A., W. S. Wise, M. O. Garcia, H. B. West, S.-T. Kwon, and A. K. Kennedy (1990), Evolution of Mauna Kea volcano, Hawaii: Petrologic and geochemical constraints on postshield volcanism, *Journal of Geophysical Research*, *95*(B2), 1271-1300.

Gaffney, A. M., B. K. Nelson, and J. Blichert-Toft (2004), Geochemical constraints on the role of oceanic lithosphere in intra-volcano heterogeneity at West Maui, Hawaii, *Journal of Petrology*, *45*(8), 1663-1687.

Gaffney, A. M., B. K. Nelson, and J. Blichert-Toft (2005), Melting in the Hawaiian plume at 1-2 Ma as recorded at Maui Nui: The role of eclogite, peridotite and source mixing, *Geochemistry Geophysics Geosystems*, *6*(10), doi: 10.1029/2005GC000927.

Galer, S. J. G., and W. Abouchami (1998), Practical application of lead triple spiking for correction of instrumental mass discrimination, *Mineralogical Magazine*, *62A*, 491-492.

Hauri, E. H. (1996), Major-element variability in the Hawaiian mantle plume, *Nature*, *382*, 415-419.

Hieronymus, C. F., and D. Bercovici (2001), A theoretical model of hotspot volcanism: Control on volcanic spacing and patterns via magma dynamics and lithosheric stresses, *Journal of Geophysical Research*, *106*(B1), 683-702.

Horwitz, E. P., D. M.L., and D. E. Fisher (1991), Separation and preconcentration of strontium from biological, environmental, and nuclear waste samples by extraction chromatography using a crown ether, *Analytical Chemistry*, *63*, 522-525.

Huang, S., and F. A. Frey (2005), Trace element abundances of Mauna Kea basalt from phase 2 of the Hawaii Scientific Drilling Project: Petrogenetic implications of correlations with major element content and isotopic ratios, *Geochemistry, Geophysics, Geosystems*, *4*(6), doi:10.1029/2002GC000322.

Huang, S., F. A. Frey, J. Blichert-Toft, R. V. Fodor, G. R. Bauer, and G. Xu (2005), Enriched components in the Hawaiian plume: evidence from Kahoolawe Volcano, Hawaii, *Geochemistry Geophysics Geosystems*, *6*(11), doi:10.1029/2005GC001012.

Jackson, E. D., E. A. Silver, and G. B. Dalrymple (1972), Hawaiian-Emperor chain and its relation to Cenozoic circum-Pacific tectonics, *Geological Society of America Bulletin*, *83*, 601-618.

King, A. J., D. G. Waggoner, and M. O. Garcia (1993), Geochemistry and petrology of basalts from Leg 136, Central Pacific Ocean, in *Proceedings of the Ocean Drilling Program, Scientific Results*, edited by R.H. Wilkens, J. Firth, and J. Bender et al., pp. 107-118, College Station, TX.

Kurz, M. D., T. C. Kenna, J. C. Lassister, and D. J. DePaolo (1996), Helium isotopic evolution of Mauna Kea volcano: First results from the 1-km drill core, *Journal of Geophysical Research*, *101*, 11,781-11,793.

Lassiter, J. C., D. J. DePaolo, and M. Tatsumoto (1996), Isotopic evolution of Mauna Kea Volcano: results from the initial phase of the Hawaii Scientific Drilling Project, *Journal of Geophysical Research*, *101*(B5), 11,769-11,780.

Lassiter, J. C., E. H. Hauri, P. W. Reiners, and M. O. Garcia (2000), Generation of Hawaiian post-erosional lavas by melting of a mixed lherzolite/pyroxenite source, *Earth and Planetary Science Letters*, *178*, 269-284.

Lassiter, L., and E. Hauri (1998), Osmium-isotope variations in Hawaiian lavas: Evidence for recycled oceanic lithosphere in the Hawaiian plume, *Earth and Planetary Science Letters, 164*, 483-496.

Le Bas, M. J., R. W. Le Maitre, A. Streckeisen, and B. Zanettin (1986), A chemical classification of volcanic rocks based on the total alkali - silica diagram, *Journal of Petrology, 27*, 745-750.

Luo, X., M. Rehkamper, D. C. Lee, and A. N. Halliday (1997), High precision $^{230}Th/^{232}Th$ and $^{234}U/^{238}U$ measurements using energy-filtered ICP magnetic sector multiple collector mass spectrometry, *International Journal of Mass Spectrometry and Ion Processes, 171*, 105-117.

Macdonald, G. A., and T. Katsura (1964), Chemical composition of Hawaiian lavas, *Journal of Petrology, 5*(1), 82-133.

Marske, J. P., A. J. Pietruszka, D. Weis, M. O. Garcia, and J. M. Rhodes (2007), Rapid passage of a small-scale mantle heterogeneity through the melting regions of Kilauea and Mauna Loa volcanoes, *Earth and Planetary Science Letters, 259*, 34-50.

McCulloch, M. T., and J. A. Gamble (1991), Geochemical and geodynamical constraints on subduction zone magmatism, *Earth and Planetary Science Letters, 102*, 358-374.

McDonough, W. F., and S.-s. Sun (1995), The composition of the Earth, *Chemical Geology, 120*, 223-253.

McDougall, I. (1969), Potassium-argon ages on lavas of Kohala volcano, Hawaii, *Geological Society of America Bulletin, 80*, 2597-2600.

Montelli, R., G. Nolet, F. A. Dahlen, and G. Masters (2006), A catalogue of deep mantle plumes: New results from finite-frequency tomography, *Geochemistry Geophysics Geosystems, 7*(11), doi:10.1029/2006GC001248.

Mukhopadhyay, S., J. C. Lassiter, K. A. Farley, and S. W. Bogue (2003), Geochemistry of Kauai shield-stage lavas: Implications for the chemical evolution of the Hawaiian plume, *Geochemistry Geophysics Geosystems, 4*(1), 1009, doi:10.1029/2002GC000342.

Niu, Y., K. D. Collerson, R. Batiza, J. I. Wendt, and M. Regelous (1999), Origin of enriched-type mid-ocean ridge basalt at ridges far from mantle plumes: The East Pacific Rise at 11°20'N, *Journal of Geophysical Research, 104*(B4), 7067–7087.

Patchett, P. J., W. M. White, H. Feldmann, S. Kielinczuk, and A. W. Hofmann (1984), Hafnium/rare earth element fractionation in the sedimentary system and crustal recycling into the Earth's mantle, *Earth and Planetary Science Letters, 69*, 365-378.

Pretorius, W., D. Weis, G. Williams, D. Hanano, B. Kieffer, and J. S. Scoates (2006), Complete trace elemental characterization of granitoid (USGS G-2, GSP-2) reference materials by high resolution inductively coupled plasma-mass spectrometry, *Geostandards and Geoanalytical Research, 30*(1), 39-54.

Regelous, M., A. W. Hofmann, W. Abouchami, and S. J. G. Galer (2003), Geochemistry of lavas from the Emperor Seamounts, and the geochemical evolution of Hawaiian magmatism from 85 to 42 Ma, *Journal of Petrology, 44*(1), 113-140.

Regelous, M., Y. Niu, J. I. Wendt, R. Batiza, A. Greig, and K. D. Collerson (1999), Variations in the geochemistry of magmatism on the East Pacific Rise at 10°30'N since 800 ka, *Earth and Planetary Science Letters, 168*, 45-63.

Reiners, P. W., and B. K. Nelson (1998), Temporal-compositional-isotopic trends in rejuvenated-stage magmas of Kauai, Hawaii, and implications for mantle melting processes, *Geochimica et Cosmochimica Acta, 62*, 2347-2368.

Ren, Z.-Y., T. Shibata, M. Yoshikawa, K. T. M. Johnson, and E. Takahashi (2006), Isotope compositions of submarine Hana Ridge lavas, Haleakala volcano, Hawaii: Implications for source compositions, melting process and the structure of the Hawaiian plume, *Journal of Petrology, 47*(2), 255-275.

Ribe, N. M., and U. R. Christensen (1999), The dynamical origin of Hawaiian volcanism, *Earth and Planetary Science Letters, 171*, 517–531.

Shafer, J. T., C. R. Neal, and M. Regelous (2005), Petrogenesis of Hawaiian postshield lavas: Evidence from Nintoku Seamount, Emperor Seamount Chain, *Geochemistry Geophysics Geosystems, 6*, doi:10.1029/2004GC000875.

Sleep, N. H. (1990), Hotspots and mantle plumes: Some phenomenology, *Journal of Geophysical Research, 95*, 6715-6736.

Staudigel, H. A., A. Zindler, S. R. Hart, T. Leslie, C.-Y. Chen, and D. Clague (1984), The isotope systematics of a juvenile intraplate volcano: Pb, Nd and Sr isotope ratios of basalts from Loihi Seamount, Hawaii, *Earth and Planetary Science Letters, 69*, 13-29.

Stevenson, R. K., and P. J. Patchett (1990), Implications for the evolution of continental crust from Hf isotope systematics of Archean detrital zircons, *Geochimica et Cosmochimica Acta, 54*(6), 1683-1697.

Stille, P., D. M. Unruh, and M. Tatsumoto (1986), Pb, Sr, Nd, and Hf isotopic constraints on the origin of Hawaiian basalts and evidence for a unique mantle source, *Geochimica et Cosmochimica Acta, 50*(10), 2303-2319.

Tatsumoto, M. (1978), Isotopic composition of lead in oceanic basalt and its implication to mantle evolution, *Earth and Planetary Science Letters, 38*, 63-87.

Vervoort, J. D., and J. Blichert-Toft (1999), Evolution of the depleted mantle: Hf isotope evidence from juvenile rocks through time, *Geochimica et Cosmochimica Acta, 63*, 533-556.

Vervoort, J. D., P. J. Patchett, J. Blichert-Toft, and F. Albarède (1999), Relationships between Lu–Hf and Sm–Nd isotopic systems in the global sedimentary system, *Earth and Planetary Science Letters, 168*, 79–99.

Weaver, B. L. (1991), The origin of ocean island basalt end-member compositions: trace element and isotopic constraints, *Earth and Planetary Science Letters, 104*, 381-397.

Weis, D., B. Kieffer, D. Hanano, I. Nobre Silva, J. Barling, W. Pretorius, C. Maerschalk, and N. Mattielli (2007), Hf isotope compositions of U.S. Geological Survey reference materials, *Geochemistry Geophysics Geosystems, 8*(6), doi:10.1029/2006GC001473.

Weis, D., B. Kieffer, C. Maerschalk, J. Barling, J. deJong, G. A. Williams, D. Hanano, W. Pretorius, N. Mattielli, J. S. Scoates, A. Goolaerts, R. M. Friedman, and J. B. Mahoney (2006), High-precision isotopic characterization of USGS reference materials by TIMS and MC-ICP-MS, *Geochemistry Geophysics Geosystems, 7*(8), doi:10.1029/2006GC001283.

Weis, D., B. Kieffer, C. Maerschalk, W. Pretorius, and J. Barling (2005), High-precision Pb-Sr-Nd-Hf isotopic characterization of USGS BHVO-1 and BHVO-2 reference materials, *Geochemistry Geophysics Geosystems, 6*(2), doi:10.1029/2004GC000852.

West, H. B., D. C. Gerlach, W. P. Leeman, and M. O. Garcia (1987), Isotopic constraints on the origin of Hawaiian lavas from the Maui volcanic complex, Hawaii, *Nature*, *330*, 216-220.

West, H. B., and W. P. Leeman (1987), Isotopic evolution of lavas from Haleakala Crater, Hawaii, *Earth and Planetary Science Letters*, *84*, 211-225.

White, W. M., F. Albarède, and P. Telouk (2000), High-precision analysis of Pb isotope ratios by multi-collector ICP-MS, *Chemical Geology*, *167*, 257-270.

Wolfe, E. W., and J. Morris (1996), Geologic map of the island of Hawaii, *Map 2524-A*, United States Geological Survey, Denver, CO.

Wolfe, E. W., W. S. Wise, and G. B. Dalrymple (1997), The geology and petrology of Mauna Kea volcano, Hawaii - A study of postshield volcanism, *U.S. Geological Survey Professional Paper 1557*, 129 pp., Menlo Park, CA.

Xu, G., F. A. Frey, D. A. Clague, W. Abouchami, J. Blichert-Toft, B. Cousens, and M. Weisler (2007), Geochemical characteristics of West Molokai shield- and postshield-stage lavas: Constraints on Hawaiian plume models, *Geochemistry Geophysics Geosystems*, *8*, doi:10.1029/2006GC001554.

Xu, G., F. A. Frey, D. A. Clague, D. Weis, and M. H. Beeson (2005), East Molokai and other Kea-trend volcanoes: Magmatic processes and sources as they migrate away from the Hawaiian hot spot, *Geochemistry Geophysics Geosystems*, *6*, doi:10.1029/2004GC000830.

Yang, H.-J., F. A. Frey, and D. A. Clague (2003), Constraints on the source components of lavas forming the Hawaiian North Arch and Honolulu Volcanics, *Journal of Petrology*, *44*(4), 603-627.

CHAPTER 4

IMPLICATIONS FOR THE NATURE OF GEOCHEMICAL HETEROGENEITIES IN THE HAWAIIAN MANTLE PLUME

4.1 SUMMARY AND CONCLUSIONS

This study of post-shield lavas from Mauna Kea, Kohala, and Hualalai volcanoes on the island of Hawaii uses major and trace element chemistry as well as Sr, Nd, Pb, and Hf isotopic compositions to characterize the geochemical changes that occur during the critical transition to the post-shield stage of ocean island volcanoes. Integration of the results of this study with the geochemistry of shield, post-shield, and rejuvenated lavas from other Hawaiian volcanoes, particularly submarine basalts from Mahukona, permits the identification of systematic spatial and temporal isotopic variations. The distinct isotopic signatures of the post-shield lavas have implications for the origin of depleted components related to Hawaiian volcanism and provide additional constraints on the geochemical structure of the Hawaiian mantle plume.

Post-magmatic alteration can significantly modify the Pb isotopic compositions of basalts from Hawaii and other oceanic islands and, if not dealt with adequately, hinders the use of Pb isotopes as a geochemical tracer. The large difference in Pb isotopic composition between unleached and leached Hawaiian basalts indicates the presence of highly radiogenic components (e.g., Mn-oxides and barite/celestite) and suggests that even young, relatively unaltered basalts must be acid-leached prior to isotopic analysis. The incomplete removal of some secondary minerals (e.g., celadonite) by acid-leaching results in poor Pb isotope reproducibility and, with the improved precision now afforded by MC-ICP-MS [e.g., *Albarède et al.*, 2004], may be the ultimate limitation on high-precision Pb isotopic compositions of ocean island basalts. The external Pb isotope reproducibility achieved in this study, discussed in Appendix A3, is better than ~150 ppm (Table A3), which allows for identification of small-scale heterogeneities in the source of the post-shield lavas.

The enriched trace element abundances of the post-shield lavas contrast with their depleted isotopic characteristics, which require contributions from a source component with high $^{143}Nd/^{144}Nd$ and $^{176}Hf/^{177}Hf$ and low $^{87}Sr/^{86}Sr$ and $^{206}Pb/^{204}Pb$. The isotopic variation observed in the post-shield lavas cannot be explained by mixing between the two principal Hawaiian shield stage end-members (Kea and Koolau) or by assimilation of the underlying Pacific lithosphere or shallow asthenosphere. This conclusion is consistent with a growing number of recent studies [e.g., *Frey et al.*, 2005; *Fekiacova et al.*, 2007; *Swinnard et al.*, in preparation, 2008] and provides compelling evidence that the depleted isotopic signatures observed in Hawaiian lavas are derived from within the Hawaiian plume. The unradiogenic Sr and Pb isotopic compositions of the post-shield lavas are consistent with those inferred for ancient (2 Ga) gabbroic lower oceanic crust and sediments. The Nd and Hf isotopic systematics provide further evidence for the presence of ancient pelagic sediments in the source of the post-shield lavas. The recognition of ancient oceanic crust and sediments in the Hawaiian plume source is well documented [e.g., *Lassiter and Hauri*, 1998; *Blichert-Toft et al.*, 1999] and supports a recycling model whereby such materials are subducted into the mantle and returned to the surface via upwelling plumes.

The depleted isotopic signature identified in post-shield lavas from Mauna Kea is also present at West Maui, East Molokai, and Haleakala [*Chen et al.*, 1991; *Gaffney et al.*, 2004; *Xu et al.*, 2005], suggesting that this component is a fundamental characteristic of the Kea source. If rejuvenated lavas are derived from the same depleted source as these four consecutive Kea-trend volcanoes, which is suggested by the isotopic systematics, then this depleted component must be a long-lived (i.e., millions of years) feature of the Hawaiian plume. The depleted component sampled by post-shield lavas from Hualalai represents the

first example of a depleted signature at a Loa-trend volcano. This indicates that more than one depleted component is present in the plume and that these components are more widely distributed, in both the Kea and Loa sources, than previously thought. Future research can take advantage of these findings in developing geodynamic and melting models to explain the physical processes that allow these depleted components to be sampled [e.g., *Ribe and Christensen*, 1999; *Regelous et al.*, 2003; *Bianco et al.*, 2005].

The presence of both Loa and Kea isotopic compositions in lavas from Mahukona and Kohala represents two more examples of a volcano with a subset of lavas that have Pb isotopic compositions characteristic of lavas from the adjacent trend [e.g., *Eisele et al.*, 2003; *Ren et al.*, 2006; *Marske et al.*, 2007; *Xu et al.*, 2007] and indicate that the compositional boundary between these two source materials is more complex than predicted by most current plume models. The Loa-like Pb isotope signatures of post-shield lavas from Hualalai and Mahukona, combined with the Kea-like signatures observed at Mauna Kea and Kohala, are inconsistent with a concentrically zoned plume and support a bilateral zonation of Pb isotope chemistry within the Hawaiian plume. The contrasting Pb isotope systematics of the consecutive volcano pairs indicates that, in addition to any horizontal zonation, vertical heterogeneity within the upwelling plume is also significant. More information from locations transverse to the axis of the Hawaiian Ridge, and particularly from the southwest side of the plume, is required to confirm these hypotheses and resolve the long-standing debate over the geochemical structure of the Hawaiian plume.

4.2 REFERENCES

Albarède, F., P. Telouk, J. Blichert-Toft, M. Boyet, A. Agranier, and B. Nelson (2004), Precise and accurate isotopic measurements using multiple-collector ICPMS, *Geochimica et Cosmochimica Acta*, *68*(12), 2725-2744.

Bianco, T. A., G. Ito, J. M. Becker, and M. O. Garcia (2005), Secondary Hawaiian volcanism formed by flexural arch decompression, *Geochemistry Geophysics Geosystems*, *6*(Q08009), doi:10.1029/2005GC000945.

Blichert-Toft, J., F. A. Frey, and F. Albarède (1999), Hf isotope evidence for pelagic sediments in the source of Hawaiian basalts, *Science*, *285*, 879-882.

Chen, C.-Y., F. A. Frey, M. O. Garcia, G. B. Dalrymple, and S. R. Hart (1991), The tholeiitic to alkalic basalt transition at Haleakala volcano, Maui, Hawaii, *Contributions to Mineralogy and Petrology*, *106*, 183-200.

Eisele, J., W. Abouchami, S. J. G. Galer, and A. W. Hofmann (2003), The 320 kyr Pb isotopic evolution of Mauna Kea lavas recorded in the HSDP-2 drill core, *Geochemistry Geophysics Geosystems*, *4*(5), doi: 10.1029/2002GC000339.

Fekiacova, Z., W. Abouchami, S. J. G. Galer, M. O. Garcia, and A. W. Hofmann (2007), Origin and temporal evolution of Koolau volcano, Hawaii: Inferences from isotope data on the Koolau Scientific Drilling Project (KSDP), the Honolulu Volcanics and ODP Site 843, *Earth and Planetary Science Letters*, *261*, 65-83.

Frey, F. A., S. Huang, J. Blichert-Toft, M. Regelous, and M. Boyet (2005), Origin of depleted components in basalt related to the Hawaiian hot spot: Evidence from isotopic and incompatible element ratios, *Geochemistry Geophysics Geosystems*, *6*(1), doi: 10.1029/2004GC000757.

Gaffney, A. M., B. K. Nelson, and J. Blichert-Toft (2004), Geochemical constraints on the role of oceanic lithosphere in intra-volcano heterogeneity at West Maui, Hawaii, *Journal of Petrology*, *45*(8), 1663-1687.

Lassiter, L., and E. Hauri (1998), Osmium-isotope variations in Hawaiian lavas: Evidence for recycled oceanic lithosphere in the Hawaiian plume, *Earth and Planetary Science Letters*, *164*, 483-496.

Marske, J. P., A. J. Pietruszka, D. Weis, M. O. Garcia, and J. M. Rhodes (2007), Rapid passage of a small-scale mantle heterogeneity through the melting regions of Kilauea and Mauna Loa volcanoes, *Earth and Planetary Science Letters*, *259*, 34-50.

Regelous, M., A. W. Hofmann, W. Abouchami, and S. J. G. Galer (2003), Geochemistry of lavas from the Emperor Seamounts, and the geochemical evolution of Hawaiian magmatism from 85 to 42 Ma, *Journal of Petrology*, *44*(1), 113-140.

Ren, Z.-Y., T. Shibata, M. Yoshikawa, K. T. M. Johnson, and E. Takahashi (2006), Isotope compositions of submarine Hana Ridge lavas, Haleakala volcano, Hawaii: Implications for source compositions, melting process and the structure of the Hawaiian plume, *Journal of Petrology*, *47*(2), 255-275.

Ribe, N. M., and U. R. Christensen (1999), The dynamical origin of Hawaiian volcanism, *Earth and Planetary Science Letters*, *171*, 517–531.

Xu, G., F. A. Frey, D. A. Clague, W. Abouchami, J. Blichert-Toft, B. Cousens, and M. Weisler (2007), Geochemical characteristics of West Molokai shield- and postshield-stage lavas: Constraints on Hawaiian plume models, *Geochemistry Geophysics Geosystems*, *8*, doi:10.1029/2006GC001554.

Xu, G., F. A. Frey, D. A. Clague, D. Weis, and M. H. Beeson (2005), East Molokai and other Kea-trend volcanoes: Magmatic processes and sources as they migrate away from the Hawaiian hot spot, *Geochemistry Geophysics Geosystems*, *6*, doi:10.1029/2004GC000830.

APPENDICES

APPENDIX A

ANALYTICAL QUALITY ASSURANCE-QUALITY CONTROL (QA-QC)

A1. Trace element abundances determined by XRF and ICP-MS

An estimate of the precision of trace element abundances reported in this study can be obtained by comparing the values determined by both ICP-MS (University of British Columbia) and XRF (University of California, Berkeley) for the same sample (Figure A1). The linear correlation coefficients for select trace elements including Sr, Zr, Ba, Rb, and Y are all greater than 0.97, except for Nb where it is 0.94. Furthermore, the slopes for Sr, Zr, Ba, and Rb are near unity (0.93-0.96). However, for Y and Nb, there is a discrepancy between the two techniques, with ICP-MS values consistently lower (by ~20-30%) than XRF values. Systematically lower Y abundances have been documented in other recent ICP-MS studies and may indicate overestimated XRF values related to correction and calibration methods [e.g., *Robinson et al.*, 1999; *Pretorius et al.*, 2006; *Robinson et al.*, 1999]. The Y concentrations determined by ICP-MS for reference materials analysed in this study are within error of the USGS recommended values as well as literature values (see Appendix A2).

A2. Trace element abundances of reference materials

The United States Geological Survey (USGS) reference materials AGV-2 and BCR-2 were run as samples to monitor the accuracy of the ICP-MS analyses during the course of this study. Values of AGV-2 show excellent agreement with both USGS [*Wilson*, 1998] and literature values [e.g., *Raczek et al.*, 2001; *Willbold and Jochum*, 2005], except for Sn where the value in this study is ~25% lower than that recommend by the USGS (Table A1). The BCR-2 standard has a composition that more closely matches the majority of the post-shield samples and was analysed three times (Table A2). Values of BCR-2 are within ±8%, and

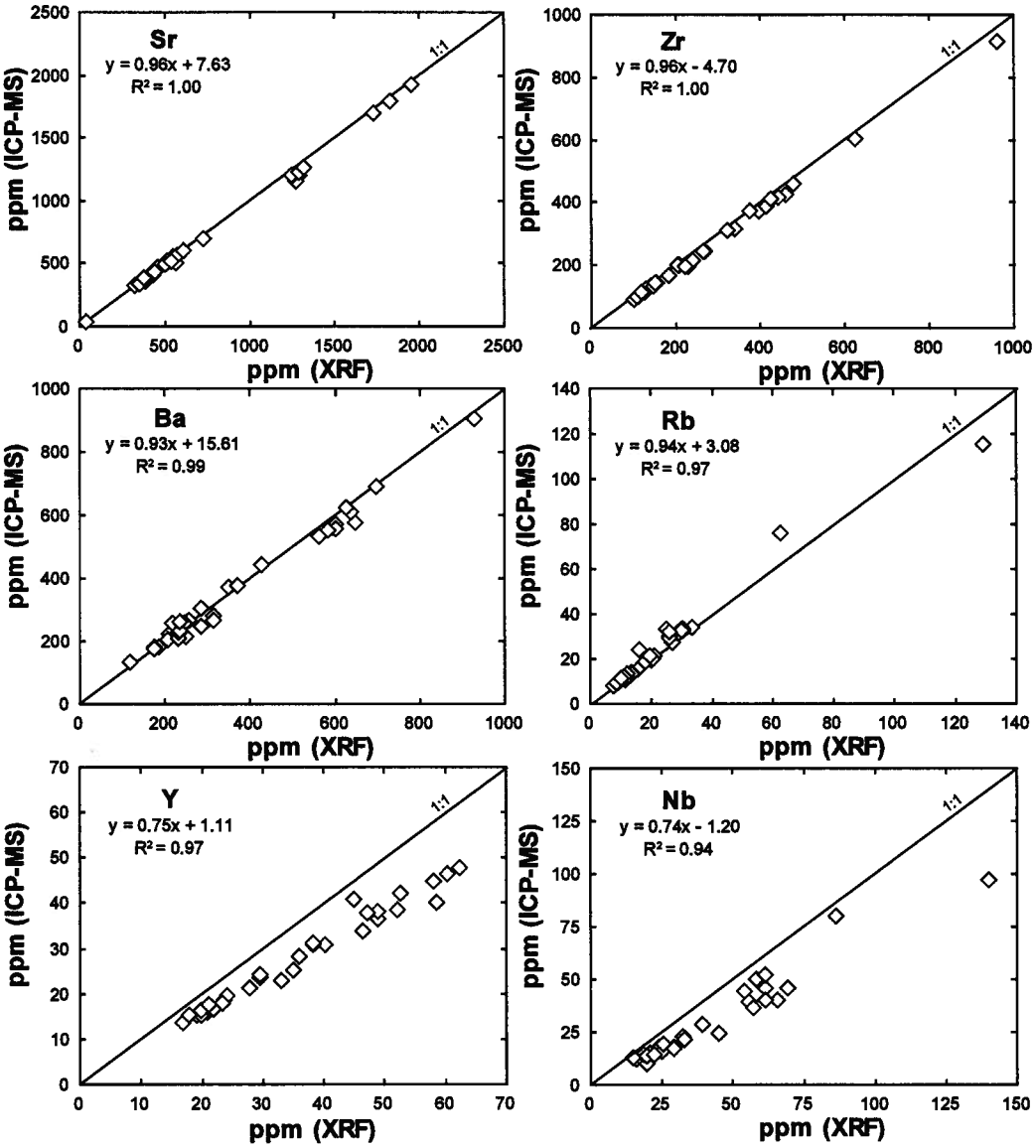

Figure A1: Comparison of select trace element abundances determined by XRF and ICP-MS. R^2 is the linear correlation coefficient. Slopes of unity are shown for reference.

Table A1: Trace Element Abundances of USGS Reference Material AGV-2[a]

	This Study (HR-ICP-MS)	USGS Recommended Values[b]			*Raczek et al.* [2001][c]	*Willbold and Jochum* [2005][d]
	AGV-2 (n=1)	Mean	1SD	%RSD	Mean (n=5)	Mean (n=3)
Sc	13	13	1	7.7		
V	125	120	5	4.2		
Cr	16	17	2	11.8		
Co	16	16	1	6.3		
Ni	18	19	3	15.8		
Cu	46	53	4	7.5		
Zn	88	86	8	9.3		
Ga	20	20	1	5.0		
Rb	66.9	68.6	2.3	3.4	66.3	65.4
Sr	675	658	17	2.6	661	657
Y	18	20	1	5.0		20.5
Zr	232	230	4	1.7		240
Nb	14	15	1	6.7		14.6
Mo	9.3					
Cd	0.34					
Sn	1.7	2.3	0.4	17.4		
Sb	0.6	0.6				
Cs	1.14	1.16	0.08	6.9		1.31
Ba	1135	1140	32	2.8	1130	1154
Hf	5.10	5.08	0.20	3.9		5.04
Ta	0.84	0.89	0.08	9.0		0.831
W	1.6					
Pb	12	13	1	7.7		14.2
Bi	0.04					
Th	6.6	6.1	0.6	9.8		6.16
U	2.00	1.88	0.16	8.5		1.81
La	41	38	1	2.6	37.9	37.8
Ce	71	68	3	4.4	68.6	67.4
Pr	8.1	8.3	0.6	7.2	7.68	7.57
Nd	30	30	2	6.7	30.5	30.2
Sm	5.5	5.7	0.3	5.3	5.49	5.36
Eu	1.53	1.54	0.10	6.5	1.53	1.49
Gd	4.44	4.69	0.26	5.5	4.52	4.51
Tb	0.62	0.64	0.04	6.3	0.641	0.636
Dy	3.4	3.6	0.2	5.6	3.47	3.43
Ho	0.67	0.71	0.08	11.3	0.653	0.651
Er	1.80	1.79	0.11	6.1	1.81	1.82
Tm	0.25	0.26	0.02	7.7	0.259	0.267
Yb	1.6	1.6	0.2	12.5	1.62	1.62
Lu	0.25	0.25	0.01	4.0	0.247	0.251

[a]All abundances in ppm. %RSD is the relative standard deviation (1SD/mean x 100).

[b]*Wilson* [1998].

[c]All abundances determined by ID-TIMS, except for Pr, Tb, Ho, and Tm, which were determined by MIC-SSMS.

[d]All abundances determined by combined isotope dilution (ID) sector field inductively coupled plasma-mass spectrometry (SF-ICP-MS).

Table A2: Trace Element Abundances of USGS Reference Material BCR-2[a]

	This Study (HR-ICP-MS)			USGS Recommended Values[b]			*Raczek et al.* [2001][c]	*Willbold and Jochum* [2005][d]
	Mean (n=3)	1SD	%RSD	Mean	1SD	%RSD	Mean (n=3)	Mean (n=3)
Sc	33	1	3.2	33	2	6.1		
V	417	18	4.2	416	14	3.4		
Cr	15.00	0.07	0.5	18	2	11.1		
Co	37.44	0.05	0.1	37	3	8.1		
Ni	11.6	0.2	1.3					
Cu	14.9	0.2	1.2	19	2	10.5		
Zn	128.1	0.3	0.2	127	9	7.1		
Ga	21.3	0.1	0.6	23	2	8.7		
Rb	47.7	0.8	1.7	48	2	4.2	46.9	47.3
Sr	347	2	0.5	346	14	4.0	340	339
Y	33	3	7.8	37	2	5.4		35.3
Zr	182	2	1.3	188	16	8.5		184
Nb	10.0	0.4	3.6					12.5
Mo	247	9	3.6	248	17	6.9		
Cd	0.90	0.04	4.4					
Sn	1.57	0.07	4.3					
Sb	0.209	0.005	2.4					
Cs	1.13	0.01	1.2	1.1	0.1	9.1		1.07
Ba	690	7	1.0	683	28	4.1	677	687
Hf	4.70	0.02	0.5	4.8	0.2	4.2		4.74
Ta	0.65	0.09	13.2					
W	0.46	0.02	3.9					
Pb	9	1	10.8	11	2	18.2		12
Bi	0.041	0.004	8.7					
Th	6.0	0.2	2.9	6.2	0.7	11.3		5.23
U	1.66	0.08	4.9	1.7	0.2	11.2		1.63
La	26	2	7.3	25	1	4.0	24.9	25.6
Ce	55	5	8.4	53	2	3.8	52.9	55.3
Pr	6.7	0.5	7.4	6.8	0.3	4.4	6.57	6.76
Nd	27	2	5.6	28	2	7.1	28.7	28.6
Sm	6.4	0.4	6.8	6.7	0.3	4.5	6.57	6.41
Eu	1.85	0.09	4.9	2	0.1	5.0	1.96	2.06
Gd	6.3	0.4	6.3	6.8	0.3	4.4	6.75	6.68
Tb	0.98	0.05	5.5	1.07	0.04	3.7	1.07	1.06
Dy	6.2	0.4	5.8				6.41	6.33
Ho	1.26	0.08	6.3	1.33	0.06	4.5	1.30	1.26
Er	3.5	0.2	6.2				3.66	3.62
Tm	0.49	0.04	7.5				0.564	0.512
Yb	3.1	0.1	4.8	3.5	0.2	5.7	3.38	3.36
Lu	0.48	0.03	6.9	0.51	0.02	3.9	0.519	0.504

[a]All abundances in ppm. %RSD is the relative standard deviation (1SD/mean x 100).

[b]*Wilson* [1997].

[c]All abundances determined by ID-TIMS, except for Pr, Tb, Ho, and Tm, which were determined by MIC-SSMS.

[d]All abundances determined by combined isotope dilution (ID) sector field inductively coupled plasma-mass spectrometry (SF-ICP-MS).

are consistently better than ±5%, of the values reported by *Raczek et al.* [2001] and *Willbold and Jochum* [2005]. For most elements, values obtained in this study are within ±7% of the USGS recommended values [*Wilson*, 1997], and are well within the reported standard deviations. Notable exceptions include Cr, Cu, and Pb, for which values in this study are ~15-20% lower than the USGS recommended values. Variable Pb concentrations have been identified in many USGS reference materials and may be related to contamination during processing [e.g., *Weis et al.*, 2005; *Weis et al.*, 2006].

A3. Reproducibility of Pb and Hf isotopic analyses

The external reproducibility of Pb and Hf isotopic analyses was determined via several sets of complete procedural duplicates, which involved a separate leaching, digestion, chemical separation, and isotopic analysis. The external precision of Pb isotopic analyses in this study is better than 166 ppm, and consistently better than 105 ppm (Table A3). This level of precision is comparable to that achieved in other recent Pb isotope studies [e.g., *Abouchami et al.*, 2000; *Eisele et al.*, 2003]. This shows that the use of thallium to correct for instrumental mass bias, particularly when all samples are analysed with the same Pb/Tl and intensity as the standards, produces data of comparable quality to the double or triple spike techniques [e.g., *White et al.*, 2000; *Woodhead*, 2002; *Albarède et al.*, 2004]. For the Hf isotopic analyses, the external precision is better than 57 ppm, with duplicate analyses commonly agreeing within $^{176}Hf/^{177}Hf = <0.000003$ (Table A4). Replicate analyses, which involved re-running the same sample solution, were also carried out during each analytical session to monitor instrument performance, and are comparable to or better than the reproducibility of duplicate analyses.

Table A3: External Reproducibility of Pb Isotopic Compositions [a]

Sample		$^{206}Pb/^{204}Pb$	2σ	$^{207}Pb/^{204}Pb$	2σ	$^{208}Pb/^{204}Pb$	2σ
		procedural duplicates (separate digestions)					
02AHU-5	#1	17.9802	0.0006	15.4473	0.0006	37.7442	0.0018
	#2	17.9805	0.0005	15.4483	0.0006	37.7470	0.0016
	mean	17.9803	0.0003	15.4478	0.0014	37.7456	0.0040
	ppm	**19**		**88**		**105**	
02AHU-13	#1	17.9426	0.0006	15.4500	0.0006	37.7119	0.0016
	#2	17.9417	0.0007	15.4491	0.0007	37.7092	0.0018
	mean	17.9421	0.0013	15.4496	0.0013	37.7105	0.0038
	ppm	**71**		**82**		**101**	
02AMK-11	#1	18.3411	0.0009	15.4717	0.0010	37.9244	0.0029
	#2	18.3411	0.0009	15.4717	0.0008	37.9268	0.0023
	mean	18.3411	0.00004	15.4717	0.00003	37.9256	0.0033
	ppm	**2**		**2**		**88**	
02AKA-4	#1	18.4394	0.0006	15.4808	0.0005	37.9949	0.0013
	#2	18.4410	0.0006	15.4824	0.0006	37.9994	0.0017
	mean	18.4402	0.0024	15.4816	0.0022	37.9972	0.0063
	ppm	**128**		**145**		**166**	
		WC/agate duplicates (separate powders)					
02AHU-1	WC	17.8877	0.0008	15.4434	0.0007	37.6712	0.0019
	agate	17.8913	0.0009	15.4459	0.0007	37.6779	0.0021
	mean	17.8895	0.0051	15.4447	0.0036	37.6746	0.0095
	ppm	**286**		**235**		**252**	
02AHU-10	WC	18.0013	0.0009	15.4592	0.0008	37.7658	0.0021
	agate	17.9992	0.0010	15.4578	0.0010	37.7621	0.0024
	mean	18.0003	0.0030	15.4585	0.0019	37.7640	0.0052
	ppm	**166**		**121**		**137**	
02AMK-12	WC	18.3463	0.0009	15.4777	0.0008	37.9536	0.0021
	agate	18.3496	0.0006	15.4788	0.0006	37.9608	0.0018
	mean	18.3480	0.0046	15.4782	0.0016	37.9572	0.0103
	ppm	**253**		**100**		**270**	
02AKA-6	WC	18.2482	0.0009	15.4713	0.0008	37.8962	0.0020
	agate	18.2482	0.0008	15.4728	0.0008	37.8989	0.0019
	mean	18.2482	0.00004	15.4720	0.0020	37.8976	0.0038
	ppm	**2**		**131**		**102**	

[a]All Pb isotopic ratios were determined by MC-ICP-MS on acid-leached sample powders [*Weis et al.*, 2005]. Pb data were corrected for fractionation by Tl spiking and then normalized to the NBS 981 triple spike values of *Galer and Abouchami* [1998] using the standard bracketing method. The 2σ error is the absolute error value of an individual sample analysis (internal error). For the mean values, the error reported is the 2 standard deviation (external error). External reproducibility is represented by the 2 standard deviation from the mean of duplicate analyses and is reported in ppm (2SD/mean $x10^6$).

Table A4: External Reproducibility of Hf Isotopic Compositions[a]

Sample		$^{176}Hf/^{177}Hf$	2σ	Sample		$^{176}Hf/^{177}Hf$	2σ
		procedural duplicates (separate digestions)					
02AHU-3	#1	0.283108	0.000005	02AHU-13	#1	0.283110	0.000004
	#2	0.283119	0.000005		#2	0.283113	0.000004
	mean	0.283113	0.000016		mean	0.283112	0.000004
	ppm	**57**			**ppm**	**14**	
02AMK-8	#1	0.283126	0.000004	02AKA-1	#1	0.283133	0.000004
	#2	0.283127	0.000004		#2	0.283133	0.000005
	mean	0.283126	0.0000003		mean	0.283133	0.0000003
	ppm	**1**			**ppm**	**1**	
		WC/agate duplicates (separate powders)					
02AMK-12	WC	0.283138	0.000007	02AKA-6	WC	0.283109	0.000004
	agate	0.283131	0.000006		agate	0.283119	0.000005
	mean	0.283135	0.000009		mean	0.283114	0.000013
	ppm	**32**			**ppm**	**47**	
		leached/unleached duplicates (separate digestions)					
02AMK-2	L	0.283127	0.000006	02AMK-4	L	0.283124	0.000005
	unL	0.283126	0.000004		unL	0.283133	0.000005
	mean	0.283126	0.000003		mean	0.283128	0.000013
	ppm	**9**			**ppm**	**45**	
02AMK-7	L	0.283125	0.000005				
	unL	0.283124	0.000005				
	mean	0.283125	0.000002				
	ppm	**7**					

[a]All Hf isotopic ratios were determined by MC-ICP-MS and have been normalized to JMC 475 $^{176}Hf/^{177}Hf$ = 0.282160 [*Vervoort and Blichert-Toft*, 1999]. The 2σ error is the absolute error value of an individual sample analysis (internal error). For the mean values, the error reported is the 2 standard deviation (external error). External reproducibility is represented by the 2 standard deviation from the mean of duplicate analyses and is reported in ppm (2SD/mean x10^6).

No systematic differences in Pb isotopic composition were observed between powders that were crushed in tungsten carbide (WC) and those that were crushed in agate (Table A3), contrary to what is observed for trace elements and Hf isotopes (see below). This is likely due to the removal of potential contaminants through acid-leaching of the powders. This is consistent with *Weis et al.* [2005] who found that differences between the USGS reference materials BHVO-1 (contaminated during processing) and BHVO-2 were significantly reduced after leaching. However, the difference between powders crushed in different materials (WC vs. agate) reaches up to 286 ppm, which is significantly larger than the external precision of powders that were crushed in the same material (Table A3). The poorer reproducibility of the WC/agate duplicates may reflect heterogeneity in the different powder splits or incomplete removal of contaminants via leaching. This emphasizes the importance of careful sample crushing and leaching in obtaining high-precision Pb isotopic compositions [e.g., *Weis et al.*, 2005; *Nobre Silva et al.*, in revision, 2008].

Contamination due to crushing in WC is a potential problem for Hf isotopes due to the isobaric interferences of ^{180}Ta and ^{180}W on ^{180}Hf. The effect of ^{180}Ta and ^{180}W can be assessed by comparing the ^{180}Hf/^{177}Hf values of the samples to the JMC 475 Hf standard, which gave an average ^{180}Hf/^{177}Hf of 1.886837 ± 0.000099 (2sd; n = 175). The samples crushed in agate gave ^{180}Hf/^{177}Hf = 1.886883 ± 0.000092 (2sd; n = 36), whereas those crushed in WC gave ^{180}Hf/^{177}Hf = 1.892 ± 0.018 (2sd; n = 7), indicating the presence of variably elevated amounts of Ta and W. This was confirmed by their anomalously high trace element abundances (up to ~16.5 ppm Ta and ~3100 ppm W) compared to the samples crushed in agate (average ~2 ppm Ta and ~1 ppm W). Some of the additional Ta and W will be removed during sample purification, and any remaining Ta and W will have a relatively

minor effect due to the size of the ^{180}Hf peak and the low natural abundances of ^{180}Ta (~0.01%) and ^{180}W (~0.1%). Regardless, any potential interference on ^{180}Hf does not affect the reported ratio of $^{176}Hf/^{177}Hf$. No systematic differences in Hf isotopic composition or reproducibility were observed between the WC- and agate-crushed powders (Table A4). Similarly, the Hf isotopic compositions of leached and unleached powders of the same sample show excellent agreement (Table A4). This reflects the low susceptibility of Hf isotopes to modification by secondary alteration and demonstrates that, unlike for Pb and Sr, samples do not need to be acid-leached prior to Hf isotopic analysis.

A4. References

Abouchami, W., S. J. G. Galer, and A. W. Hofmann (2000), High precision lead isotope systematics of lavas from the Hawaiian Scientific Drilling Project, *Chemical Geology, 169*, 187-209.

Albarède, F., P. Telouk, J. Blichert-Toft, M. Boyet, A. Agranier, and B. Nelson (2004), Precise and accurate isotopic measurements using multiple-collector ICPMS, *Geochimica et Cosmochimica Acta, 68*(12), 2725-2744.

Eisele, J., W. Abouchami, S. J. G. Galer, and A. W. Hofmann (2003), The 320 kyr Pb isotopic evolution of Mauna Kea lavas recorded in the HSDP-2 drill core, *Geochemistry Geophysics Geosystems, 4*(5), doi: 10.1029/2002GC000339.

Nobre Silva, I. G., D. Weis, J. Barling, and J. S. Scoates (2008), Leaching systematics for the determination of high-precision Pb isotope compositions of ocean island basalts, *Geochemistry Geophysics Geosystems*, paper # 2007GC001891 (in revision).

Pretorius, W., D. Weis, G. Williams, D. Hanano, B. Kieffer, and J. S. Scoates (2006), Complete trace elemental characterization of granitoid (USGS G-2, GSP-2) reference materials by high resolution inductively coupled plasma-mass spectrometry, *Geostandards and Geoanalytical Research, 30*(1), 39-54.

Raczek, I., B. Stoll, A. W. Hofmann, and K. P. Jochum (2001), High-precision trace element data for the USGS reference materials BCR-1, BCR-2, BHVO-1, BHVO-2, AGV-1, AGV-2, DTS-1, DTS-2, GSP-1 and GSP-2 by ID-TIMS and MIC-SSMS, *Geostandards Newsletter, 25*(1), 77-86.

Robinson, P., A. T. Townsend, Y. Zongshou, and C. Munker (1999), Determination of scandium, yttrium and rare earth elements in rocks by high resolution inductively coupled plasma-mass spectrometry, *Geostandards Newsletter: The Journal of Geostandards and Geoanalysis, 23*(1), 31-46.

Weis, D., B. Kieffer, C. Maerschalk, J. Barling, J. deJong, G. A. Williams, D. Hanano, W. Pretorius, N. Mattielli, J. S. Scoates, A. Goolaerts, R. M. Friedman, and J. B. Mahoney (2006), High-precision isotopic characterization of USGS reference materials by TIMS and MC-ICP-MS, *Geochemistry Geophysics Geosystems, 7*(8), doi:10.1029/2006GC001283.

Weis, D., B. Kieffer, C. Maerschalk, W. Pretorius, and J. Barling (2005), High-precision Pb-Sr-Nd-Hf isotopic characterization of USGS BHVO-1 and BHVO-2 reference materials, *Geochemistry Geophysics Geosystems, 6*(2), doi:10.1029/2004GC000852.

White, W. M., F. Albarède, and P. Telouk (2000), High-precision analysis of Pb isotope ratios by multi-collector ICP-MS, *Chemical Geology, 167*, 257-270.

Willbold, M., and K. P. Jochum (2005), Multi-element isotope dilution sector field ICP-MS: A precise technique for the analysis of geological materials and its application to geological reference materials, *Geostandards and Geoanalytical Research, 29*(1), 63-82.

Wilson, S. A. (1997), The collection, preparation, and testing of USGS reference material BCR-2, Columbia River, basalt, *Open-File Report*, United States Geological Survey, Denver, CO.

Wilson, S. A. (1998), Data compilation and statistical analysis of intra-laboratory results for AGV-2, *Open-File Report*, United States Geological Survey, Denver, CO.

Woodhead, J. D. (2002), A simple method for obtaining highly accurate Pb-isotope data by MC-ICPMS, *Journal of Analytical Atomic Spectrometry*, *17*, 1381-1385.

APPENDIX B

SUPPLEMENTARY SAMPLES

B1. Mahukona basalts

Mahukona is a submerged volcano located off the northwest coast of the island of Hawaii, ~50 km west of Kohala (Figure B1). The proposed existence of Mahukona as an independent Hawaiian shield volcano [*Moore and Cambell*, 1987] was not confirmed until recently [*Garcia et al.*, 1990], and as a result much debate still exists over the location of its summit, whether or not it reached sea level, and what growth stage it was in when it became extinct [*Garcia et al.*, 1990; *Clague and Moore*, 1991]. Mahukona is of particular importance because it fills the gap on the Loa trend, between Hualalai and Kahoolawe, in the paired sequence of Hawaiian volcanoes [*Dana*, 1849; *Jackson et al.*, 1972]. The location and age of Mahukona permits comparison with the adjacent Kohala volcano (on the Kea trend) and the younger Hualalai volcano (on the Loa trend), thus providing both spatial and temporal constraints on the evolution of volcanism related to the Hawaiian mantle plume.

To better characterize Mahukona volcano, 13 samples from Mahukona were selected for geochemical analysis (Figure B1; Table B1). Two samples (MA-12 and MA-32) were collected by dredging with the R/V Atlantis II near the summit high of the volcano [*Garcia et al.*, 1990]. One additional sample (F2-88-HW D16-6) was collected by dredging with the R/V Farnella on the west ridge of Mahukona [*Clague and Moore*, 1991]. The remaining samples were collected by the Pisces V submersible during three separate dives on ridges that radiate to the west-southwest, southwest, and southeast from the summit high [*Garcia et al.*, 1990; M. Garcia, personal communication]. All of the lavas recovered from Mahukona are basalts, which can be divided into two separate groups, tholeiitic basalts and transitional to weakly alkalic basalts (Figure B2).

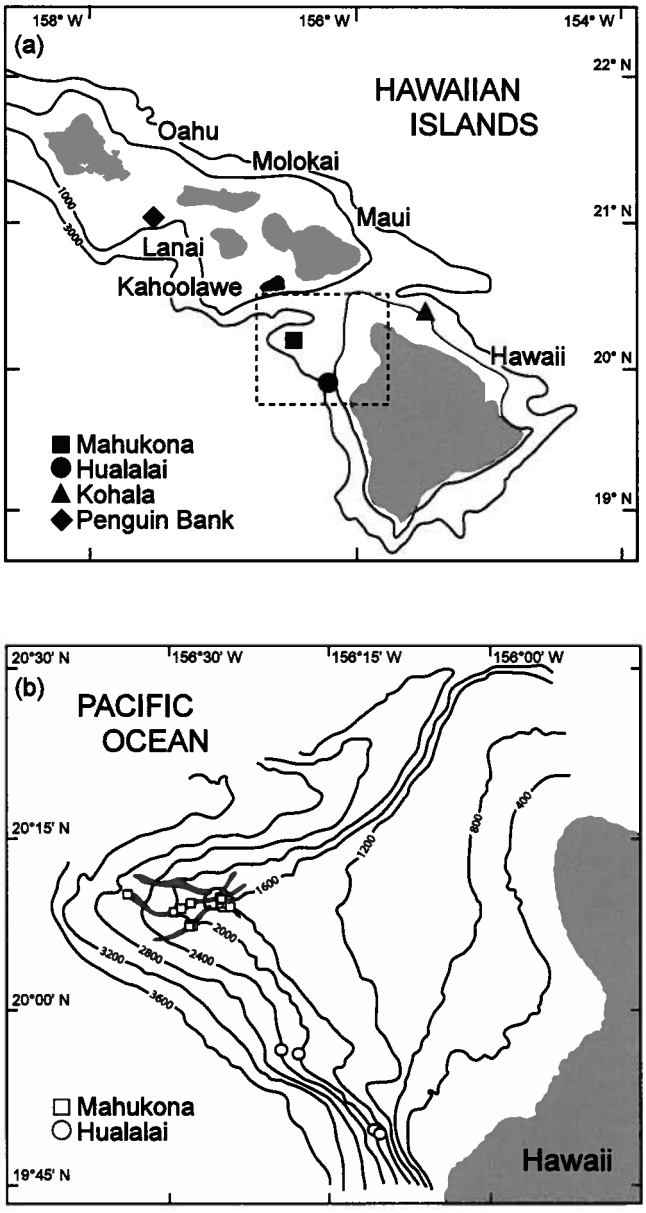

Figure B1: (a) Map of the Hawaiian Islands showing the sample locations of the submarine lavas from Mahukona, Hualalai, Kohala, and Penguin Bank. The dashed box indicates the area shown in (b). (b) Bathymetric map of the seafloor to the northwest of the island of Hawaii (after *Garcia et al.* [1990] and *Clague and Moore* [1991]) showing the locations of submarine samples from Mahukona volcano and the northwest rift zone of Hualalai volcano. Contour interval is 400 m. Prominent ridges radiating from the summit high of Mahukona are shaded along their crests.

Table B1: Pb, Hf, Sr, and Nd Isotopic Compositions of Mahukona Basalts[a]

Sample	$^{208}Pb/^{204}Pb$	2σ	$^{207}Pb/^{204}Pb$	2σ	$^{206}Pb/^{204}Pb$	2σ	$^{176}Hf/^{177}Hf$	2σ	$^{87}Sr/^{86}Sr$	2σ	$^{143}Nd/^{144}Nd$	2σ
MA-12	38.0624	21	15.4683	7	18.3147	8	0.283086	5	0.703686	7	0.512942	6
							0.283090	4				
MA-32	38.1446	19	15.4820	7	18.3795	8	0.283089	4	0.703674	7	0.512929	6
P5 159-1	37.9719	47	15.4670	17	18.1879	19	0.283063	7	0.703769	7	0.512907	6
P5 159-4	38.1066	20	15.4776	8	18.3412	8	0.283089	4	0.703689	8	0.512929	7
P5 159-6	38.0952	22	15.4703	7	18.3488	7	0.283095	4	0.703699	9	0.512945	6
P5 160-1	38.1232	22	15.4771	7	18.3661	8	0.283089	4	0.703696	6	0.512938	6
P5 160-2	38.0636	18	15.4719	7	18.3076	8	0.283092	5	0.703682	9	0.512932	6
P5 160-5	38.0494	16	15.4697	6	18.2944	6	0.283084	4	0.703689	7	0.512925	6
P5 160-6	38.0495	16	15.4699	6	18.2936	6	0.283088	5	0.703687	7	0.512939	6
P5 161-1	37.9514	23	15.4669	8	18.2983	9	0.283125	6	0.703586	9	0.513001	6
	37.9512	17	15.4665	6	18.2980	7	0.283125	4	0.703581	7	0.513013	7
P5 161-2	37.9395	29	15.4611	10	18.2913	11	0.283126	8	0.703569	7	0.512991	7
P5 161-4	37.9750	25	15.4680	11	18.1901	11	0.283067	6	0.703776	9	0.512911	6
F2-88-HW D16-6	37.9879	15	15.4752	5	18.2967	6	0.283117	7	0.703644	10	0.512974	7

[a]All Pb and Hf isotopic ratios were determined by MC-ICP-MS; Pb data were corrected for fractionation by Tl spiking and then normalized to the NBS 981 triple spike values of *Galer and Abouchami* [1998] using the standard bracketing method; Hf data were normalized to JMC 475 $^{176}Hf/^{177}Hf = 0.282160$ [*Vervoort and Blichert-Toft*, 1999]. All Sr and Nd isotopic ratios were determined by TIMS; Sr data were normalized to SRM 987 $^{87}Sr/^{86}Sr = 0.710248$; Nd data were normalized to La Jolla $^{143}Nd/^{144}Nd = 0.511858$, except for F2-88-HW D16-6, which was normalized to the Berkeley Ames standard $^{143}Nd/^{144}Nd = 0.510939$. The 2σ error is the absolute error value of an individual sample analysis (internal error) and applies to the last decimal place(s). Samples labeled "D" represent procedural duplicate analyses carried out on separate powder aliquots.

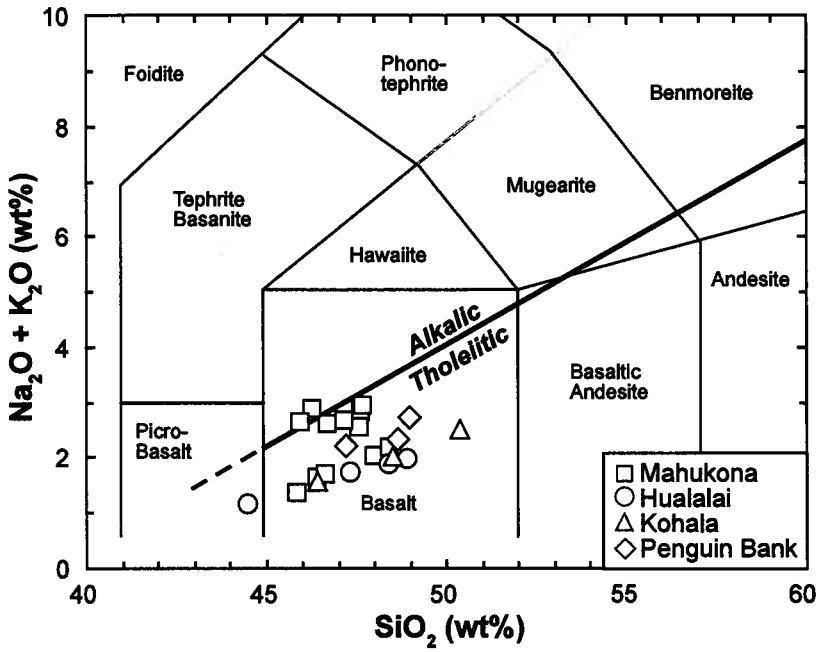

Figure B2: Total alkalis vs. silica classification diagram (modified from *Le Bas et al.* [1986]) for the submarine lavas from Mahukona, Hualalai, Kohala, and Penguin Bank. The tholeiitic-alkalic dividing line is from *Macdonald and Katsura* [1964]. The majority of the Hawaiian submarine lavas are tholeiitic to transitional basalts.

Three of the samples were selected for $^{40}Ar/^{39}Ar$ dating at Oregon State University. The deepest of these samples, recovered from a depth of 1970 mbsl on the WSW rift, is a tholeiite with an age of 653 ± 74 ka. The shallowest sample, collected near the summit of Mahukona (~1200 mbsl) on the SE rift, is a transitional basalt that yields the youngest age of 351 ± 32 ka. Another transitional basalt, located midway between the other two samples at a depth of 1685 mbsl on the SW rift, has an intermediate age of 479 ± 75 ka. The significantly younger ages of the shallower and more alkaline basalts from Mahukona support the interpretation that these lavas erupted during the post-shield stage [*Clague and Moore*, 1991] rather than the pre-shield stage [*Garcia et al.*, 1990]. The observed range of ages for tholeiitic to transitional volcanism on Mahukona coincides with the period of shield to late-shield volcanism (Polulu Volcanics) on the neighbouring Kohala volcano [*Spengler and Garcia*, 1988], and allows for direct comparison of the geochemistry of lavas from this pair of volcanoes.

Sr, Nd, Pb, and Hf isotopic compositions (Table B1) were determined at the PCIGR, University of British Columbia, using procedures described in Section 3.3 (see also *Weis et al.* [2006] and *Weis et al.* [2007] for complete chemical and analytical protocols). The Sr, Nd, and Hf isotopic compositions of the Mahukona basalts generally overlap the field defined by Mauna Loa, except for three samples with the lowest $^{87}Sr/^{86}Sr$ and highest $^{143}Nd/^{144}Nd$ and $^{176}Hf/^{177}Hf$ that overlap with Mauna Kea (Figure B3). These Kea-like samples also have distinct Pb isotopic compositions and plot on the Kea side of the Pb isotopic division in Pb-Pb space [*Abouchami et al.*, 2005] (Figure B4). The majority of the Mahukona basalts, however, are characteristically Loa-like in their Pb isotope systematics. The transitional to weakly alkalic basalts extend to more radiogenic compositions

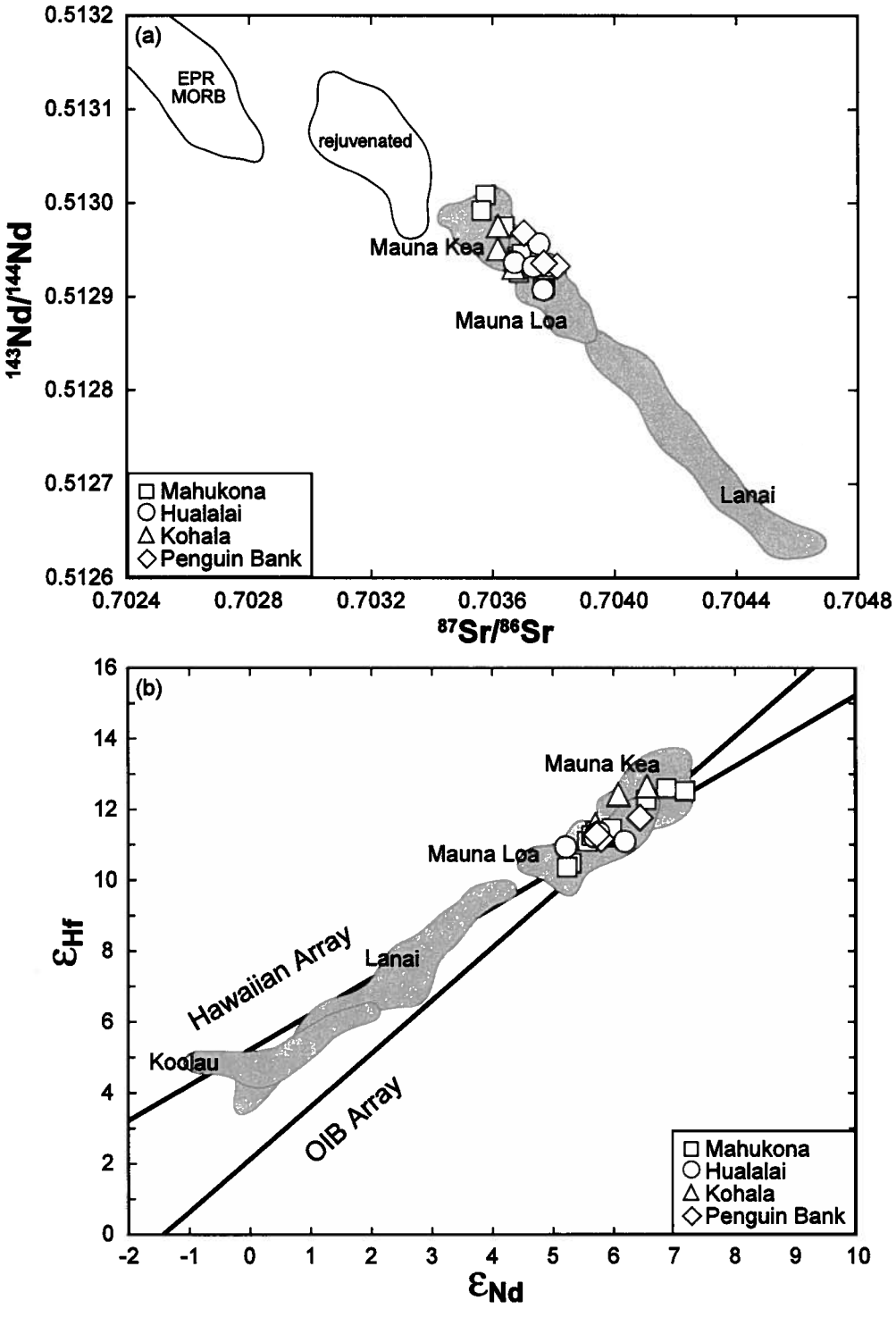
(a)
EPR MORB
rejuvenated
Mauna Kea
Mauna Loa
Lanai
Mahukona
Hualalai
Kohala
Penguin Bank
0.5132
0.5131
0.5130
0.5129
0.5128
0.5127
0.5126
143Nd/144Nd
0.7024
0.7028
0.7032
0.7036
0.7040
0.7044
0.7048
87Sr/86Sr
(b)
Mauna Kea
Mauna Loa
Lanai
Hawaiian Array
Koolau
OIB Array
Mahukona
Hualalai
Kohala
Penguin Bank
16
14
12
10
8
6
4
2
0
εHf
-2
-1
0
1
2
3
4
5
6
7
8
9
10
εNd

Figure B3

Figure B3: (a) $^{143}Nd/^{144}Nd$ vs. $^{87}Sr/^{86}Sr$ and (b) ε_{Hf} vs. ε_{Nd} for for the submarine basalts from Mahukona, Hualalai, Kohala, and Penguin Bank compared to selected Hawaiian shield stage lavas. Also shown in (a) are fields for Hawaiian rejuvenated stage lavas and EPR MORB. The Hawaiian and OIB arrays in (b) are from *Blichert-Toft et al.* [1999]. Data sources are the same as in Figure 3.8.

($^{206}Pb/^{204}Pb$ =18.38; $^{208}Pb/^{204}Pb$ = 38.14) than the tholeiites and overlap with the field for Loihi (Figure B4).

The Loa-like isotopic compositions of the majority of the Mahukona basalts, and in particular their similarity to lavas from Mauna Loa and Loihi, confirm that Mahukona is compositionally a Loa-trend volcano, consistent with its location on the Loa spatial trend. The exclusively Loa-like Pb isotope systematics of the transitional to weakly alkalic basalts preserve the Loa-Kea Pb isotopic division [*Abouchami et al.*, 2005] (Figure B4). If these lavas belong to the post-shield stage, as suggested by the age relationships, this implies that the Loa source extends to the plume margin and supports the bilaterally zoned plume model [*Abouchami et al.*, 2005; *Xu et al.*, 2007] (Figure 3.12). This is consistent with post-shield lavas from Hualalai, Mauna Kea, and Kohala, which retain their respective Loa- and Kea-like Pb isotope signatures (see Section 3.5.3 for discussion).

The three anomalous Kea-like samples are tholeiites and are the deepest samples in the study (~2000-2700 mbsl), suggesting that they may belong to the adjacent Kohala volcano. This would imply that the large submarine feature interpreted to be Mahukona volcano instead corresponds to Kohala's westward-trending rift zone. In such a scenario, the Loa-like summit high may represent a large (post-shield?) cone developed on this rift zone. Alternatively, a more plausible explanation is that the compositions of these lavas reflect sampling of the Kea source by this Loa-trend volcano. The sampling of source material from the adjacent trend has been documented at numerous other Hawaiian volcanoes [e.g., Mauna Kea: *Eisele et al.*, 2003; Haleakala: *Ren et al.*, 2006; Kilauea: *Marske et al.*, 2007; West Molokai: *Xu et al.*, 2007]. This indicates considerable heterogeneity in the melting region and suggests that the Hawaiian plume has more complex

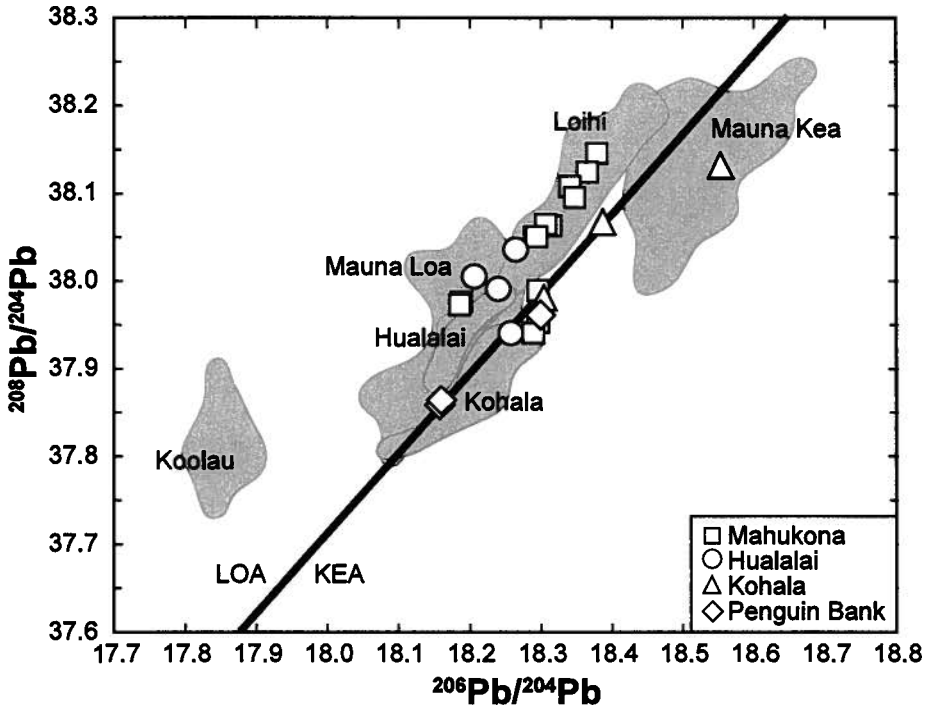

Figure B4: $^{208}Pb/^{204}Pb$ vs. $^{206}Pb/^{204}Pb$ for the submarine basalts from Mahukona, Hualalai, Kohala, and Penguin Bank compared to selected Hawaiian shield stage lavas. The thick black line represents the Loa-Kea Pb isotopic division defined by *Abouchami et al.* [2005]. Data sources are the same as in Figure 3.8.

geochemical structure than predicted by either the concentrically or bilaterally zoned models [e.g., *Hauri*, 1996; *Kurz et al.*, 1996; *Lassiter et al.*, 1996; *Abouchami et al.*, 2005].

Comparison of the Pb isotope systematics of Mahukona with Kohala, its neighbour on the Kea-trend, shows that lavas from both volcanoes become more radiogenic in Pb with time (Figure 3.11a). In contrast, the younger pair of volcanoes, Hualalai and Mauna Kea, shows the opposite relationship and become less radiogenic in Pb during the shield to post-shield transition (Figure 3.11b). The sampling of isotopically distinct components by these consecutive pairs of volcanoes suggest that, in addition to any horizontal zoning, vertical heterogeneities within the upwelling plume also contribute to the geochemical variability observed in Hawaiian lavas [*Blichert-Toft et al.*, 2003]. During the late stages of volcanism at Mahukona and Kohala, a contribution from an enriched source with radiogenic Pb isotopic compositions is required. Although lavas from these two volcanoes could share one common component, the linear Pb-Pb array of Mahukona trends towards higher $^{208}Pb/^{204}Pb$ for a given $^{206}Pb/^{204}Pb$ than that of Kohala, indicating that each volcano sampled a different enriched component (Figure 3.11a). Similarly, the sub-parallel Pb-Pb arrays of Hualalai and Mauna Kea suggest that more than one depleted component may be involved during the post-shield stage (Figure 3.11b). The depleted signature (relatively unradiogenic Sr and Pb isotopic compositions) identified in post-shield lavas from Hualalai and Mauna Kea is distinct from the MORB source (see Section 3.5.2 for discussion). The observed isotope systematics of lavas from these volcanoes reflect derivation from a heterogeneous source with both enriched and depleted components of varying composition from within the Hawaiian plume.

B2. Submarine Hawaiian basalts from Hualalai, Kohala, and Penguin Bank

Ten additional samples collected from the NW rift of Hualalai, NE flank of Kohala, and Penguin Bank, were also selected for isotopic analysis (Figure B1; Table B2). All of the submarine samples are tholeiitic basalts (Figure B2), except for one picritic sample from Hualalai that has ~30 wt% MgO. Pb and Hf isotopic compositions were determined at the PCIGR, University of British Columbia, and Sr and Nd isotopic compositions were determined at the CIG, University of California, Berkeley using procedures described in Section 3.3.

Submarine basalts from Hualalai and Penguin Bank have Sr, Nd, and Hf isotopic compositions that plot within the field defined by Mauna Loa, whereas basalts from Kohala coincide with those from Mauna Kea (Figure B3). This is consistent with the location of Hualalai and Penguin Bank on the Loa-trend, and Kohala on the Kea-trend. The Pb isotopic compositions of the submarine lavas show less overlap and allow for better distinction between the three volcanoes (Figure B4). Submarine basalts from Hualalai are Loa-like and similar to subaerial shield lavas from Hualalai. In contrast, submarine basalts from Kohala are more radiogenic than their subaerial counterparts and trend towards the field for Mauna Kea. The Pb isotopic compositions of submarine basalts from Penguin Bank lie along the Loa-Kea Pb isotopic division [*Abouchami et al.*, 2005].

Due to the location of Penguin Bank west of the main Hawaiian Ridge, the geochemical characteristics of these lavas are critical for evaluating the concentric and bilateral models of plume zonation [e.g., *Hauri*, 1996; *Kurz et al.*, 1996; *Lassiter et al.*, 1996; *Abouchami et al.*, 2005]. The Loa-like Sr, Nd, and Hf isotopic compositions of Penguin bank lavas are consistent with a bilaterally zoned plume. However, the Pb isotopic

Table B2: Pb, Hf, Sr, and Nd Isotopic Compositions of Submarine Hawaiian Basalts[a]

Sample	$^{208}Pb/^{204}Pb$	2σ	$^{207}Pb/^{204}Pb$	2σ	$^{206}Pb/^{204}Pb$	2σ	$^{176}Hf/^{177}Hf$	2σ	$^{87}Sr/^{86}Sr$	2σ	$^{143}Nd/^{144}Nd$	2σ
					Hualalai (NW rift)							
KK 10-1	37.9392	38	15.4649	15	18.2583	53	0.283084	6	0.703758	11	0.512956	6
KK 14-7	37.9897	26	15.4634	10	18.2402	11	0.283092	6	0.703660	8	0.512952	6
							0.283090	5	0.703696	10	0.512918	11
F2-88-HW D26-1	37.9998	19	15.4676	7	18.2048	7	0.283088	5	0.703742	10	0.512931	6
	38.0095	14	15.4700	6	18.2107	6						
F2-88-HW D27-2	38.0343	19	15.4626	7	18.2647	6	0.283080	6	0.703773	8	0.512906	6
					Kohala (NE flank)							
T302 R19	38.1322	15	15.4898	6	18.5563	7	0.283129	4	0.703620	8	0.512975	8
P5 406-12	37.9780	19	15.4676	8	18.3026	9	0.283122	6	0.703620	8	0.512950	6
	37.9816	19	15.4695	7	18.3029	6						
P5 407-4	38.0666	27	15.4771	9	18.3867	10	0.283098	6	0.703674	11	0.512931	5
					Penguin Bank							
P5 255-7	37.8579	19	15.4618	7	18.1587	9	0.283091	6	0.703813	24	0.512932	4
P5 255-8	37.8631	13	15.4635	6	18.1606	6	0.283087	5	0.703775	11	0.512935	6
P5 255-11	37.9613	13	15.4730	5	18.2985	5	0.283104	5	0.703706	8	0.512968	9

[a]All Pb and Hf isotopic ratios were determined by MC-ICP-MS; Pb data were corrected for fractionation by Tl spiking and then normalized to the NBS 981 triple spike values of *Galer and Abouchami* [1998] using the standard bracketing method; Hf data were normalized to JMC 475 $^{176}Hf/^{177}Hf = 0.282160$ [*Vervoort and Blichert-Toft*, 1999]. All Sr and Nd isotopic ratios were determined by TIMS; Sr data were normalized to SRM 987 $^{87}Sr/^{86}Sr = 0.710248$; Nd data were normalized to the Berkeley Ames standard $^{143}Nd/^{144}N$ = 0.510939. The 2σ error is the absolute error value of an individual sample analysis (internal error) and applies to the last decimal place(s). Samples labeled "D" represent procedural duplicate analyses carried out on separate powder aliquots.

compositions are not explicitly Loa- or Kea-like and prevent a definitive distinction between the two models. This may support the hypothesis that the Loa-Kea compositional trends do not extend beyond the Molokai Fracture Zone [*Abouchami et al.*, 2005]. The Molokai Fracture Zone is a complex large-offset fracture zone that coincides with a change in the strike of Pacific plate motion, and may have had a significant influence on Hawaiian volcanism and the plume components sampled by different Hawaiian shields [e.g., *Basu and Faggart*, 1996; *Abouchami et al.*, 2005; *Xu et al.*, 2007].

B3. References

Abouchami, W., A. W. Hofmann, S. J. G. Galer, F. A. Frey, J. Eisele, and M. Feigenson (2005), Lead isotopes reveal bilateral asymmetry and vertical continuity in the Hawaiian mantle plume, *Nature*, *434*, 851-856.

Basu, A. R., and B. E. Faggart (1996), Temporal isotopic variations in the Hawaiian mantle plume: The Lanai anomaly, the Molokai Fracture Zone and a seawater-altered lithospheric component in Hawaiian volcanism, in *Earth Processes: Reading the Isotopic Code*, edited by A.R. Basu, and S.R. Hart, pp. 149-159, AGU, Washington, D.C.

Blichert-Toft, J., D. Weis, C. Maerschalk, A. Agranier, and F. Albarède (2003), Hawaiian hot spot dynamics as inferred from the Hf and Pb isotope evolution of Mauna Kea volcano, *Geochemistry Geophysics Geosystems*, *4*(2), doi: 10.1029/2002GC000340.

Clague, D. A., and J. G. Moore (1991), Geology and petrology of Mahukona volcano, Hawaii, *Bulletin of Volcanology*, *53*, 159-172.

Dana, J. D. (1849), Geology, in *United States Exploring Expedition, 1838-1842*, vol. 10, pp. 756, C. Sherman, Philadelphia.

Eisele, J., W. Abouchami, S. J. G. Galer, and A. W. Hofmann (2003), The 320 kyr Pb isotopic evolution of Mauna Kea lavas recorded in the HSDP-2 drill core, *Geochemistry Geophysics Geosystems*, *4*(5), doi: 10.1029/2002GC000339.

Garcia, M., M. D. Kurz, and D. W. Muenow (1990), Mahukona: The missing Hawaiian volcano, *Geology*, *18*, 1111-1114.

Hauri, E. H. (1996), Major-element variability in the Hawaiian mantle plume, *Nature*, *382*, 415-419.

Jackson, E. D., E. A. Silver, and G. B. Dalrymple (1972), Hawaiian-Emperor chain and its relation to Cenozoic circum-Pacific tectonics, *Geological Society of America Bulletin*, *83*, 601-618.

Kurz, M. D., T. C. Kenna, J. C. Lassister, and D. J. DePaolo (1996), Helium isotopic evolution of Mauna Kea volcano: First results from the 1-km drill core, *Journal of Geophysical Research*, *101*, 11,781-11,793.

Lassiter, J. C., D. J. DePaolo, and M. Tatsumoto (1996), Isotopic evolution of Mauna Kea Volcano: results from the initial phase of the Hawaii Scientific Drilling Project, *Journal of Geophysical Research*, *101*(B5), 11,769-11,780.

Marske, J. P., A. J. Pietruszka, D. Weis, M. O. Garcia, and J. M. Rhodes (2007), Rapid passage of a small-scale mantle heterogeneity through the melting regions of Kilauea and Mauna Loa volcanoes, *Earth and Planetary Science Letters*, *259*, 34-50.

Moore, J. G., and J. F. Cambell (1987), Age of tilted reefs, Hawaii, *Journal of Geophysical Research*, *92*, 2641-2646.

Ren, Z.-Y., T. Shibata, M. Yoshikawa, K. T. M. Johnson, and E. Takahashi (2006), Isotope compositions of submarine Hana Ridge lavas, Haleakala volcano, Hawaii: Implications for source compositions, melting process and the structure of the Hawaiian plume, *Journal of Petrology*, *47*(2), 255-275.

Spengler, S. R., and M. O. Garcia (1988), Geochemistry of the Hawi lavas, Kohala volcano, Hawaii, *Contributions to Mineralogy and Petrology*, *99*, 90-104.

Weis, D., B. Kieffer, D. Hanano, I. Nobre Silva, J. Barling, W. Pretorius, C. Maerschalk, and N. Mattielli (2007), Hf isotope compositions of U.S. Geological Survey

reference materials, *Geochemistry Geophysics Geosystems*, *8*(6), doi:10.1029/2006GC001473.

Weis, D., B. Kieffer, C. Maerschalk, J. Barling, J. deJong, G. A. Williams, D. Hanano, W. Pretorius, N. Mattielli, J. S. Scoates, A. Goolaerts, R. M. Friedman, and J. B. Mahoney (2006), High-precision isotopic characterization of USGS reference materials by TIMS and MC-ICP-MS, *Geochemistry Geophysics Geosystems*, *7*(8), doi:10.1029/2006GC001283.

Xu, G., F. A. Frey, D. A. Clague, W. Abouchami, J. Blichert-Toft, B. Cousens, and M. Weisler (2007), Geochemical characteristics of West Molokai shield- and postshield-stage lavas: Constraints on Hawaiian plume models, *Geochemistry Geophysics Geosystems*, *8*, doi:10.1029/2006GC001554.